Dynamic Wearable Technology: Designing and Deploying Small Climbing Robots for Sensing and Actuation on the Human Body

by

Artem Dementyev

B.S., University of Maryland, College Park (2009)
M.S., University of Washington (2013)

Submitted to the Program in Media Arts and Sciences,
School of Architecture and Planning
in partial fulfillment of the requirements for the degree of

Doctor of Philosophy in Media Arts and Sciences

at the

MASSACHUSETTS INSTITUTE OF TECHNOLOGY

September 2019

Signature redacted

Author ....
Program in Media Arts and Sciences,
August 9, 2019

Signature redacted

Certified by..... .....
Joseph Paradiso, PhD
Alexander W. Dreyfoos (1954) Professor and Associate Head,
Media Arts and Sciences

Signature redacted

Accepted by ... .
Tod Machover
Academic Head, Program in Media Arts and Sciences

Dynamic Wearable Technology: Designing and Deploying Small Climbing Robots for Sensing and Actuation on the Human Body

by

Artem Dementyev

Submitted to the Program in Media Arts and Sciences,,
School of Architecture and Planning
on August 9, 2019, in partial fulfillment of the
requirements for the degree of
Doctor of Philosophy in Media Arts and Sciences

Abstract

This thesis introduces the idea of Dynamic Wearable Technology - a concept of wearable devices as small autonomous robots that can move on and around the human body. Ecosystems in the natural world have static and dynamic organisms such as plants vs. animals. In our wearable ecosystem, all our current devices are static, thus limiting their functionality. Adding robots could significantly increase the usability of wearable devices and/or open up entirely new avenues of application.

This thesis develops and evaluates two approaches to wearable robots. First, Rovables, an on-clothing climbing robot that pinches fabric with magnetic rollers, and second, Epidermal Robots that use controlled suction to attach to the skin. The robots contain on-board navigation that uses inertial measurement units, motor encoders, and occasional ground truth from on-skin features or beacons to estimate position. In this thesis, we analyze important aspects of such robots: size, localization, weight, power consumption, and locomotion.

Dynamic wearable technology has potential applications in many areas, such as medicine, human-computer interactions, fashion, and art. We explore several applications in each of these areas. We focus on how the robots can help to systematically collect health information, such as the mechanical, optical, and electrodermal properties of tissues. Robots like these will provide new avenues of autonomous or guided medical assessment and treatment as well as new venues for the artistic and interfacial exploration of relationships between our bodies and our devices.

Thesis Supervisor: Joseph Paradiso, PhD
Title: Alexander W. Dreyfoos (1954) Professor and Associate Head,
Media Arts and Sciences

Dynamic Wearable Technology: Designing and Deploying Small Climbing Robots for Sensing and Actuation on the Human Body

by

Artem Dementyev

The following people served as readers for this thesis:

Signature redacted

Thesis Reader .....

Canan Dagdeviren, PhD
Assistant Professor
MIT Media Lab

Signature redacted

Thesis Reader .....

Aaron Parness, PhD
Robotics Engineer
NASA Jet Propulsion Laboratory

Acknowledgments

The path to my thesis had been supported by many people along the way.

My advisor Joe Paradiso for continuous support, encouragement to do novel research, and wise advice during my years at the Media Lab.

My thesis committee Canan Dagdeviren and Aaron Parness for inspiration, great advise, and support.

My research collaborators during my time at the Media Lab, who contributed significantly to this thesis and my research directions. Inrak Choi for sharing his amazing mechanical engineering skills. Inrak's advise on mechanisms essential for Rovables and SkinBot projects. Sean Follmer for his great insights into the HCI field and helping to frame the concept of wearable robots. Javier Hernandez for continuous support and encouragement in the SkinBot project, even after resubmitting the paper four times. Cindy Kao for providing different perspectives, and help in the Rovables Project. Christian Holz for teaching me rigorous data analysis. Alice Hong for helping with many aspects of Epidermal robots. Also, my collaborators with who I worked on other projects: Judith Amores, Ken Nakagaki, Hiroshi Ishii, Chris Schmandt, Jifei Ou, and Jie Qi

My colleagues at the Responsive Environments Group. Clemont Duhart, Nan Zhao, Bryan Mayton, Gershon Dublon, Nan-Wei Gong, Mark Feldmayer, Katia Vega, Donald Derek Haddad, Spencer Russell, Robert Richer, Amna Carriero, and others.

Many other friends at the Media Lab who gave me a lot of advice and feedback. Sang-Wong Leigh, Lining Yao, and Irmandy Wicaksono.

The undergraduate students who helped me with the research: Rianna Jitosho, Viktor Urvantsev, Justina R Yang, Gregory Young, Diana Lamaute, Lucas Santana and Kyle Joba-Woodruff.

My previous mentors. Alexander Gorbach for introducing me to research by giving me a chance to work at NIH. Joshua Smith for being a kind mentor and advisor at the University of Washington during my masters. Steve Hodges and Stuart Taylor for introducing me to human-computer interactions during my internship at Microsoft

Research. Bunnie Huang for introducing the manufacturing world in China. Alanson Sample for teaching me many things about electrical engineering.

My family and friends for supporting me. Sergey Dementyev, Yulia Dementyeva, Vlada Dementyeva, and Tammy Lan.

Contents

List of Figures

List of Tables

Chapter 1

Introduction

Recently there have been great advances in wearable electronics. In parallel, there are rapid improvements in machine learning [3, 4], mainly driven by an increased amount of collected data, improved algorithms and computing power, as governed by Moore's law[1]. The machine learning approaches are useful in finding patterns in complex data such as physiological signals.

To leverage the advantages of computing power, we need to find better ways to collect data on our bodies systematically. Supervised learning algorithms require repeatable, quantitative, and labeled data. Robots are well suited for such data collection task. As evident by the smartwatches domination of the wearable sensor market [5], the current paradigm of wearable sensors enables us to collect data or actuate just from one location. Furthermore, they require manual manipulation and placement. Almost for all wearable sensors, their position plays a significant role. If we look at nature for inspiration, we find that a healthy ecosystem has static (e.g., forests) and dynamic organisms such as animals and insects. The digital ecosystem around our bodies has only static devices, severely limiting its functionality.

This thesis proposes and explores wearable devices that move autonomously on the human body as mini-robots. We named this idea *Dynamic Wearable Technology (DWT)*. Specifically, the thesis introduces two complementary robots: *Epidermal Robots* that can move on the skin, and the *Rovables* that move on the clothing. The

[1] Moore's law states that transistor count roughly doubles every year

specification of the two robots are summarized in Table 1.1.

Robotics is a relatively new field, with the first industrial robots appearing in the early 1960s [6]. As a result, there is not much crucial historical context. Miniature robots require sophisticated electronics with low power consumption and MEMS fabrication. Such robots have only become accessible in recent years, due to improvements in microfabrication. On the other hand, living creatures were used on the human body for a long time. For example, in Mexico and ancient Egypt, a beetle on a chain was used as jewelry [7]. Maggots are used for chronic diabetic ulcers [8] and leeches have been used for medical purposes for more than 2500 years [9].

	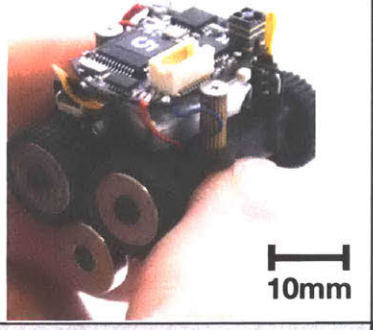	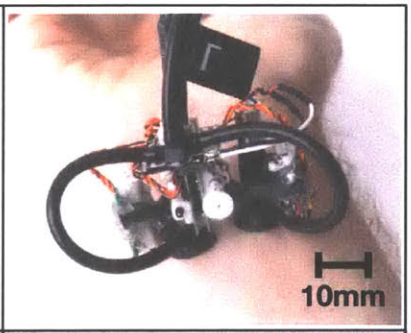
Specs	**Rovables**	**Epidermal Robots**
Movement mechanism	Magnetic wheels	Suction cups
Movement surface	Fabric	Skin
Weight	20 grams	20 grams
Size	2.6 x 3.6 x 4 cm	2.7 x 2.0 x 4.2 cm
Power source	100 mAh battery	Tether
Untethered	yes, wireless	no
Mechanism	2 geared motors	4 linear motors, 1 gear motor, 2 pumps
Controller	ARM Cortex M0	ARM Cortex M4F
Sensors	2 wheel encoders, IMU	IMU

Table 1.1: Selected specification of the two designed robots.

There are three inspirations for this work. First, the Nixie bracelet drone [10] from

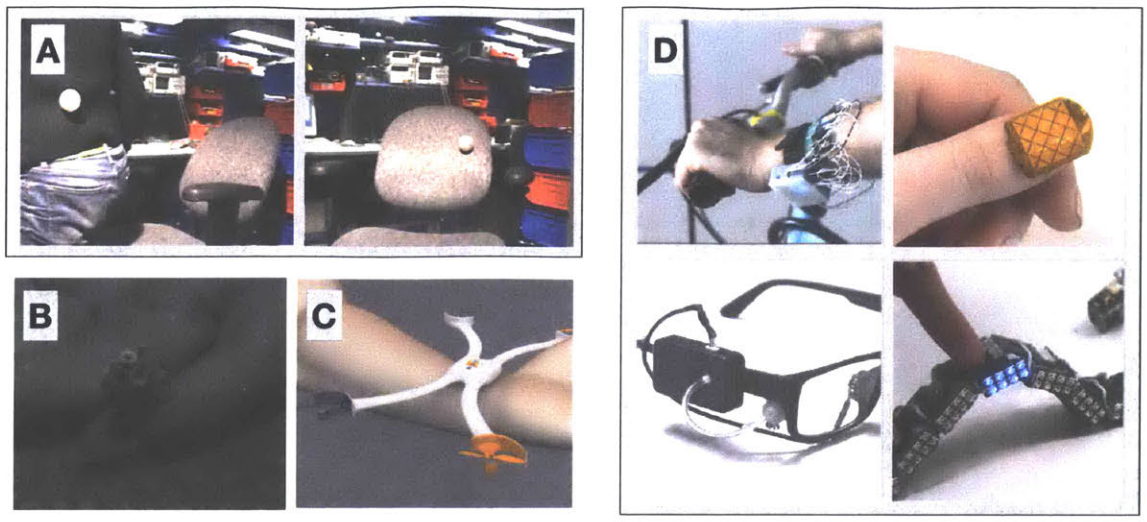

Figure 1-1: Inspirations for DWT. A) Parasitic mobility. Robots attached to the person, than to the chair. B) SkinSucka from Studio XO. A concept video with skin crawling robots. C) Nixie, a drone thats also a bracelet. D) My previous research in wearables and robotics.

2014 Intel Make it Wearable contest, led me to believe that wearable technology does not need to be static. Second, a concept of parasitic mobility [11] was developed in 2005 in our research group: Responsive Environments at the MIT Media Lab. This concept showed sensor nodes that can hitchhike on a person, and detach where they are needed. Third, the previous work I did in medical imaging [12, 13] , wearables [14, 15] and robotics [16, 1]. Doing those projects allowed me to understand the limitations of the current technologies and build up the technical skill required for this thesis. Those three ideas lead to the Rovables project.

We explored using Rovables as a platform for Human-Computer Interactions (HCI) and fashion applications. For example, we used Rovables to provide localized tactile feedback and as a moving fashion accessory. For such applications, the untethered ability to move on clothing worked well. As a disadvantage, the Rovables did not make skin contact.

Skin contact is required for almost all physiological sensing and medical applications, and I was interested in exploring such applications. Furthermore, I was interested in the technical challenge of designing the robots that climb the skin, as

it has not been done before. This lead to the development of the SkinBot and the area of Epidermal Robots. Among some applications, we use the robot to detect and classify lumps under the skin. Concept video [17] from a design firm Studio XO had demonstrated the idea of Epidermal Robots well, a few years before we started such development. In the video, swarms of small robots moved around the body and applied makeup.

Such small climbing robots could be used for other purposes than wearable devices. For example, they could be used for finding cracks in an airplane engine or scale mountain terrain. General climbing robots has been explored in robotics field in great detail before (e.g., [18, 19]). This thesis examines only wearable applications to avoid broad but shallow exploration of this topic. Also, I believe that the blend of wearable electronics and robotics is a new area of research.

1.1 Dynamic wearable technology (DWT)

In this section, we attempt to outline the main design criteria of DWT robots. Each of those criteria is discussed in separate chapters in the thesis. To satisfy those criteria, the system design of the DWT robot needs certain subsystems. In Figure 1-2 we provide a block diagram of a DWT robot.

- **Small size (chapter 8)**. The robots should be well below an order of magnitude smaller than the human body, millimeters to few centimeters in size. First, small robots are less obtrusive to the human host. Second, it is easier for a small robot to move around a complex surface such as the human body. Coarsely, the human body can be thought of as cylindrical. surfaces [20]. To a robot that is an order of magnitude smaller, such surfaces will appear flat.

- **Ability to move freely (chapter 6)**. The robots should have the ability to move freely on human clothing or skin. They should be able to move vertically as well.

- **Autonomous (chapter 5)**. The robots should be able to navigate the human

body on their own. Navigation requires a localization method and a map. The robot operation should not require any external sensors or devices.

- **Platform (chapter 9).** DWT should be able to support different types of sensors or actuators, to allow the development of different applications.

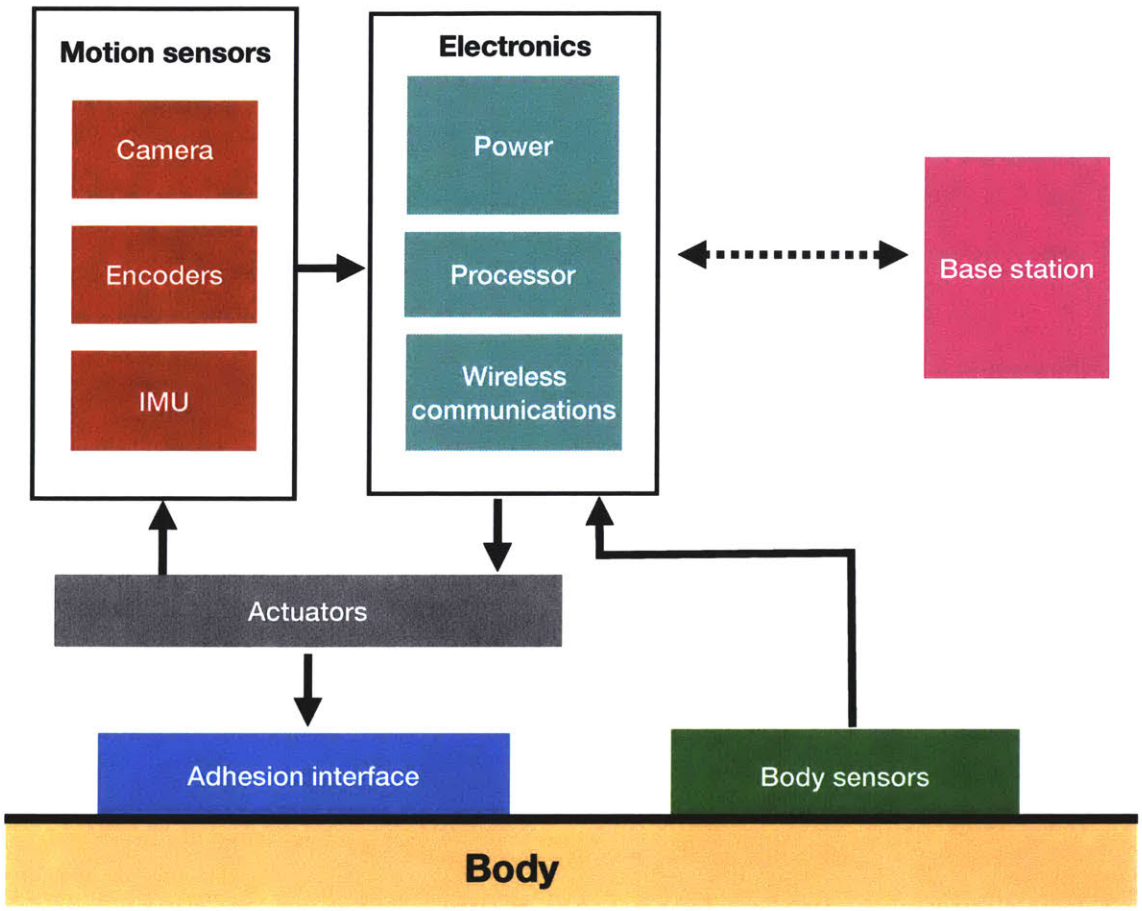

Figure 1-2: The overall system diagram of DWT robots. The arrows show the information flow between the subsystems.

1.2 Why is DWT important

Let's imagine a future scenario where we already have small robots that fulfill the previous requirements. Medicine is becoming more personalized and data-driven and will continue to do so in the future [21]. Potentially, DWT will become our first

line of defense against diseases. To do a yearly medical check, instead of going to a doctor or a hospital, one would order online a personalized box of robots, tailored for a specific purpose. After receiving the robots, the person would put the robots on, perhaps while going on through an everyday routine or sleeping during the night. The robots will take repeatable and high-resolution measurements of the body. The robots could see things that are impossible for a doctor to see with a naked eye. For example, robots can test the mechanical properties of the skin to detect very early signs of cancers. All the data is collected and analyzed with powerful computers remotely. If the robots discover something, they could use a precise laser to remove the problematic skin cells. Also, the robots can see invisible signals of the body, such as bioelectrical potentials (EKG and EMG). Once the robots finish, they can be shipped back, just like returns in online shopping.

DWT can be used in many fields, such as medical sensors, human-computer interactions, body-care, arts, and fashion. I will provide specific example applications throughout the thesis. Currently, I believe the most productive use is medical sensing, as it can have an immediate improvement in our lives. Chapter 2 (Background) provides a thorough comparison to other technologies. Below, I will attempt to summarize the benefits of DWT. All DWT robots have the following characteristics.

- **Continous and repeatable measurements**. The robots eliminate errors and uncertainties associated with human operators.

- **Variable and accurate spatial resolution** As the robot can adjust their step size, they can sample with both high and low resolution. This allows robots to obtain 2D and 3D data.

- **Full-body coverage**. The robots can access any location on the body.

- **Easy to transport** The small and lightweight robots are easy to transport to a remote location or home. This is a great benefit for individuals with limited mobility or in remote locations with no access to sophisticated instruments.

- **Privacy and comfort** Some users might not feel comfortable to be examined

by another person. Robots can potentially provide complete privacy.

Depending on the applications, the robots might have additional benefits:

- **Ability to work in swarm**. The robots could work together to coordinate tasks to accomplish them faster or to create sensor arrays. For example, one robot could serve as a transmitter and other as a receiver.

- **Sophisticated sensors and actuators**. The robots are not limited to simple sensors, as many current wearables. As a payload, the robots can carry sophisticated sensors, such as cameras.

1.3 Chapter and thesis summaries

The thesis has four main parts: The first part (**Chapters 1,2**) provides an overview of DWT, as well as describes previous work and technologies. A second part (**Chapters 3,4**) dives deep into the implementation of Epidermal Robots and Rovables. This part is primarily based on my previously published work on this topic [1, 22, 23, 24]. The third part (**Chapters 5,6,7,8**) provides a discussion of the main design criteria of DWT, such as power consumption, navigation, climbing, and size. The fourth part (**Chapters 9,10,11**) discusses applications of DWT, as well as limitations, future work, and concluding remarks.

1.4 Contributions of the thesis

This thesis makes the following contribution:

1. We introduce a new area of *Dynamic Wearable Technology.*

2. As two instances of DWT, we develop Epidermal Robots and Rovables. Epidermal robots can move on the surface of the skin. Rovables can move on the clothing. All the design files and instructions are open-sourced online on Github[2]

[2]https://github.com/adementyev

3. We discuss and study various points of DWT such as power consumption, size, and localization.

4. We showcase various applications of DWT in medicine, human-computer interactions, and art domains.

Chapter 2

Background

In this chapter, DWT is positioned against existing technologies. Since DWT is a blend of robotics and wearable electronics, backgrounds for both fields will be provided. Figure 2-4 summarizes complex relationships between DTW and other technologies. This chapter will look into each technology in the graph in detail, and discuss their advantages and disadvantages. This graph demonstrates the unique and unexplored space that DWT occupies. By looking at the graph, DWT provides variable body coverage while maintaining the size of wearable devices.

2.1 Wearable Electronics

Wearables first appeared in the early 1960s. The first instance of wearable technology appeared in 1961 as an electric device hidden in the shoe to improve gains at a game of roulette [25]. Another example of an early wearable device from the late 1960s is a spacesuit, which contains a portable life support system. (e.g., Apollo 15-17 EMU) The idea of wearable technology was explored and popularized by Thad Starner and Steve Mann at the MIT Media Lab, with untethered wearable cameras and head-mounted display [26].

Today due to electronics miniaturization, many wearables have reached the consumer market. For example, smartwatches are popular. They can provide easily accessible information, as well as sense activity, and provide limited physiological

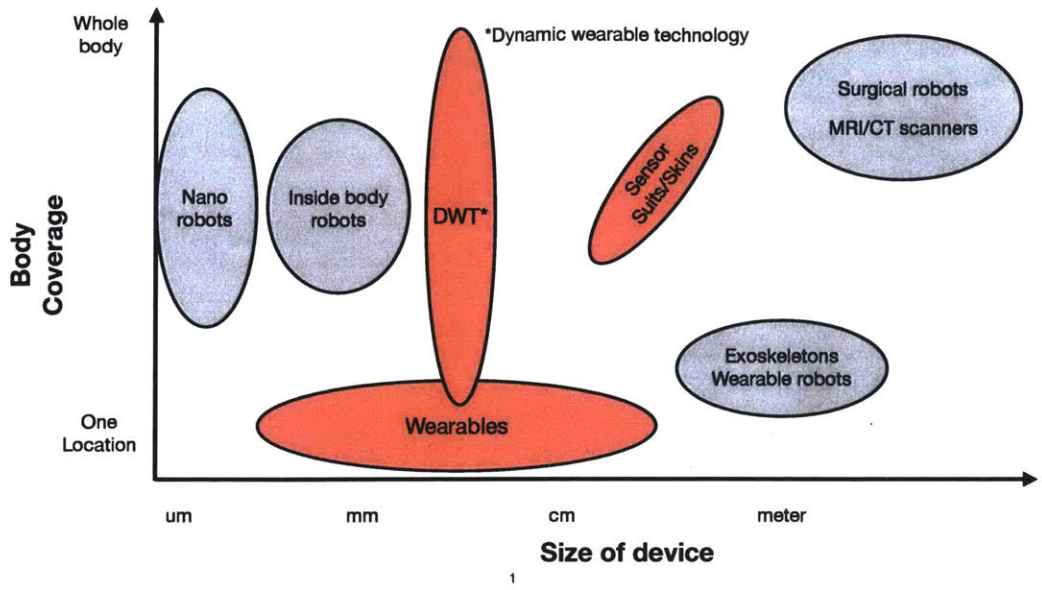

Figure 2-1: Dynamic wearable technology (DWT) and related technologies. Approximate body coverage of the technology in comparison to it's size. In my previous research and this thesis I explored the technologies highlighted in red.

signals such as heart rate using photoplethysmogram (PPG) with near-infrared spectrometry [27]. Research in Human-Computer Interactions (HCI) has explored many aspects of smartwatches. For example, using motors to provide haptic feedback [28] or to move the watch [29]. Also, researchers explored additional sensing such as electric field [30] on a watch form factor. Today the cutting edge wearable devices research are stretchable tattoo-like epidermal electronics, which have been pioneered by the Rogers group at Urbana Champaign [31]. Also, starting with iSkin [32], multiple projects [33, 34] in human-computer interactions demonstrated tattoo-like wearables.

Wearable devices, including commercial examples and state-of-art research prototypes, are designed to be fixed in one location to perform a specific function. Even though they can vary in size from millimeters to centimeters, wearables cover single point coverage.

However, there are a few exceptions, where researchers and designers looked at moving wearable devices. In a Ph.D. thesis from MIT Media Lab, Zipperbot [35]

Figure 2-2: Examples of state-of-the-art wearable devices. A) Epidermal electronics: microfabricated stretchable electronics. B) iskin, an on-skin electronics using conductive ink. C) Apple watch with the green LED tuned on, which is used for measuring heartrate and blood oxygen level.

attaches to a zipper and can zip and unzip clothing. Other robots did not climb directly on the clothing but demonstrated cloth climbing ideas. The concept of Daily Support Robots [36] showed a robot that moves on the body to provide notifications, using a rail on the arm for climbing. It is one of the earliest examples of moving wearables in the Human-Computer Interaction field. Movelet is an arm brace that can move up and down, providing haptic feedback [37].

Fashion designer Hussein Chalayan has done multiple fashion shows with transforming clothing [38], where motors and pulleys were used to move the dresses. Behnaz Farahi designed a 3D-printed garment that moves based on other peoples gazes [39]. Other designers showed fabrics that can change shape, such as using magnets embedded inside the fabric [40].

2.2 Sensor fabrics and materials

A brute force approach to increase body coverage of sensors is to increase the number of sensors. With this approach, the coverage is directly proportional to the number of sensors. The common approach is using e-textiles, where electronics are integrated into the fabric. This was investigated early at the MIT Media Lab [41] with embroidery of conductive threads. A research community sprung up around this area, creating many new fibers, techniques, and applications for sensate garments [42, 43, 44].

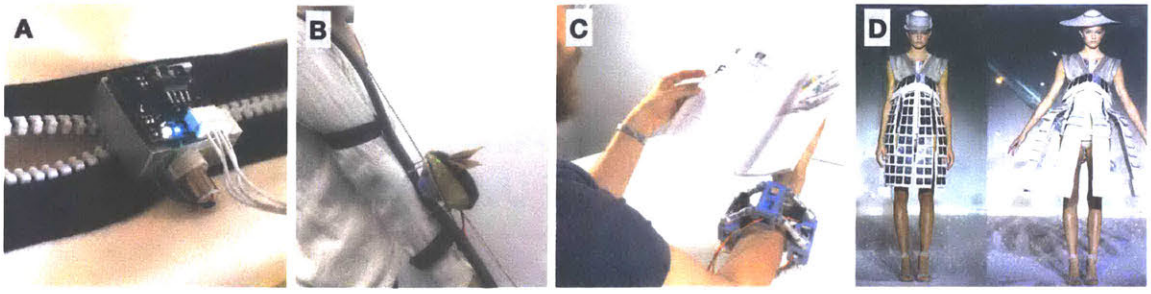

Figure 2-3: Explorations of moving wearable devices and clothing. A) Zipper-bot; a robot that zips clothing. B) Daily support robots, a mouse-looking robot that moves on a rail. C) Movelet, a bracelet that moves up and down the arm for haptic applications. D) Hussein Chalayan fashion show with transforming clothing.

E-textile were further popularized by Leah Buechley with an introduction of Lily-Pad kit, which made it easier to create e-textiles [45] using friendly form factor and the Arduino platform. This approach has been investigated by Google ATAP recently commercialized jackets with capacitive sensing for gestures [46]. A state of the art approach is to integrate semiconductors into textile fibers [47] directly. Some approaches do not require the sensors to be embedded in the fabric. For example, placing 17 inertial measurement units (IMUs) in pre-defined body locations allows for full 3d body tracking [48]. In this approach, a suit is used to ensure that the sensors always stay in the same place. Another approach is to create flexible sensor skins with various sensors, instead of integrating electronics into the fabrics. For example, Takao Someya's group at the University of Tokyo demonstrated a flexible pressure sensor array for robotic applications [49]. As a precedent to DWT, we demonstrated SensorTape, a dense sensor network distributed along a length of a flexible tape-like circuit board. It could be used as a wearable sensor skin to track posture, as well as be cut to different sizes [50].

There are multiple disadvantages to using sensor-laden materials. First, they require custom fitting fabrics to ensure good contact with the skin. Second, there is a scaling problem with an increasing number of sensors. The size, complexity, price, and power consumption increases with the area coverage. It is not a huge issue for simple sensors such as electrodes but becomes a problem with multiple complex sensors such

as cameras. Third, the spatial resolution is limited by the physical sensor layout. This could be a disadvantage in applications where a variable or custom resolution is required. For example, different areas might require distinct resolutions or resolution could be adapted based on collected data. Nevertheless, this approach is promising. With the improvements in electronics size and power, we can integrate more and more sensors into clothing.

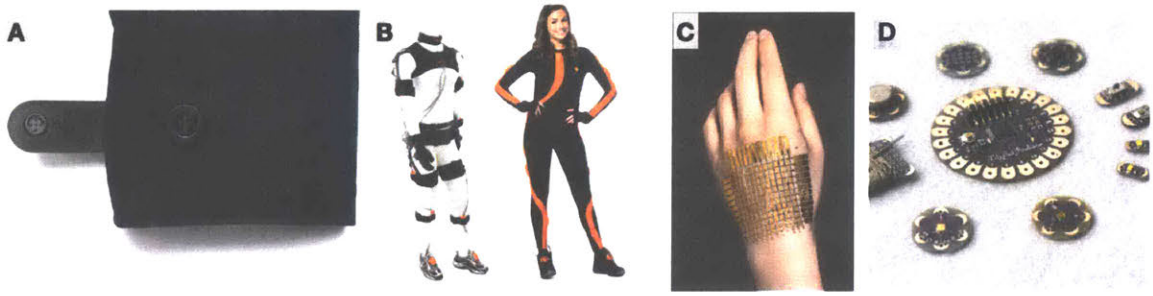

Figure 2-4: Examples of sensor suits and skins. A) Denum Jacket with capactive sensing conductive fibers. B) Body motion capture suit from Xsens. C) Pressure sensor skin from Takao Someya's group. D) LillyPad Arduino, a kit for wearable electronics.

2.3 Micro and nano robots

Nanorobots and microrobots that go inside the body is an area of active research. The advantage of microrobots is that they can be non-invasively injected into the body. There are significant challenges to realizing this, such as power and size, so off-the-shelf technology cannot be used. There have been robots proposed to move inside blood vessels [51]. Many microrobots are steered by external magnetic fields [52]. Some exciting work has focused on how a swarm of robots can be inserted through a needle and assembled inside the eye [53]. Some biomedical microbots were actuated by shape memory alloy wires [54] or vibrations [55].

The main disadvantage of micro/nanorobot is its limited functionality. It is not yet technically possible to integrate computing and energy sources into such robots, so they lack autonomy. Usually, they are driven by an external machine, so the person

remains tethered to a specific location.

2.4 Mini-robots inside the body

The mini-robots also go inside the human body but are larger than the nano and microrobots. They are usually at a millimeter to a centimeter scale. At this size, they can potentially be autonomous, as they can contain computing and a power source. There are task-specific medical prototype robots, such as a small bone-mounting robot for spine surgery [56], a snake-like robot that goes into the airways [57], and an endoscope robot to look inside the body cavities [58]. Most relevant to DWT is HeartLander [59, 60], Carnegie Mellon's robot that uses suction to locomote on the surface of the heart and deliver injections. This robot has been tested on a beating pig heart. The robot was developed in the early to mid-2000s and appeared to be in the commercialization stage since.

The disadvantage of mini-robots is that they are invasive. Such robots are too large, so they require an invasive entry into the body. DWT is on the same size scale, but it is not invasive.

2.5 Room-size devices

Full body coverage can be achieved by putting the person inside a large machine or having a large robot with a long reach. Typically, a large machine such as a CT or MRI scanner is used. Another approach is using non-contact sensing, such as radio signals [61] or cameras [62] to sense heart rate and respiration.

Some surgical robots are already being used in medicine. There are large robots that can perform surgery with teleoperation. There are two main such robots: the research robot Raven [63] and commercial Da Vinci robot [64].

The main disadvantage of large machines is that the person requires to be enclosed by the device or remain in a specific location, so this approach can not be used in an ambulatory or remote setting.

2.6 Exoskeletons

Currently, the term wearable robots refer to exoskeletons. Exoskeleton's role is to improve or restore human abilities. Some can be purely medical, such as an active prosthesis, for example, an artificial hand controlled by EMG signals [65] or an active leg prosthesis [66]. The applications of such robots are straightforward: to restore the function of a missing or damaged limb. The second application of exoskeletons is to improve abilities or to add haptics. For example, an upper arm exoskeleton was developed by Columbia University [67]. Other researchers made additional appendages such as fingers [68] or arms [69]

2.7 Chapter Summary

In this section, various technologies regarding body coverage and size were presented. There are advantages and disadvantages to each technology. DWT occupies a unique niche in this space. As seen in the Graph 2-4 DWT can provide variable coverage at the size of a small wearable device. Also, we found that the small on-body robots have not been extensively explored before, and this provides a lot of opportunities for future exploration

Chapter 3

Epidermal Robots

This chapter describes the design and manufacturing of Epidermal Robots. Also, it attempts to rationalize the design decisions of the robot. The first functional Epidermal Robot is called *SkinBot*, and is the main focus of this chapter. In the future, Epidermal Robots should be made from soft materials, so they match the elasticity of the skin and are more resilient. The soft robotics prototype is briefly described at the end of the chapter.

3.1 Introduction

To perform their tasks successfully, Epidermal Robots need to meet several specific requirements. First, the robots need to be **lightweight and small** (under 80 grams and centimeter-sized according to our experiments) to minimally disrupt the person while exploring the different parts of the body. The weight requirement was experimentally determined in chapter 6. Second, Epidermal Robots need to have direct **access to the skin**. Human skin is not only the largest organ of the human body but also offers a good proxy to capture relevant information about the skin (e.g., appearance, texture) and inner body responses such as physiological signals (e.g., electrocardiograms, electrodermal activity). Third, the robot needs the **ability to adhere and locomote** over the non-uniform skin, which contains many irregularities such as wrinkles, joints, and hair. Moreover, the locomotion should be robust

to different robot orientations. Fourth, Epidermal Robots should offer **multimodal sensing**. The human body contains a large range of information that requires different types of sensing modalities. To ensure the robot can successfully digitize the human body, the sensing module should contain as many sensors as possible, while still satisfying the previous considerations. Finally, Epidermal Robots should have the ability of accurate **self-localization** on the body (under 18 mm error rate, due to the camera's field of view, detailed in Chapter 5), which is key for autonomous operation and mapping of the human body.

3.2 Implementation

For reference and reproduction, all the design files and software can be found in an online repository[1].

3.2.1 Skin Adhesion

Human skin has complex mechanical behavior and is elastic at small loads. In particular, it has Young's modulus [2] ranges from about 0.1MPa to 1.1MPa [70], with a high dependence on the test subject's age, the analytical model, and the measurement instrument [71]. Also, the human body has some degree of curvature and features such as hair which makes adhesion even more challenging. Since skin is a complex surface, we conduct *in vivo* experiments as much as possible. However, in some cases such as testing specific skin curvature, we perform experiments on artificial skin created with silicone (Ecoflex 00-30, Smooth-On)[3] which has a similar Young's modulus as the skin.

We designed and built a total of six robot prototypes that considered different locomotion systems (Fig. 3-2). On the one hand, some adhesion approaches such as pinching the skin were not practical and were excluded from the start. On the

[1]https://github.com/adementyev/SkinBot

[2]Young modulus is a measure of material's stiffness. Young modulus is defined by the relation between strain and stress

[3]https://www.smooth-on.com/products/ecoflex-00-30/

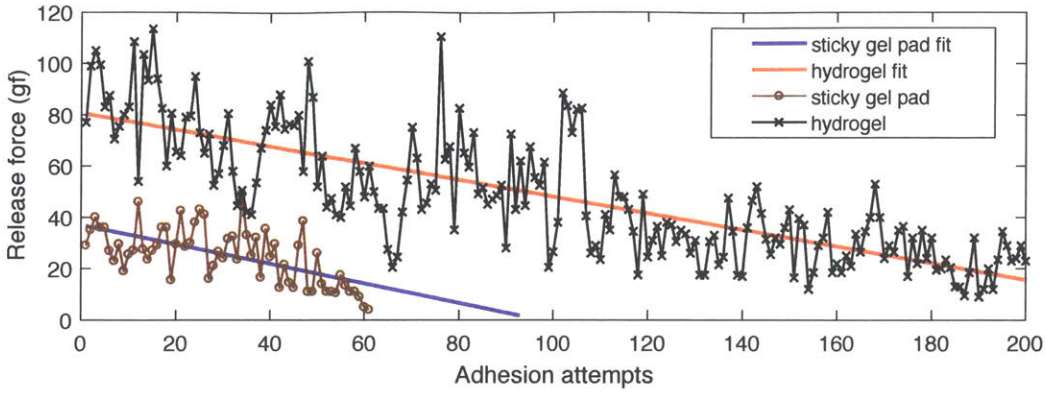

Figure 3-1: Testing of two adhesives for repeated sticking and releasing on the skin. Linear fits are overlayed on the data. We tested a hydrogel and a sticky gel pad. The hydrogel worked for more adhesions than sticky gel pad, before losing adhesive properties. The release forces had large variations from sample to sample. The testing was conducted with a 20N force gauge, and peak force was recorded.

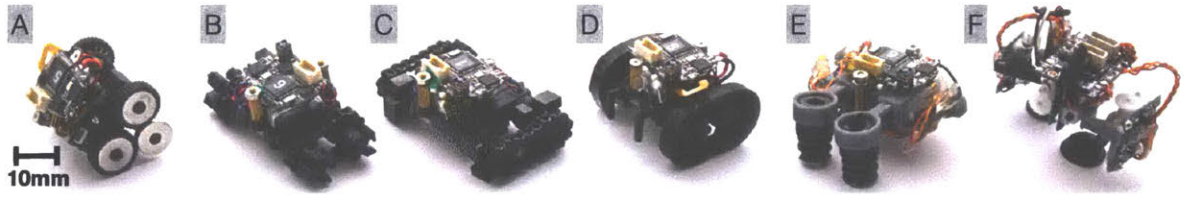

Figure 3-2: The iterative design process of SkinBot showing different prototypes. A) Rovables [1], cloth climbing robot. The initial designs were based on Rovables platform. B) Prototype based on a wheel-leg climbing robot design in [2]. Tracks on the outside were used to synchronize the wheels. This prototype does not have enough contact area to adhere to the skin reliably. C) Similar wheel-leg design, but contains tracks on the inside. This design also does not have enough contact area. D) Prototype with sticky tracks. E) Initial suction-based robot with two servo motors that allows suction cups to extend and contract. We found that two motors are not enough for reliable movement, as the suction cups need to be pushed down to create a reliable seal. F) Current robot design, which is explained in detail in this paper.

other hand, adhesive wheels and tracks did not provide consistent adhesion force. For instance, the adhesive force of two commercial adhesives (Katecho and Premium Fixate Cell Pads, CloudValley) decreased with each peel by about half a percent (Fig. 3-1) while having significant variations between peels. With the continuous attachment and detachment cycles, required for locomotion, the adhesive force quickly

degrades. Also, the hydrogel adhesive picks up dirt, oil, and dead epithelial from the skin, thus requiring periodic cleaning. After considering different methods, we finally selected a suction-based approach which was inspired by living organisms such as leeches and cephalopods (e.g., squid, octopus).

In suction-based locomotion, a suction force appears when a lower pressure is created inside a cup, and the pushing of the atmospheric pressure causes an adhesion force. While suction cups used in the industrial applications are usually made of soft rubber, we found that rigid cups can be used with the skin. Under vacuum, the flexible skin gets pulled into the cup to seal the skin-cup interface (shown in Fig. 3-3C). While rigid suction cups can be quickly prototyped with a standard 3D printer, flexible suction cups require a multi-part silicone mold. We found that the bell-shaped cup worked well with the skin. The bell provided a large inside volume, into which the skin can expand. A similar bell design is often used in cupping therapy, alternative medicine in which suction cups are applied to reduce pain and swelling.

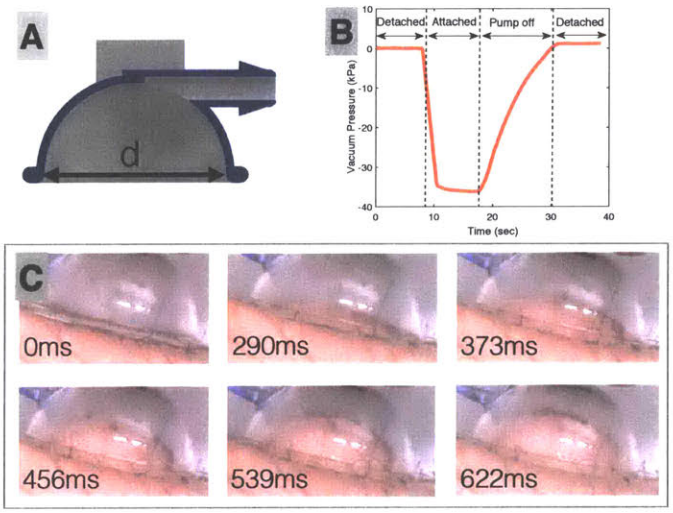

Figure 3-3: Suction cup design for skin attachment. A) The cross section of the suction cup CAD model. B) The vacuum pressure changes during the suction cup attachment and detachment. C) Snapshots of suction cup attachment to the skin. The pictured suction cups were made from clear 3D printed material.

The final implementation of SkinBot uses two 9mm-diameter suction cups. To make the suction cups as well as all other mechanical parts, we used a 3D printer (Form 2, Formlabs, gray resin). The 9mm suction cup provided the best size-to-

adhesion-force tradeoff and is analyzed in more detail in Chapter 6. This configuration provided a maximum of 200gf (gram-force) adhesion force, which is enough to hold the 20-gram SkinBot securely. The minimum vacuum pressure required for skin adhesion was measured to be about -10kPa. However, we pull the maximum vacuum of -30kPa using a small membrane diaphragm pump (SC3101PM, Skookum Electronic co.). This pressure was determined by the construction of the pump, specifically by the piston displacement volume. When the vacuum pump is turned off, due to leakage, the pressure slowly returns to atmospheric pressure. To speed up this process, we added a solenoid valve (S070C-SDG-32, SMC Pneumatics) that vents the vacuum line. Using a diaphragm pump also has some problems such as the loudness (55 dB at 30cm) and the large size (32x8x18mm). We also considered piezoelectric pumps, but current commercial models (e.g., mp5, Servoflo) only provide a maximum of -10kPa which does not leave any safety factor for air leaks, hair and pump variations that can make adhesion less reliable.

3.2.2 Skin Locomotion

We wanted to achieve locomotion with the ability to turn with a minimum number of motors as they are one of the largest components. The selected gait was inspired by an inchworm mechanism where climbing is achieved by creating an anchor point and pushing the body away from that point. At a minimum, this motion requires one actuator to extend and contract the robot's body. In our case, however, we used two linear servo motors to extend and contract the body to allow independent left and right side control. In particular, we used linear servo motors (SPMSA2005, Spektrum) with a 9.1mm throw, commonly used in small radio-controlled airplanes that can pull 100gf (gram-force) and weight around 1.8 grams. Furthermore, at least two independent anchor points are required, which can be detached and attached on demand. Thus, two independent pumps and suction cups were used to provide controllable attachment. Also, we added two of the same linear motors to move the suction cups up and down. This prevented dragging of the end effector during extension and contraction and gave the robot the ability to attach to non-uniform

surfaces. Finally, we added a planetary gear motor (TGPP06-D-136, TT Motor) and a motor controller (DRV8835, Texas Instruments) to add turning ability around one of the suction cups.

One of the critical challenges with skin locomotion is to ensure reliable adhesion at the new end-effector position. To address this, we added an air pressure sensor (MPXV611, NXP) in each of the vacuum lines to detect if the suction cup is attached. The pressure data were collected at 100Hz and filtered by a moving average of 20 samples to remove oscillations of the pump. The attachment was insured by moving the suction cup down in small increments and checking for adhesion each time. The whole locomotion was controlled by a finite state machine with 6 states and was implemented on an ARM Cortex M3 microcontroller (Teensy 3.6, PJRC). As shown in Fig. 3-4A, the transitions of the state machine were controlled by the pressure sensors. We conducted the testing using a tethered prototype, which contained valves, pumps, power, and control electronics on a separate master board, shown in Fig. 3-5. The overall system architecture is shown in Fig. 4-5A.

3.3 Soft epidermal robots

This section briefly describes the current and future direction of the soft Rpidermal Robot. We found multiple problems with the current rigid robot design. The rigid robot has limited degrees of freedom, which limits its reach around tight curvatures. Also, the robot would break if it gets squished, which can happen if a person rolls over during sleep. To have multiple degrees of freedom as well as a resilient structure, we created a prototype of a soft Epidermal Robot. Soft robotics has become a popular research topic and has a promising future, especially for robots that are near humans. I initially became involved in soft robotics as we looked at how to integrate air pouch-based actuators inside flexible circuit boards [72].

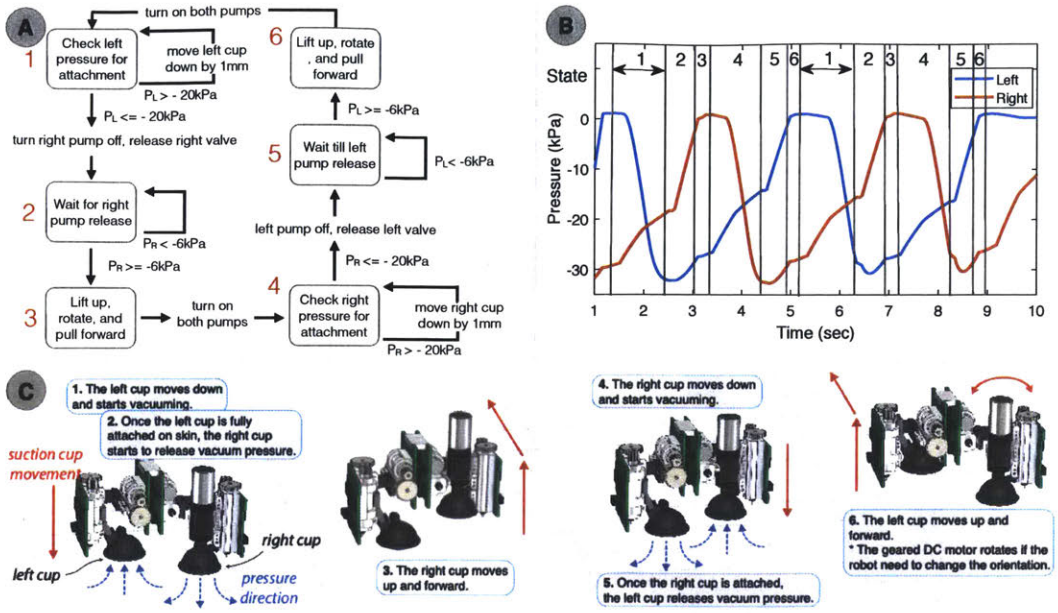

Figure 3-4: Locomotion mechanism overview. A) Finite state machine diagram for the robot locomotion. The rounded rectangles and arrows represent the states and transitions, respectively. The red numbers next to the circles indicate specific states. The pressure sensors control the state machine. States 1 and 4 involved reattaching suction cups, which was done by moving the suction cup down in increments and checking the pressure each time. B) Pressure changes during the locomotion sequence, which was measured independently on the right and the left suction cups. The diagram also shows the corresponding states of the finite state machine on the top. C) Model representing physical locomotion.

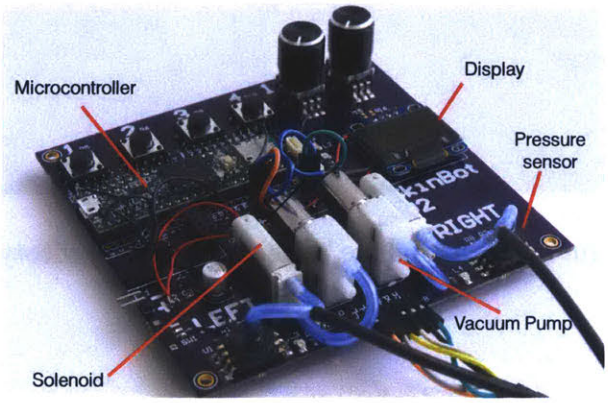

Figure 3-5: The master circuit board image. This board contains all the components required to run the tethered robot. The master board connected to the computer through the USB for communications and programming. The pumps, solenoids and servo motors run off separate power supply at 3.3V

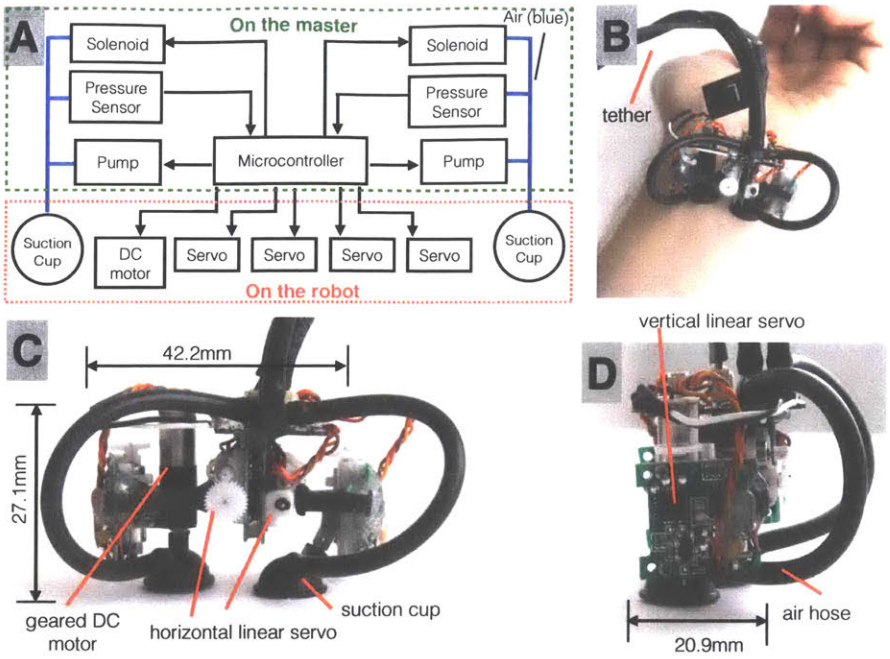

Figure 3-6: SkinBot design. A) The system diagram of the main components of SkinBot. B) Robot attached to the arm. C) The front of the robot. The robot combined four linear servo motors and a DC gear motor to allow translation and rotation. D) The side view of the robot.

Figure 3-7: An image of the soft robot prototype

3.3.1 Design

Our design criteria for the soft robot is that we employ soft materials only and keep the size of the robot to a few centimeters. The robot design is based on the multi-module variable stiffness manipulator [73]. We modified the manipulator to make it smaller and removed the central channel for stiffness control. Mainly we reduced the thickness of the walls to 2mm, as we experimentally determined that 2mm thickness

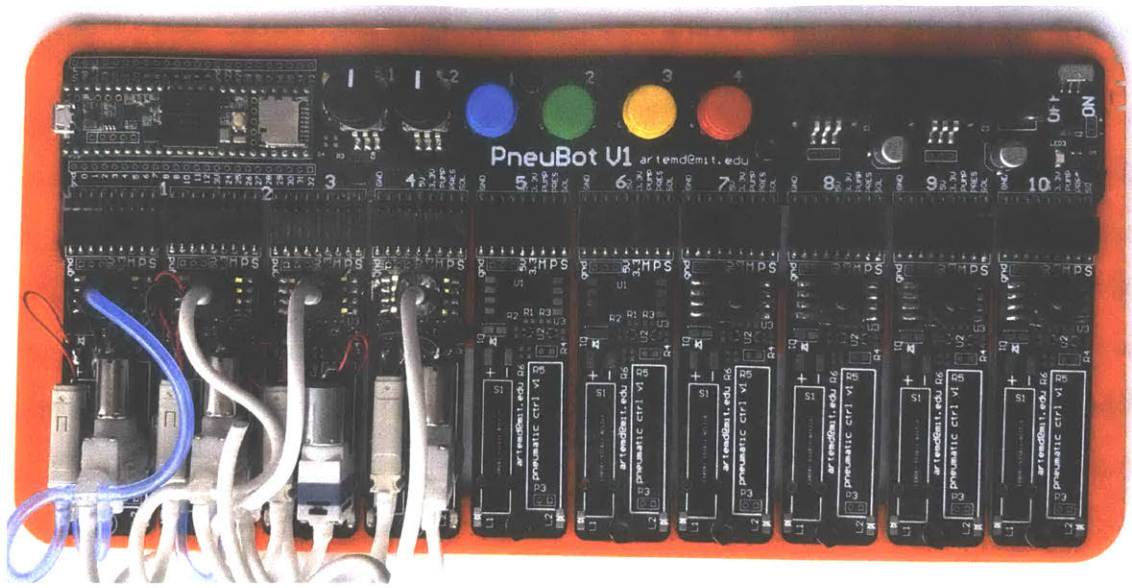

Figure 3-8: Pneumatic control board for the soft robot.

could be reliably manufactured by molding.

Using three individual air pouches, this design can bend and elongate in any direction. Inflation of one pouch causes bending. Inflation of all three pouches at the same time causes the actuator to elongate. To avoid inflation of silicone in the radial direction, a plastic sleeve was added. Sleeve allowed elongation and bending, but could not be stretched radially.

The robot was tethered to a control board, as shown in Figure 3-8. The control board was based on the Epidermal Robots control board. In comparison to Epidermal Robots control board, instead of two channels, this board supported up to 10 modular pneumatic channels. Each channel was removable and contained pressure sensor, solenoid (S070C-SDG-32, SMC Pneumatics) and a pump (SC3101PM, Skookum Electronic co.). The diaphragm pump could be wired for either vacuum or inflation. In the case of our robot prototype, we had three inflation channels and two vacuum channels for the suction cups.

The controls were implemented on a Teensy 3.6 microcontroller. The controls were based on pressure sensors. The channels could be inflated to specific pressures, to provide a coarse approximation for a bend angle.

3.3.2 Manufacturing

We primarily used an FDM 3D printer (i3 MK3S, Prusa) with PLA filament to make the molds for silicone. We attempted to use an SLA printer but found that the resin can contaminate the silicone and inhibit curing of thin features. We used Ecoflex 00-30 (Smooth-On) as the primary material. Ecoflex is a popular choice in soft robotics as it allows for large (>200%) expansion without tearing and has a quick cure time of 4 hours. We also used Dragon Skin 30 (Smooth-On) for stiffer parts such as suction cups.

As silicone cures, it becomes an inert material, making it very challenging to interface with other materials. Fortunately, silicone can stick to itself, and Ecoflex could be used as glue between silicone parts. This property allowed us to assemble a robot using six consecutive molding steps. We used silicone tubing (5236K502, McMaster-Carr) with 1/16" ID and 1/8" OD for connections, as it adhered to silicone, creating airtight segments. We experimented with another tubing such as Vinyl, and Teflon and could not get airtight adhesion.

3.3.3 Soft Robot Discussion

We did limited experimentation with the robot, as our initial goal was to develop the proof of concept. The robot could easily attach to the skin with the suction cups, and only weight 35.5 grams. The three-segment actuator allows for a wide range of movements. We found that designing climbing robots with silicone is challenging as they lack a rigid structure, which can transfer loads during climbing. The two suction cup design does not have good stability. The robot can wobble and tumble sideways during climbing. In the future revisions, we will solve this by making the robot lighter and implementing four suction cup design for improved stability. We believe that soft robots are an attractive option for Epidermal Robots to become more reliable and comfortable.

In the current implementation, the robot did not have a closed-loop control of the actuators. We used pressure as a proxy for bend angles, which can change based

on the manufacturing variations as well as external forces. In robotics, closed-loop control is important for reliable operation. In the future implementation, we hope to achieve closed lool control by adding bend sensors on the robot. Sensors such as IMUs could be potentially used.

3.4 Chapter summary

This work demonstrates the first Epidermal Robot with the ability to move over the surface of the skin and capture a large range of body parameters. We identified and met five critical design considerations for Epidermal Eobots: lightweight and small, have access to the skin, can adhere and locomote, and provide multimodal sensing. We found that suction-based locomotion worked better than adhesive-based methods. The main challenge of skin climbing was the adhesion of the end effector (suction cup) to a new position. In our solution, we used a feedback approach, with pressure sensors and servo motors to attach to complex surfaces. Also, we probe a future direction of Epidermal Robots by looking into soft robotics.

Chapter 4

Clothing Robots

This chapter describes the design of Rovables, small untethered robots that can move on clothing. As shown in Figure 4-1, a swarm of Rovables can potentially move around the body. The robots employ mostly off-the-shelf parts, custom-designed PCB, and 3D printed body. The central insight in Rovables is the magnetic fabric attachment mechanism, which allowed robots to cling to clothing without consuming any energy. The Rovables were the first tangible exploration of DWT and mainly geared towards HCI applications as novel wearable devices. To our surprise, Rovables received much interest in the HCI community and media, encouraging us to explore this topic further.

4.1 Design criteria

The following considerations guided the design and implementation of Rovables:

1. **Small form-factor**. The devices should be as small and as lightweight as possible. Since the device is close to the body, smaller size and weight is less obtrusive for the human host. Furthermore, clothing has limited space for travel, especially places such as sleeves. The size should be limited to 1.5cm x 1.5cm, the diameter of a small wristwatch.

2. **Navigation** The robot should be able to track its positions on unmodified clothing. Such a system should not require external aids, such as cameras. This

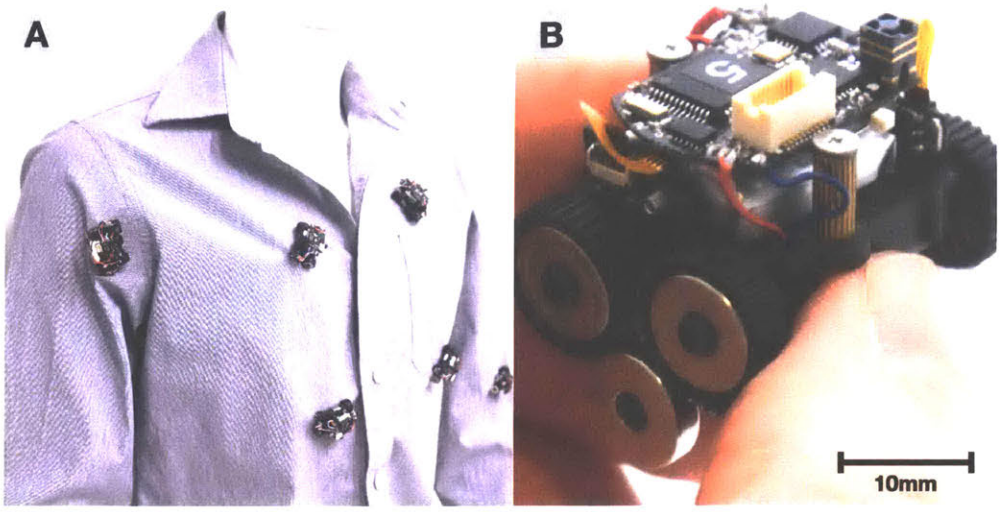

Figure 4-1: a) Multiple Rovables are climbing a shirt to show swarm abilities. b) close-up of one robot.

will allow autonomous movement on the host's clothing, without disturbing or limiting the wearer.

3. **Mobility** The device should move freely vertically on unmodified clothing. Furthermore, it should be able to move on loose and wrinkled clothing. The device should be able to carry a payload, allowing it to actuate clothing or to carry sensors.

4. **Communications** The device's basic functionality should include wireless communications with external devices. This will allow coordination between multiple robots and interaction with devices such as PCs and mobile phones. Communications between robots will enable more complex behavior and tasks.

5. **Power** As manually charging multiple robots can be time-consuming, the robot should have an ability to charge itself. Also, the robot's battery should last for at least 30 minutes of movement, and 8 hours without movement. This will provide enough time for the robot to perform any of the tasks that were proposed in the interaction space and return to the charger.

6. **Platform** The system should be designed as a platform so that anybody can

build and experiment with wearable robots. The system should be inexpensive to build, modular, and flexible enough to add more components and interfaces easily.

4.2 Implementation

In this section, we will describe the mechanical and electrical design of Rovables. All the design files are open-sourced at github.com/rovables

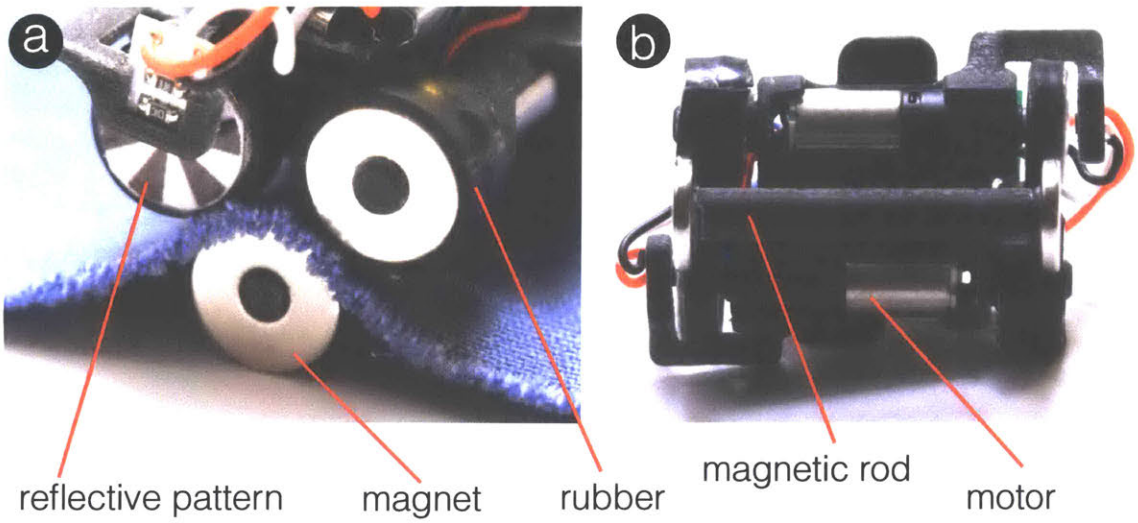

Figure 4-2: Illustration of the magnetic drive system. a) The fabric is held between the top two wheels and magnetic rod on the other side. All the wheels are circular neodymium magnets. The reflective pattern on the wheels is used for the infrared encoder. b) Underside view of the chassis, with the fabric, removed. Two motors are visible in this view.

4.2.1 Cloth climbing

The magnetic-drive chassis is shown in Figure 4-2. We used two 136:1 planetary gear motors (TGPP06-D-136, TT Motor) for movement. Such motors are only 6mm in diameter and have a high gear ratio. The gear motors were attached to neodymium magnet wheels (9mm diameter). Next, to the drive wheels, another set of neodymium magnet wheels was used to stabilize the movement. Those wheels were connected by

miniature ball bearings (4mm diameter), to reduce friction. Both sets of wheels were covered with 1mm-thick Neoprene rubber tires to reduce slippage. On the other side of the fabric, a rod with two neodymium wheels locked into the upper wheels. Because of magnetic attraction, the magnetic rod is moved with the upper wheels. This holds the robot in place, regardless of its orientation. The body of the robot was 3D printed in one piece using an Objet Eden260VS (Stratasys)

Other works used different mechanisms for climbing, such as by pinching the fabric [74]. Although our approach requires a magnet on the backside, we picked it for simplicity and ease of miniaturization.

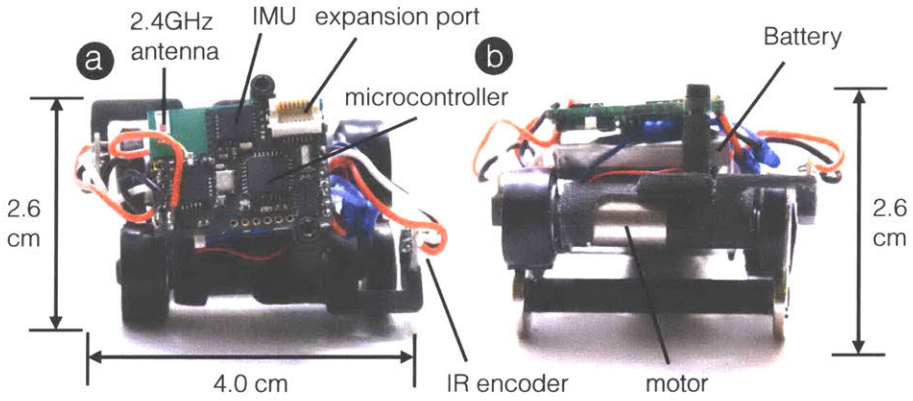

Figure 4-3: Picture of the electronics and sensors. a) Top view. The custom-designed circuit board is visible on the top. Infrared encoders are placed on the left and right wheels. The expansion port on the top is used to add more functionality. b) Side view. As visible in this view, the battery is sandwiched between the motors and the circuit board.

4.2.2 Hardware

The system diagram is shown in Figure 4-5. To reduce the size and weight, we made a custom 1mm-thick PCB (printed circuit board), as shown in Figure 4-3. We added a 14-pin connector so shields can be added for more functionality (e.g., additional sensors). We exploit this feature in the applications section. The main processor is an ATmega328p (Atmel). The system is powered by a 100 mAh lithium polymer battery.

For radio communications with the base station, we used a 2.4GHz radio; nRF24L01+ (Nordic Semiconductors). We decided to use a custom wireless protocol versus standard a (Bluetooth, WiFi) to allow control of multiple robots without significant latency while reducing power consumption. Furthermore, the 2.4GHz frequency allowed for a miniaturized antenna. The base-station contained the same nRF24L01+ radio with extended range antenna. It also contained an ATmega32u4 (Atmel) microcontroller to communication to PC over USB, and to control the radio. We used a server-client architecture for communications. On the PC side, C++ based openFrameworks was used to control Rovables, plus process and visualize data. In this configuration, the base station is the server, and the robots are the clients. The robots send the data to the server at 10Hz intervals. To prevent data collisions with multiple radios, the retry period was randomized for each robot.

For orientation sensing, we used an MPU6050 (InvenSense) inertial measurement unit (IMU). It contains a 3-axis gyroscope and 3-axis accelerometer, and can calculate 3-D orientation onboard. To estimate the traveled distance and the speed, we designed incremental infrared optical encoders with a GP2S60A (Sharp). The encoders work by measuring the changes in infrared reflectance of a disk with alternating white and black stripes. The disk was printed on glossy poster paper and glued on the wheels. To generate digital interrupts, the encoders were connected through a Schmidt trigger. We did not use magnetic encoders because of interference from magnetic wheels. For IR proximity sensing, four TSSP77P38 (Vishay) were used. The sensors were mounted on the removable display shield, which is further described in the applications section and Figure 9-13.

4.2.3 Wireless Charging

By putting an inductive coil (WR221230-36M8-G, TDK) on the undercarriage, Rovables can charge wirelessly. The coil is shown in Figure 4-4. The coil is only 0.5 mm thick, so it does not interfere with movements. The charging was done using the 13.56 MHz Qi wireless power standard. As a secondary purpose, the charger can serve as home, for the dead-reckoning system, described in the next section. When the device

goes home, it can re-calibrate to reset the accumulated error.

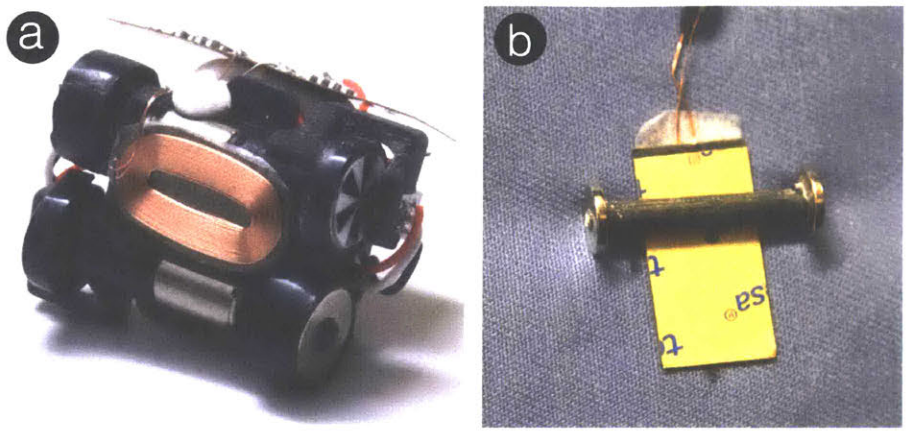

Figure 4-4: The wireless charging system. a) The receiver coil is mounted on the underside of the chassis. b) The yellow transmitter coil can be taped on the backside of the fabric. The Rovable is parked on the coil, as seen by its magnetic rod. The main body is on the other side of the fabric.

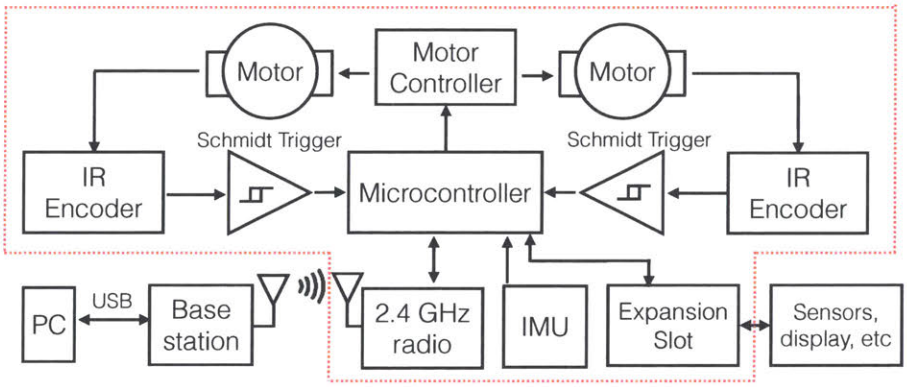

Figure 4-5: System diagram. The parts inside the red dashed lines are on the main board.

4.2.4 Wireless communications

Each Rovable transmits and requests a 32-byte packet every 100ms, providing a data rate of 0.32Kb/sec. The network supports up to 3 robots reliably. With more robots, data collisions become more frequent and cause errors and high latency. In the future, collisions can be avoided with synchronization and by allocating transmissions into slots.

4.3 Chapter summary

This chapter described the implementation and design of Rovables. The robots are capable of clinging on clothing and untethered operation.

Initially, we did not believe we would be able to create a functional robot. We prototyped many ideas, such as using magnetic fabrics, fabrics with slots and grooves, but nothing seemed to work. Once we developed the magnetic pinch mechanism, the design was straightforward, and we made 12 functional robots.

The surprisingly tricky part was the design of autonomous operation. As the robots operating in the open world with inexpensive sensors, it is hard to precisely and repeatably track their position. If I were to design the robots again, I would not underestimate the tracking and develop it from the start. In the next chapter, we will discuss the navigation in greater detail.

We took the robots around the world and demonstrated them at ARS Electronica (With Tangible Media exhibition), UIST conference demo, and as Kino: Living Jewelry in multiple venues. The public interest in the robots encouraged us to work more in this area.

Chapter 5

Navigation

This chapter provides a detailed overview of how robots can autonomously move around the human body. Also, this chapter provides an overview of existing localization and tracking methods. To be autonomous, robots need to know their location. We envision localization to be done onboard each robot, without the use of external devices. Such a goal has been one of the most difficult to achieve during the design of the robots. There are no small off-the-shelf trackers that can be clipped to the robot; therefore, we had to design our own system. In the literature review, we will take a look at some of the possible navigation methods.

There are three main parts to navigation: 1) Generating a map of the landscape, which is the map of the body or clothing in this case. 2) Finding the absolute position of the robot on the map, using navigation markers on the skin or the fabric. 3) Finding the relative position of the robot, using dead-reckoning.

Our ideal navigation localization system would have the following specifications. In our design, we try to make a system that follows those specifications as closely as possible.

- Accuracy of one millimeter or less and no drift. The accuracy largely depends on the application. To allow all applications, the smallest vasculature features on the body are on a millimeter scale [75]. The accuracy is discussed in more detail in the next section.

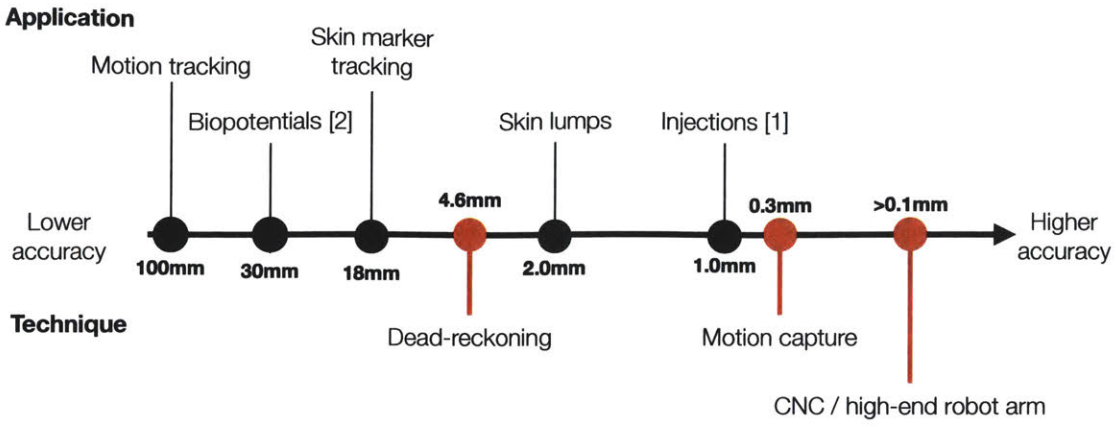

Figure 5-1: Accuracy required for different applications, and accuracy obtained from different localization techniques.

- Does not use external devices. The system is completely integrated into the robot. Alternatively, part of the system can be placed in the pocket or clipped on the clothing.
- Low power consumption. To respect the power constraints of the small robot, the system should not use significant energy.
- Not disruptive to the user. The system does not emit any visible light or sounds.
- Provides absolute tracking. The robot should know where it is on the body.

5.0.1 Accuracy requirements

It is challenging to determine what specific accuracy and resolution are required for the robot. Ideally, the accuracy is as small as possible, but improving accuracy potentially sacrifices other areas, such as power consumption and cost. The minimum accuracy is 18mm, and beyond that, it largely depends on the application. Figure 5-1 shows the range of accuracies required for different applications and our tracking methods. The accuracy largely depends on the application. Applications such as biopotentials and motion capture do not require high accuracy. The accuracy of around 30 mm is acceptable. Motion capture trackers only have to be positioned

between the joints, such as anywhere on the forearm is fine. EKG electrodes provide similar data if they are positioned within 30mm proximity to the original spot [76].

Reproducibility is another important factor in navigation systems and robots. It is especially important in precise industrial robots. We have not studied reproducibility in detail in our system, as our navigation is not yet robust enough to collect statistically significant data.

5.1 Literature review

A standard outdoor positioning system is GPS, but it is not practical for the small robots, because of large errors and signal blockages. For indoor localization, there are various methods such as optical, magnetic, acoustic, radio, but no widely accepted solutions [77, 78]. In this section, I will provide an overview of indoor systems, as they are relevant to DWT.

5.1.1 Optical tracking

Optical tracking systems usually employ cameras and infrared light, as it is not visible to human eye [79] and more resilient to shadows and ambient light. The object is equipped with LED-based active [80, 81] or reflective passive infrared tags (e.g Optitrack[1]) and multiple cameras or photodetectors to locate the tags. Sometimes a special infrared light pattern is projected (e.g., Microsoft Kinect or Vive Lighthouse). Time-of-flight for the pulsed light could also be used but is difficult to measure in practice as the system needs picosecond time resolution, which is beyond the performance of most electronics. In some cases, visible light is used for object tracking [82]. It can be done with standard cameras, but it is susceptible to environmental conditions, so it is rarely used in commercial systems. Any optical tracking is sensitive to occlusions and ambient light. Many commercial infrared optical trackers provide sub-millimeter accuracy at high speed (100 to 1000Hz range). We use infrared optical tracking system (Optitrack) to get the ground truth in this thesis.

[1]https://optitrack.com/

5.1.2 Magnetic tracking

Magnetic tracking uses the changes in magnetic fields in space to track objects. One way is to transmit a field with an active tracker [83]. This method has been employed in multiple off-the-shelf products (MotionStar, Polhemus). Some magnetic trackers do not need to be tethered and measure the orientation and strength of a permanent magnet [84, 85]. The disadvantages of magnetic tracking include small range at up to a few meters and high power consumption. Another way is to map the magnetic fields in the environment and then use known fields for localization [86].

I believe magnetic tracking has promise for DWT as it does not require line-of-sight since the human body is practically transparent to magnetic fields. The current systems require large trackers, which can not be placed on the robot.

5.1.3 Radio-frequency

Since RF signals are ubiquitous in communications, there has been much interest in using them for tracking. Some systems employed signal intensity to localize objects. [87] To alleviate the multi-path problem, some systems use time-of-flight of radio signals [88, 89] Another ubiquitous technique is using low-frequency near-field communications (NFC) tags for short-range localization [90]. Higher frequency RFID tags have been tested for localization at longer range (few meters to tens of meters) [91, 92]. An issue with using RF tracking is that accuracy is fundamentally dependent on the wavelength. For example, the wavelength at 2.4GHz is 12 cm, so the system is less than 12cm. There are higher frequency systems that use 5GHz and higher. For example, off-the-shelf module DecaWave DWM1000[2] uses 3.5GHz to 6.5GHz. A disadvantage of such high-frequency systems is sophisticated instrumentation, as well as limited range.

[2]https://www.decawave.com/product/dwm1000-module/

5.1.4 Accoustic

Acoustic systems use ultrasound for localization. Ultrasound provides some advantages, as it is significantly slower than light, therefore allowing easier time of flight measurements. There are two prominent examples of indoor acoustic localization: Active bat [93] and Cricket systems [94]. Acoustic systems use a significant amount of energy and use a relatively long wavelength, which negatively impacts resolution.

5.1.5 Dead-reckoning

Dead-reckoning is the navigation method where the current position is estimated from the previous position. It provides a relative position and is used where there are no external position markers. For example, a car cannot use GPS in a tunnel because the satellite signal is blocked, or a rocket in space does not have access to GPS. The main disadvantage of dead-recking is an accumulation of error; therefore, dead-reckoning is often aided by absolute beacons or markers.

Dead-reckoning can be done in various ways. In terms of robotics, it is often done using inertial navigation, where gyroscopes, magnetometers, and accelerometers are used to estimate position via integration and estimation technique like Kalman filters [95]. Another way to dead-reckon is odometry, which uses encoders, sensors that measure the rotation of the wheels or linear displacement of motors. In most practical approaches, inertial navigation and odometry are used together [96, 97]. Another way is using optical sensors to estimate optical flow. For example, an optical mouse calculates displacement from changes in images from low-resolution camera [98]. Mobile robots have used mouse sensors [99] or cameras [100] for optical flow estimates.

5.1.6 Application to DWT

As can be seen in Figure 5.1, It is evident that there is no single localization method that can satisfy our requirements. A multisensor approach is required. This section describes the three main subsystems used for navigation.

	GPS	Optical (IR trackers)	Magnetic (active)	High Frequency RF	Acoustic	Dead-reckoning
Accuracy	Meters	Millimeters	Milimeters	Centimeters	Centemiters	Millimeters
Power Consumption	Medium	Medium	High	Low	High	Low
Human body occlusion	No	Yes	No	Yes	Yes	No
Drift	None	None	None	None	None	Yes
Tracker size	Small	Large	Medium	Small	Medim	Small

Table 5.1: Summary comparison of studied localization methods. The colors indicate if the specification satisfies DWT requirements. Green color is acceptable and red color is not.

5.2 Navigation design

To attempt to satisfy our requirements, we designed a custom system. The system uses two methods: dead-reckoning for relative position and machine vision markers for providing absolute position.

5.2.1 Dead-reckoning with inertial sensors and odometry

In particular to DWT, the dead-reckoning method estimates the position of the robot with the two following equations:

$$x_n = x_{n-1} + qh\cos(\theta_n)$$

$$y_n = y_{n-1} + qh\sin(\theta_n)$$

where x and y indicate the position in a 2D plane and x_{n-1} and y_{n-1} are the previous position estimates. h is the linear traveled distance, θ_n is the rotation angle, and q is a scaling factor used for conversion of the sensor data onto centimeters. Figure 5-2

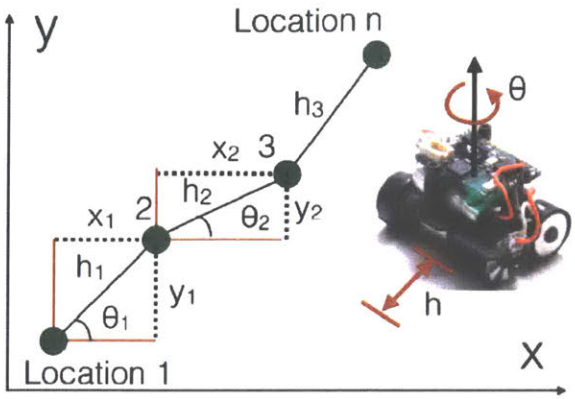

Figure 5-2: The graphical representation of the dead-reckoning algorithm. The location is determined by previous location, yaw angle, and the traveled distance.

shows how this algorithm works in practice for three consequative approximations.

The linear distance is obtained from the encoders on the motors. The rotation angle is obtained by integrating the gyroscope x-axis rotation rate and using the following equation:

$$\theta_n = \theta_{n-1} + d\theta_n - ct$$

,where c is the gyroscope drift constant, which we measured by logging stationary gyroscope rotation angle, t is the elapsed time, and $d\theta_n$ is the gyro rotation rate. Specifically, we used a 3-axis accelerometer and 3-axis gyroscope (MPU6050, Invensense). We did not include a magnetometer, because of possible interference nearby magnetic wheels. Since dead-reckoning is based on integration, any errors will accumulate over time.

Although, in reality, the robot moves in 3D, the 2D navigation is easier to employ in practice and use for estimation. We assume that the robot is always bound to some surface. With small step approximation, the surface can be unwrapped in 2D, whether the fabric or human body.

5.2.2 Getting a map

As with most navigation, the map of the space is required to make sense of the position estimates. For the clothing robots obtaining the map is straightforward. Almost

all clothing is made from 2D sheets of fabric that are sewn together. The original templates that were used to make the clothing can be used as a map. Getting a map of the body is harder, as every individual is different. The body map can be obtained from a 3D scanner. In particular, we used an affordable off-the-shelf scanner (Sense 3D, 3D Systems). With this scanner, we could digitalize a hand or head. For a whole body, a stationary scanner is needed, as the human subject cannot remain completely still during scanning. There are few such booths for commercial use (Shapify Booth, Artec 3D) Alternatively, a body map can be obtained using photogrammetry [101], where photos from different angles are stitched together into a 3D mesh.

The map is represented as a triangulated surface mesh, as it is obtained from a 3D scanner or a generated model. Such representation is the easiest to manipulate programmatically and provides the best approximation of the complex geometry of the human body. Each vertex has x,y,z coordinates as well as information on connections with neighboring triangles.

After the map is obtained, localization of SkinBot is as follows: 1) the robot's coordinates are scaled to the texture map, 2) all the texture coordinates were searched to find X-Y coordinates in the vicinity of robot's coordinates. 3) the Euclidean distance[3] between the found X-Y neighboring coordinates and robot coordinates were computed, and 4) the coordinate with the smallest Euclidean distance to the robot was assumed to be the robot's location. Therefore the robot moves by jumping from different vertices, and the density of the vertices limits the resolution.

5.2.3 Passive navigation markers

Dead-reckoning provides only relative position and will accumulate drift. To alleviate these issues, some absolute position sensing is required. We employ a method of placing markers on the fabric or the body in the predetermined locations. The markers reset the robot's dead-reckoning errors as well as provide an anchor to the digital map. Each marker contains heading and distance information. To simplify the manual placement, markers do not have a unique identifier.

[3] $d(x,y) = \sqrt{(x_1 - x_2)^2 + (y_1 - y_2)^2}$

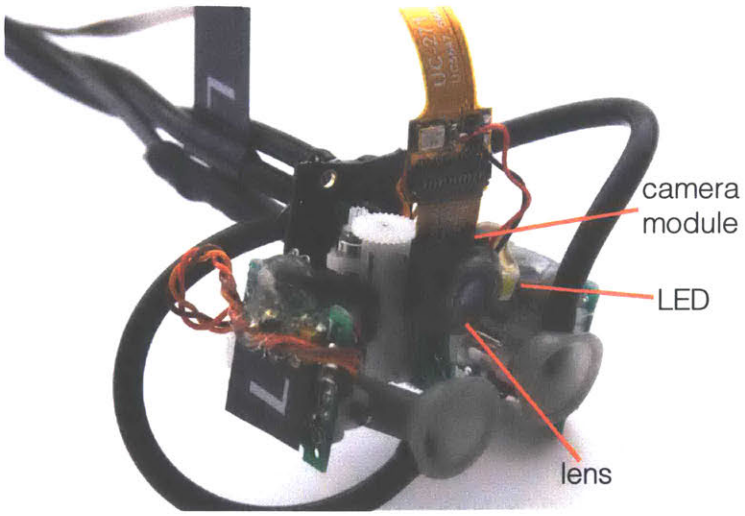

Figure 5-3: Picture of the robot equiped with the camera

In particular, we printed markers on temporary tattoo paper (A4 Laser Printer, RoryTory) which does not interfere with the robot's suction of the skin and are easily removed. The markers are 2cm in diameter. We designed a visible guide for initial manual robot placement and fiducials to recalibrate the robot's dead-reckoning position, as shown in Fig. 5-4 . The fiducials are recognized with the robot's camera, as shown in Figure 5-3 and custom machine vision methods (OpenCV 3.4.1) that run on Raspberry PI 3.

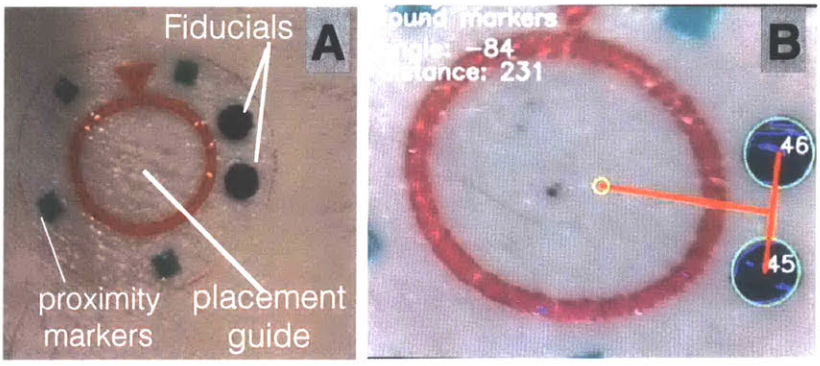

Figure 5-4: Temporary tattoo markers. a) Closeup of the marker. The fiduals and proximity markers are for the camera. The red placement guide is for initial robot placement. b) The marker as seen by the machine vision.

The markers were used in the following steps: 1) The camera image was grayscaled and thresholded to look for black color only 2) The contours on the thresholded image

were computed. 3) If contour was a circle of a predefined size, it meant it was the fiducial. 4) The centers of the two fiducials were calculated 5) A line was drawn between the two fiducial centers. To that line, a perpendicular line was drawn to the center of the view. 6) The length of the perpendicular line was used as the robot distance offset. 7) The angle of the perpendicular line was used as the angle offset.

Due to the drift of the dead-reckoning, it might be hard to find the position of the fiducials. The green proximity markers helped to find the fiducial markers, as they indicated that the fiducials markers are nearby, even if they are not in view.

To anchor to the 3D map, the markers have to be placed in the predefined position and rotation. Currently, such markers would have to be placed manually, as shown in the Figure 5-5. To visually guide consistent placement, we printed black-colored guides on the cover of the temporary tattoo marker. We developed a simple smartphone (Google Pixel 2 with Android 8.1.0) camera application, which shows a contour of the hand and where to place the marker. The user aligns their hand with the contour on the camera for the marker placement. The contour guide is automatically generated from the 3D map. With the clothing, it is simpler to position the markers. The markers can be placed permanently during the manufacturing of the clothing. With digital manufacturing such as flat-bed knitting machines, the markers can be stitched into clothing directly.

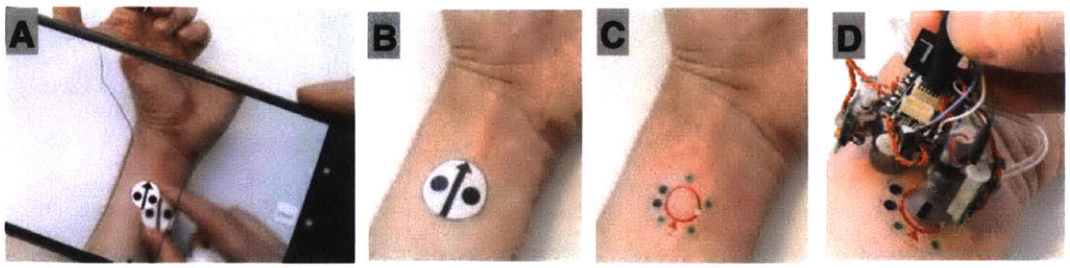

Figure 5-5: Guided attachment of the markers. a) The phone is used to guide the placement. The cover of the marker has a sticker for visual rotation. b) The marker is attached before the sticker is removed c) The cover sticker is removed d) The robot is placed on the marker as the starting point.

5.2.4 Active navigation markers

Initially, we have considered and designed active navigation markers as well. The main advantage of active markers is that it can signal its position to the robot remotely, so the robot does not need to be close to the marker to use it. The main disadvantage is higher power consumption, as well as an additional piece of hardware. Furthermore, it would be hard to attach to the skin unless it is in the form of a bracelet or another wearable.

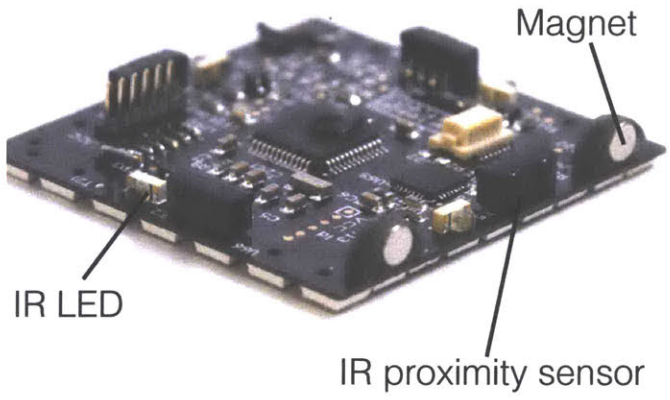

Figure 5-6: Four infrared proximity sensors for active navigation markers.

We used infrared (IR) active markers, as shown in Figure 5-6. The Rovables robot was equipped with 4 IR proximity sensors (TSSP77P38, Vishay) on each side. This sensor measured the intensity of 38kHz modulated infrared light at 940nm. A 940nm directional infrared LED light source was pinned to the clothing to work as the navigation marker. By measuring the intensity of the light on each side, the robot can determine the direction of the light, as well as the distance from the intensity.

In practice, intensity-based infrared proximity is unreliable[4]. A more sophisticated time-of-flight approach would be more appropriate. Most fabrics are very reflective in the infrared spectrum. It is challenging to determine the location of the beacon, as there are many reflective paths the IR light takes.

[4]As seen in the kitchen taps and toilet flush

5.2.5 Localization during body motion

The motion of the body will throw off the gyroscope measurements; therefore, the current dead-reckoning can only be performed on the stationary body. If any external motion is detected, the robot stops and turns off the gyroscope integration. When no motion is detected, the robot resumes its course.

The external motion is classified with the IMU. During localization, the accelerometer is sampled for sudden changed by thresholding the derivative of acceleration.

5.2.6 Path planning

The computer (server) does not control the movement of the robots directly. It transmits the commands for the robots to accomplish. This is because the radio communication can be faulty and unpredictable as well as suffer from latency. The server also keeps tracks of the overall map and where robots are in relation to each other.

In the current implementation, path-planning is simple. The robot takes the shortest path to the destination. There are three basic commands: (1) move specified distance forward, (2) move specified distance backward, and (3) turn to a specific angle. Using these three movements, a complex path can be followed. Each of the three movements was executed with different PID (proportional-integral-derivative) controllers. Without the PID controller, the robot would not follow a straight path, as the fabric or body surface is not even, and motors are not symmetrical. The IMU yaw angle was used to correct the course. Also, the yaw angle was used to control turning.

5.2.7 Localization with external optical system

With localization, there are always tradeoffs. In some cases, it is acceptable to have external trackers. Some reasons might include: the subject is confined to one room or cannot move, submillimeter accuracy or high update rate(>100Hz) is required or for development and system validation.

We used an optical motion capture system (Optitrack) and equipped the robots with four reflective markers, as seen in Figure 5-8.

Specs	On-board	Optical Motion Capture
Mechanism	Inertial, odometer and machine vision	Infrared reflective markers
Accuracy	4.6mm	0.3mm
Update rate	10Hz	100Hz
Drift	None	None
Occlusion	no	Yes
Coverage area	Unlimited	Bound by field of view
Wearable	Yes	No

Table 5.2: The table provides comaprison between the on-board navigation systems and using external optical motion capture system. In some cases an optical motion capture system can be used instead of dead-reckoning.

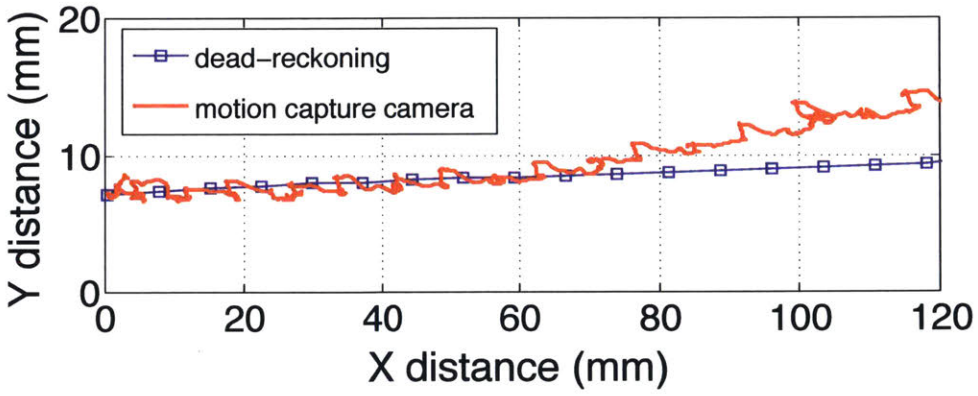

Figure 5-7: Example of SkinBot localization with the dead-reckoning approach (blue) and a motion capture system (red).

5.3 Evaluation

In this section, we describe how the localization systems were evaluated.

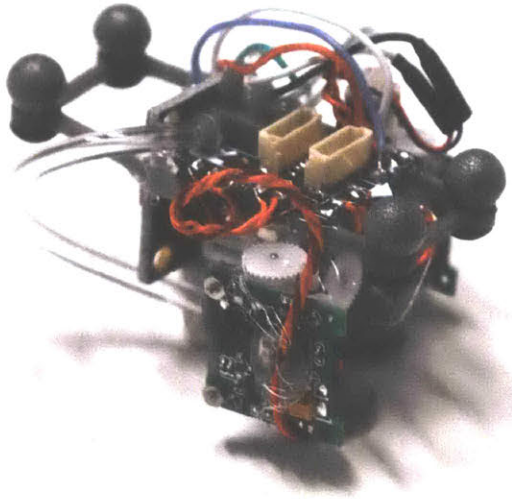

Figure 5-8: SkinBot with four reflective markers for optical tracking

5.3.1 Cloth robot

As shown in Figure 5-9, for the clothing robot, we tested localization accuracy using onboard sensors and a reference camera. The path was recorded on a calibration fabric, which is shown in Figure 5-10. The robot's movement from the camera was manually analyzed and was assumed to be the ground truth. We found that our localization algorithm has a mean error of 19.5mm and a standard deviation of 10.3mm. As Figure 5-9 shows, there is an error is both linear distance (encoders) and yaw angle (IMU).

The possible sources of error include limited resolution of the encoder (2.4mm) and wheel slippage. Furthermore, the IMU had a yaw angle error of about 6.4 degrees, as measured with reference angles as the ground truth. The IMU did not experience significant drift, as on-chip algorithms corrected for it.

After testing the robot on a 2D sheet, we developed a 3D testbed, as shown in 5-11. This setup better reflected real-world usage.

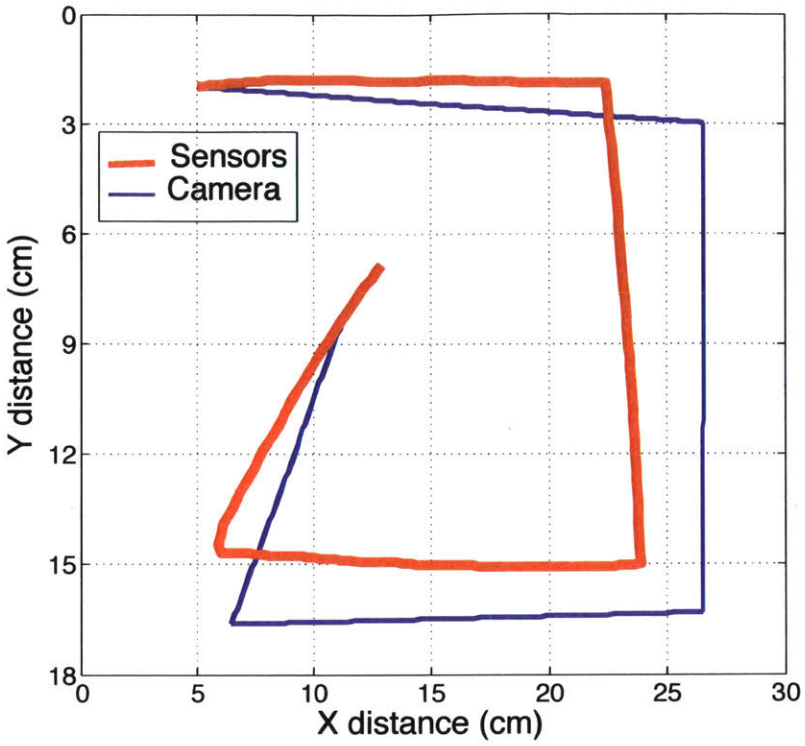

Figure 5-9: Localization accuracy on a 2D fabric. Comparison of a camera (ground truth) and on-board sensors for localization of one path.

5.3.2 Skin robot

To evaluate on-body robot localization, we collected data of the SkinBot moving horizontally on the forearm for 20 cm and repeated the process three times. SkinBot was initially placed on a navigation marker. Gold standard localization was obtained by adding four infrared reflective markers on the robot and using a camera-based motion tracking system (Flex 13, OptiTrack). After the three repetitions, the mean error of the dead-reckoning algorithm was 4.60mm (SD:±4.1mm). Figure 5-7 shows an example of localization with the onboard sensors (blue) and the motion tracking system (red). One of the main sources of discrepancy between the two measures is due to the angle error from the gyroscope. In particular, the robot experienced some wobbling while moving (visible in motion tracking data), which slightly affected its heading. As expected, there was also a cumulative error as the robot moved at a rate of 0.63mm per step. To address this, SkinBot needs to recalibrate its position using

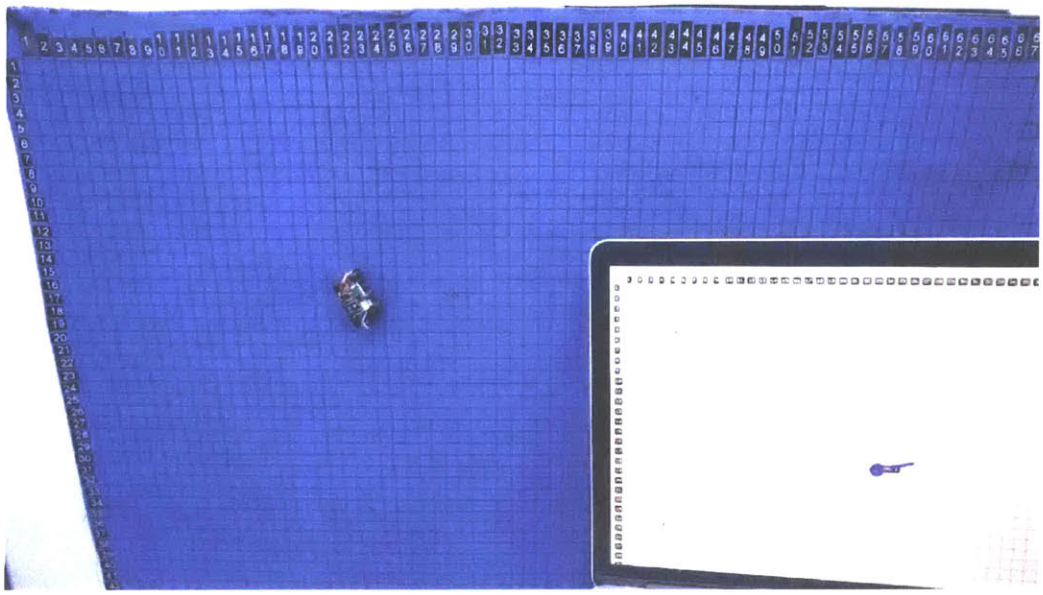

Figure 5-10: Fabric test bed used to develop the navigation and control algorithms

the skin markers occasionally. To do so, the robot has to find at least a small piece of the marker in the camera's field of view. As the field of view is limited to about 18x18mm, the onboard localization accuracy should be under 18mm. Considering the position drift, the robot will need recalibration after 21 cm of locomotion, or even less depending on the application.

5.4 Navigation without markers

Usage of navigation markers unavoidably makes the system harder to use, as it requires manual placement of the markers. It would be favorable not to use any markers. The human body contains many unique features that could potentially serve as markers. Employing our previously developed vision system, we test melanocytic nevus (moles) as natural navigation markers.

In some cases, melanocytic nevus manifest itself with excess skin pigment thus has a different color from surrounding skin. An example of a mole is shown in Figure 5-13A. The moles are typically oval or circular in shape and between 1 and 3 mm in diameter. Moles tend to appear in the first 30 years of life, and people usually have between 10 and 50 [102]. Moles are captured as a texture with a high-resolution 3D

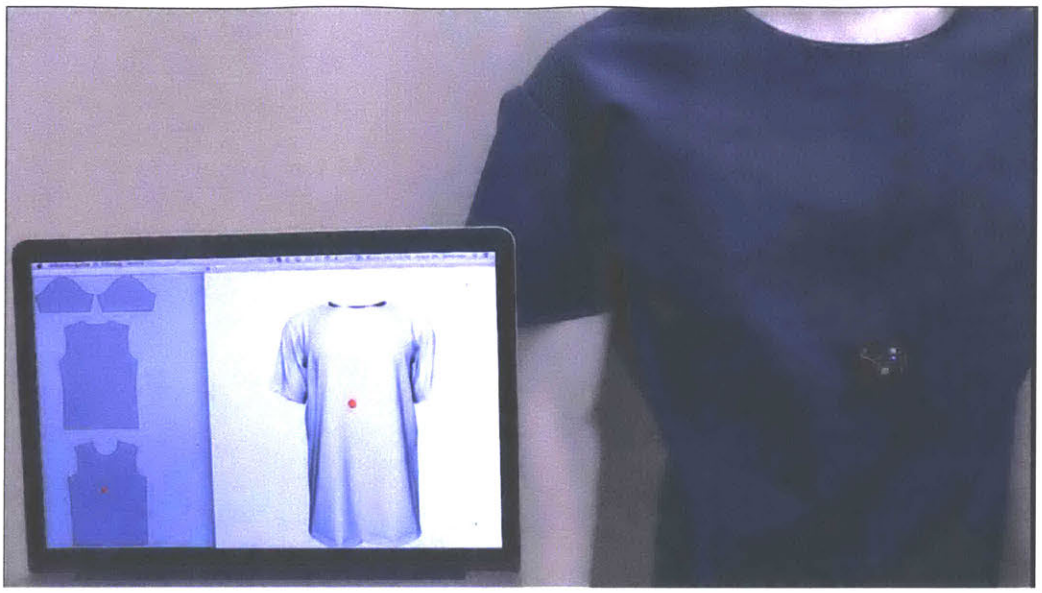

Figure 5-11: Localization of the robot on a fabric in 3D space.

scan. An example of a high-resolution skin texture map is shown in Figure 5-12, as obtained by photogrammetry. We use moles to create a proof-of-concept markerless navigation system. We also considered two other methods. In the next paragraphs, we provide more details about those methods and reasons why we did not use them.

Blood vessels have unique branching strucutres [103]. There are peripheral blood vessels that run close to the skin surface, so they can be seen optically. We did not use the blood vessels because we found it difficult to distinguish them with our camera vision system. Typically, an infrared camera or ultrasound is required for better accuracy. [104]

Also, biosignals such as biopotentials can provide a rough location. For example, the EEG signal on the chest and near the heart is different than on the arm. We did not employ the biopotentials, because their spatial resolution is about 30cm [76]. We would not be able to get sub-centimeter accuracy required for many applications.

5.4.1 Moles as passive markers

We applied previously developed machine vision algorithm (See Section 5.2.3 for detail), which was developed for passive navigation markers, to detect moles. As

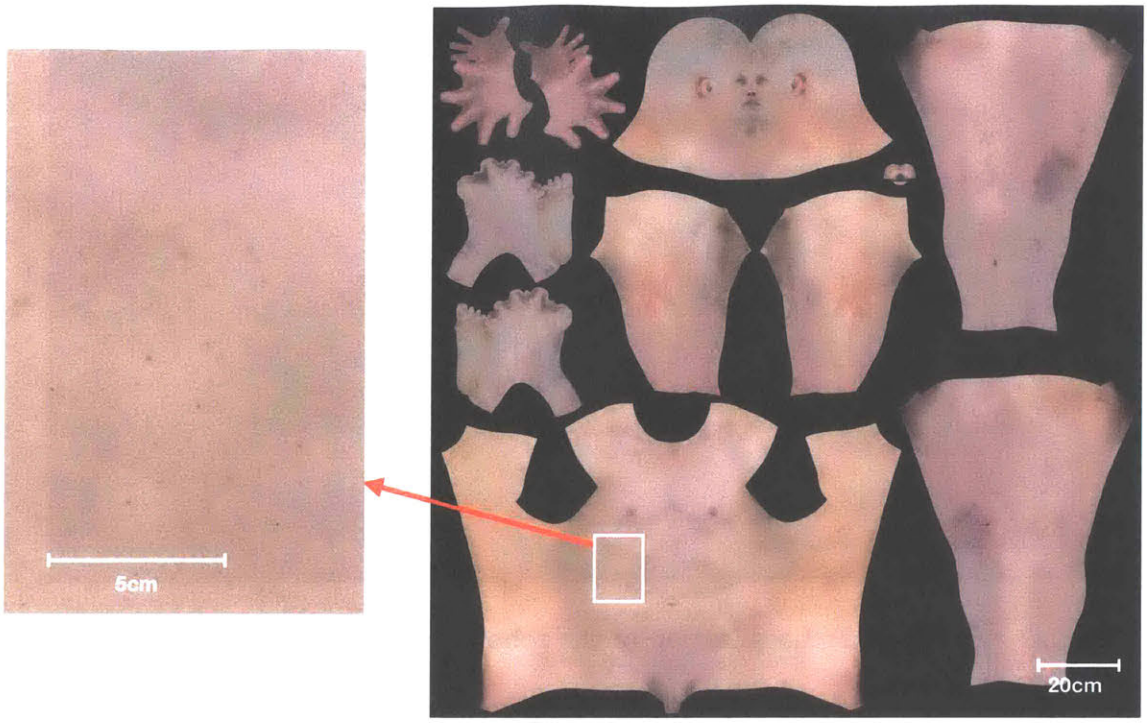

Figure 5-12: Using two birthmarks on the forearm for navigation. a) Picture of the two birthmarks that were used. b) The birthmarks as seen by the machine vision. c) The threshold applied by the machine vision algorithm to find the birthmarks.

moles usually have a slightly different color than surrounding skin, we modified the algorithm to a threshold based on a range of color, instead of using grayscale. An example of this algorithm is shown in Figure 5-13, as it was used on two moles on an upper arm.

Not any mole could serve as an optical fiducial, as they need to encode both angle and positional information. In our case, we look if there are two moles in the camera field of view, less than 18mm apart. To avoid confusing the vision algorithm, there should be no other moles in the camera field of view. Also, the moles should have stark contrast difference with the surrounding tissue. In the future, an automated algorithm could scan the texture map and find the moles that fit the criteria. The size and color of those moles would be passed to the machine vision for the on-board camera. In our current implementation, we manually find suitable moles.

To understand how common are moles that fit our criteria, we manually examined

two high-resolution body scans (Ultimate Textured Male And Female Base Mesh Bundle, 3D Scan Store). We found the male model contained eight potential markers, and female model contained five markers. The torso contained the most number of markers.

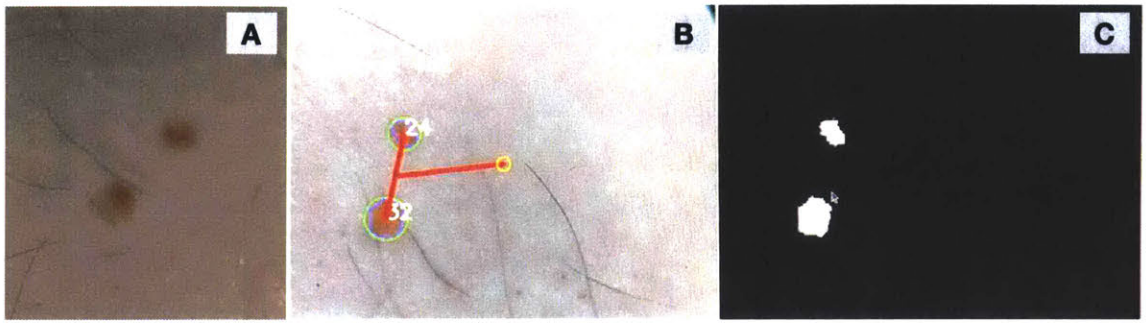

Figure 5-13: Using two birthmarks on the forearm for navigation. a) Picture of the two birthmarks that were used. b) The birthmarks as seen by the machine vision c) The threshold applied by the machine vision algorithm to find the birthmarks.

5.5 Discussion

5.5.1 Fully autonomous operation

In here, I will describe how the fully autonomous operation should function. Since mobiles phones are ubiquitous and powerful, they can act as a base station for the robots. The phone provides high-level control of the robots. The phone would be loaded with the map, either from the 3D scan or garment manufacturer. The robots would communicate to the phone through Bluetooth.

Before activating the robots, the user would put on the markers. The phone augmented camera guide would be used to help to put the markers in the right location. Some clothing might already have the markers woven in, so no manual placement would be needed. In some cases, if the 3D scan contains suitable natural markers (e.g., moles), the user will not need to place any markers.

Once the markers are configured or attached, the user would place the robots on the markers. At this point, the robots would go about their business using dead-

reckoning, occasionally going to the markers to recalibrate. If the robots detect sudden user movements, they would stop and wait until there is no movement.

5.5.2 Localization accuracy

Accurate body localization of robots proved to be more challenging than expected. We showed that body localization could be done with the onboard inertial tracking and vision markers, but it only allowed for around 21 cm of locomotion before the position drift became significant. While one marker should be sufficient to locomote on smaller areas such as the forearm, upper arm, or the upper leg, multiple markers would be required to locomote larger surfaces such as the torso. Also, inertial navigation only works on a stationary body which requires the robot to stop locomoting whenever large motion is detected.

While we hope the onboard navigation will improve in the future, whole body location is still better addressed with an external setup such as the infrared tracking system that was used in our experiments. Alternatively, Epidermal Robots could be teleoperated with an external camera view.

There are a number of things that can improve the localization accuracy. Many practical localization systems use Kalman or particle filters, where multiple types of input are fused to increase accuracy. For example, to estimate the rotation of the robot encoder readings, motor commands, and IMU data can be fused to provide a better estimate.

5.6 Chapter summary

Accurate localization is essential for autonomous operation of the DWT robots. This chapter provided an overview of potential navigation methods. Unfortunately, none of the existing methods are directly applicable to the on-body scenario. Therefore, we developed a novel navigation method that utilizes both dead-reckoning with IMU and position sensors and optical markers for absolute positioning. Initial testing provided promising results (<10mm error), but deployment in the real-world will

require greater robustness. We also evaluated markerless navigation, that uses skin moles as absolute optical markers. We found that markerless navigation is promising and possible. We are hopeful that MEMS inertial sensors will significantly improve in the near future.

Chapter 6

Climbing the human body

This chapter considers how DWT robots move around the human body. Attaching and moving on the human body or clothing is a challenging problem. The robots have to attach and climb on highly malleable and non-uniform surfaces.

We will discuss previous research in the area of vertical climbing robots. Afterward, we will provide experimental data and analysis of locomotion on skin and fabric with DWT robots. We focus on the exploration of skin climbing since it is a new area of research. We believe such analysis and experimentation is useful for future researchers.

6.1 Previous research

This section looks at the previous research in climbing robots. A few robots are capable of climbing on the fabrics [105, 74]. Besides this work, there are no examples that the author knows of robots that climb directly on the skin.

6.1.1 Bio-inspired adhesion

Many organisms use adhesion, so it important to look at bioinspired approaches. For light insects, it is fairly easy to climb any surface, due to a large number of tiny hairs utilizing Van Der Waals Forces or capillary forces. However, due to unfavor-

able scaling, larger insects, animals, and robots have to utilize a different mechanism. Although geckos appear to use Van Der Waals forces [106], they possess a highly sophisticated foot structure to increase surface area. Leeches [107] and octopuses [108] utilize suckers to adhere and climb vertical surfaces. Such suckers create negative pressure from muscle contractions. Some bioinspired robots have attempted to emulate such suckers, using shape memory alloy [109] or electroactive polymers to create artificial muscles [109].

6.1.2 Cloth-climbing robots

Although robotic fabric handling and automated sewing machines date to at least the 1980s [110], clothing and fabric climbing robots were demonstrated in research fairly recently (Figure 6-1). The first fabric climbing robot CLASH [105] was made in 2011. This robot used legs with needles to penetrate and adhere to the fabric. In 2012 a cloth climbing robot Clothbot was shown [74, 111]. It pinched the fabric between two wheels. In 2013 this project was improved and was renamed Rubbot [112]. In this thesis, Rovables [1] used a different mechanism, a magnetic pinch roller on the back for fabric adhesion.

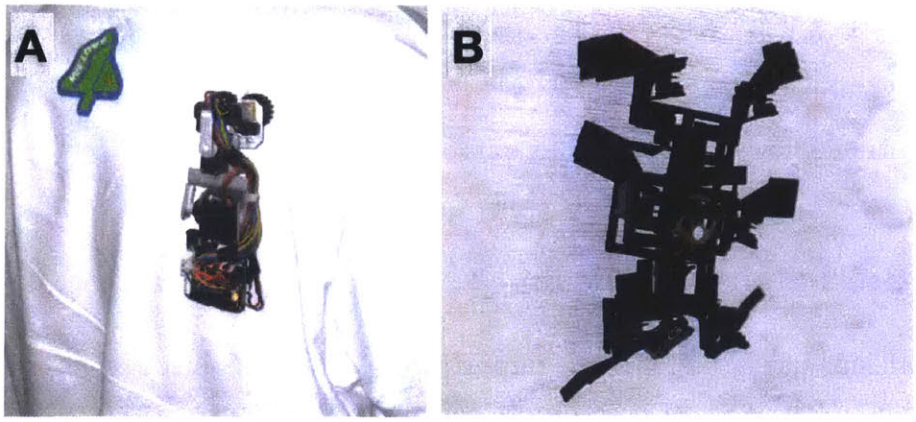

Figure 6-1: A) Clothboth climbing on a shirt using gripper wheels. b) CLASH robot.

6.1.3 Wall climbing robots

There are more examples of wall climbing robots, in contrast to cloth climbing. There are more practical applications for such robots like inspection and cleaning of inaccessible surfaces in nuclear power plants. Waalbot [113] used pressure adhesive wheels to climb vertical surfaces. Some robots used artificial gecko skin adhesive to climb surfaces [114]. This method uses micromachined hair-like structures to increase surface area and allow adhesion through Van der Waals forces. Other robots used vacuum suction to adhere to vertical surfaces [115]. Another robot used tracks with permanent magnets to climb metallic surfaces [19] and grippers [18] to climb trees and poles.

6.1.4 Soft climbing robots

Soft robotics is a relatively new area of robotics. Instead of using rigid bodies, soft robotics looks at highly compliant materials (e.g., silicone) [116]. Soft robots are especially useful for interfacing with the human body, as they provide a close match to the compliance of the human body. Soft robots have been used to create exoskeletons [117, 118]. Researchers have looked at wearable robots that can grow on the human body for providing haptic feedback [119]. This robot wraps itself over an arm by inflating in a coil.

6.2 Robot movement on the skin

This section evaluates the basic properties of SkinBot, such as locomotion, adhesion, and power requirements. Also, we conduct several experiments to understand some of the unique challenges of skin locomotion such as skin stretchability, its curvature, and hair presence. We also test the dead-reckoning localization method. Finally, we conduct a user study to assess the user perception of SkinBot.

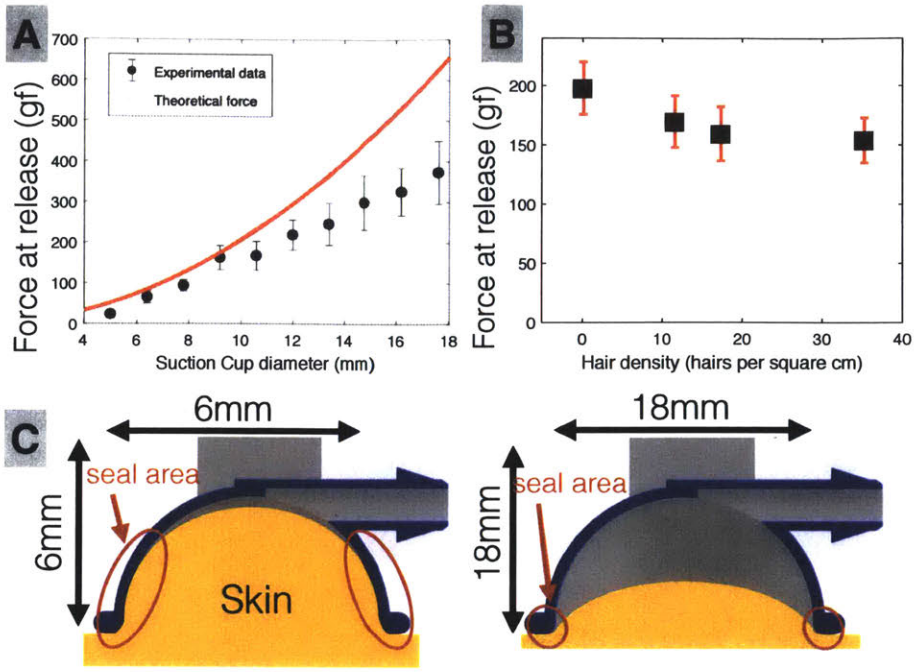

Figure 6-2: Skin attachment experiments. A) Maximum adhesion forces with different suction cup diameters as indicated by force at release. B) Presence of hair on the skin reduces the maximum adhesion force. C) Diagram illustrating the vertical displacement of the skin under suction. The suction cup of 6mm and 18mm diameters are shown in the illustration. The 6mm diameter cup creates a better cup-skin seal, as it has a larger seal area.

6.2.1 Adhesion

Suction provides a strong and reliable adhesion approach to the skin. In the case of SkinBot, the adhesion strength is between 150gf and 200gf when attached to a single cup and between and 300gf and 400gf when attached to the two suction cups simultaneously. This range provides enough adhesion to sustain the current weight of the robot, which is 20g. Thus, when the robot is hanging upside down, there is at least a 7.5x safety factor that can be used to account for different skin types and irregularities.

To help study adhesion, we define adhesion force as the peak force at which a suction cup pulled in the normal direction to the skin becomes detached from the skin. In theory, the maximum adhesion force is directly proportional to the size of

the suction cup, with the governing equation:

$$F = PA, \ and \ A = \pi(d/2)^2$$

where F is the maximum adhesion force, P is the vacuum pressure, A is the skin contact area of the suction cup, and d is the diameter of the circular contact area. Therefore, larger suction cups have higher adhesion forces. While the theory generally agrees with *in vivo* experimental data (see Figire 6-2A), the suction cups over 10mm diameter consistently had lower adhesion forces than the theoretical ones. To help further understand this effect, we 3D-printed transparent suction cups with various diameters and video-recorded the skin under the vacuum. After careful examination, we believe this discrepancy occurred due to two main factors. First, suction cups over a 10mm have small skin-cup seal area, as shown in Figure 6-2C. In other words, while the skin is displaced by the same amount for the small and large suction cups, the displacement is spread over a larger area for the larger cups. Second, larger suction cups require a more substantial seal area around its diameter. When the suction cup is being slowly pulled off, there are more chances for gaps in the seal before reaching the maximum theoretical adhesion force.

In our experiments, we noticed that hair presence could negatively impair adhesion performance. To study this effect, we measured adhesion forces on skin surfaces with different amounts of hair (see Figure 6-2B). For each of the experimental skin locations, hair density was manually counted by using a microscope. Moderate presence of hair on the skin reduces the adhesion force by around 30% to 150 gf but still allowed attachment. Beyond that, excessive hair (above 35 hairs per cm^2) prevented suction cups from making the necessary skin-cup seal.

For all adhesion measurements, we used the 20N digital force gauge (DFS20, Nextech). All measurements were done on the forearm and repeated five times in different locations. The mean of the five trials was reported as a result. The attachment experiments were done on a 30-year old male. The suction cups were pulled manually, and the peak force was recorded, as the maximum pull-off force. For the measurements,

the suction cups were 3D-printed with a custom force gauge attachment so that they can be pulled in a normal direction to the adhesion surface.

6.2.2 Locomotion

Figure 6-3 shows a snapshot of the movement of SkinBot on an inclined arm. Figure 3-4B shows the details of air pressure changes during the locomotion. The achieved vertical climbing speed of the robot is 31cm/min with solenoid valves and 6.3cm/min without solenoid valves. However, adding the solenoid valves increases the power consumption by 50 mW, and the weight of the robot by 10g. Without the valves, the vacuum release time is around 16sec, greatly limiting the climbing speed. In particular, the robot has to wait to reach atmospheric pressure by air leakage as the servo motors are not strong enough to lift an attached cup. By opening the vacuum line to atmospheric air with a 3-way solenoid valve, the time can be significantly reduced to 0.5sec. A potential future alternative would involve using mechanical cams driven by existing actuators to break the vacuum.

The robot can effectively walk backward by running the horizontal servos in reverse mode. The robot can rotate 30^o in 20 milliseconds to change its direction. Due to the possible tangling of vacuum tubes, the rotation radius has been limited to be between -30^o and 30^o per locomotion step. By combining multiple steps, the robot can potentially rotate to any angle.

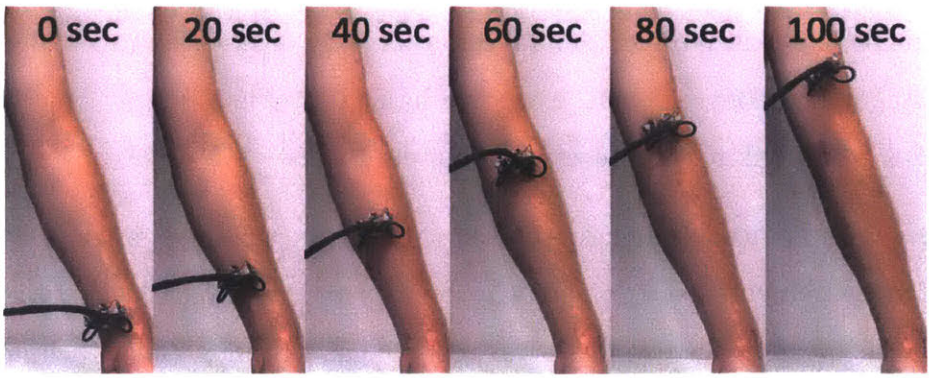

Figure 6-3: Robot locomotion on the arm. SkinBot climbing on the arm during 100 seconds.

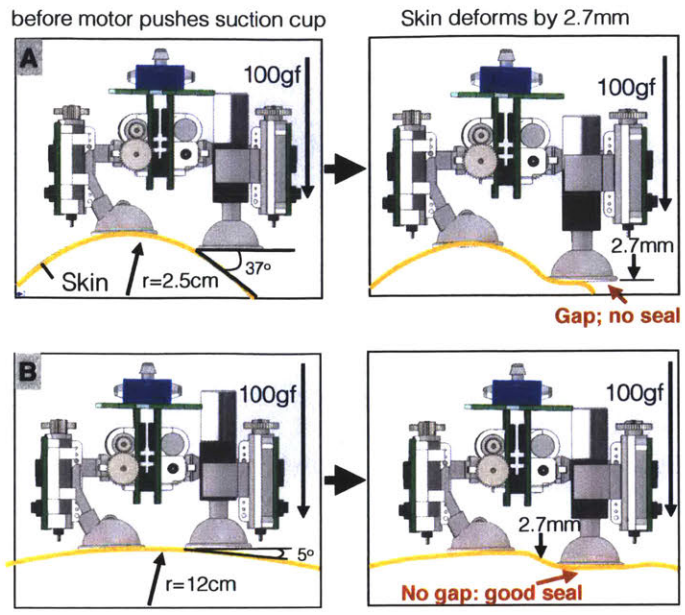

Figure 6-4: Attachment to a curved skin. A) Robot attachment to a cylindrical surface with a 2.5cm radius. Left: robot before it engages the vertical servo motor to push the suction cup down. Right: suction cup displaces the skin by about 2.7mm, which is not enough to make a reliable cup-skin seal. B) Robot attachment to a cylindrical surface with a 12.5cm radius. In this case, a reliable cup-skin seal is created.

6.2.3 Skin Curvature

The human body has many degrees of curvatures, which may negatively affect the locomotion of SkinBot. To facilitate the analysis of curvature, previous studies have approximated the body with spheres and ellipsoidal cylinders [120]. In this work, we simplify each of the body parts with cylinders. In particular, we use cylinders with radii from 2.5cm (wrist-size) to 12cm (torso-size) to help cover some of the main adult-sized areas in which we envision SkinBot exploring. Ideally, suction cups should always be normal to the skin to maximize attachment. However, this may be challenging for cylinders with a small radius (i.e., a high degree of curvature) as the suction cups cannot reliably create the skin-cup seal. In our design, the suction cup is pushed towards the skin, causing indentation and allowing attachment with some degree of skin curvature. In particular, the skin can compress by 2.7 mm (SD: ± 0.71) when pushed by the linear servo motor before the motor stalls. Figure 6-4 shows a visualization of this process. The skin compression distance can be affected by many

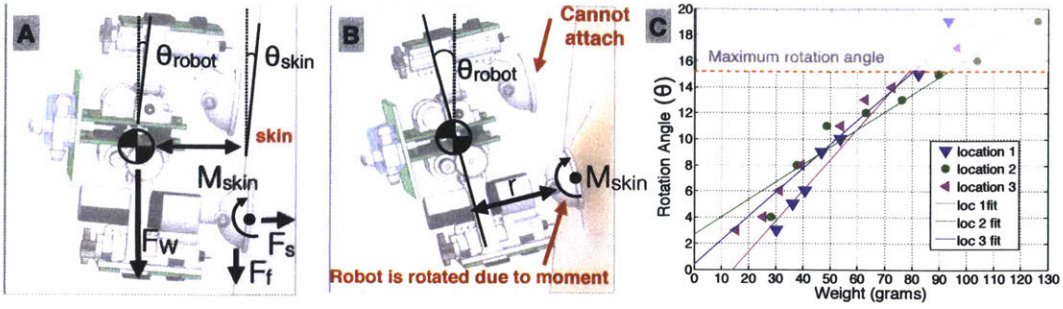

Figure 6-5: Rotation of the robot due to sagging of the skin. A) Free force diagram of the robot in a vertical position. One foot is detached, as the robot is taking a step. B) An example scenario where the robot is rotated into a position that does not allow attachment. This is caused by sagging of the skin caused by torque (M_{skin}) on the skin, due to the weight of the robot. C) The experimental data from three locations on the arm. The data shows the relationship between the robot rotation angle ($\theta_{robot} - \theta_{skin}$) and its weight. Linear fitting lines are shown.

factors, such as skin thickness and its elasticity. Theoretically, a 2.7mm compression distance allows an attachment to a minimum of 4.4 cm radius cylinders or a 15^o angle between the skin and the suction cup. To confirm this, we tested the robot on silicone (EcoFlex 00-30, thickness = 3.0 mm) placed over various 3D-printed cylinders and obtained similar results. In the future, the attachment to curved surfaces could be improved by adding the ability to pivot the suction cups to at least 37^o so it can attach to 2.5 cm cylindrical surfaces. Alternatively, the robot locomotion mechanism could be shrunk by a factor of 2.2, from 9.1mm to 4.1mm distance between the centers of the suction cups to help circumvent smaller skin features.

6.2.4 Skin Sagging

Skin is stretchable and flexible surface; therefore, it can affect the robot locomotion and orientation. These properties can create situations in which the skin sags, thus rotating the robot into unfavorable orientations. Figure 6-5B, for instance, shows an example in which the robot is unable to attach the suction cup to the skin. Sagging is caused by the moment on the skin created by the weight of the robot. As determined in the previous section, the robot cannot reattach if the suction cup angle is larger than 15^o in relation to the skin. To fully understand how the weight of the robot creates

skin sagging, we measured how different suction cups rotate at different moments. In particular, we determined that to keep the angle under 15°, the weight of the robot should be under 80g (see Fig. 6-5C).

As shown in Figure 6-5A, the moment on the skin (M_{skin}) caused by the robot is defined as:

$$M_{skin} = rF_w, \ and \ F_w = mg, \ so \ M_{skin} = rmg$$

where r is the distance to the center of mass of the robot, F_w is the force due to the weight of the robot, m is the mass of the robot, and g is gravity constant. The rotational stiffness is defined as:

$$k = M_{skin}/\theta, \ where \ \theta = (\theta_{robot} - \theta_{skin})$$

where θ is the rotational angle of the robot in relation to the skin. It follows that the rotational angle depends on the following:

$$\theta = M_{skin}/k$$

$$\theta = rmg/k$$

As in the above equation, the experimental data shows that θ changes linearly ($r^2 = 0.96$) with the weight of the robot. The slope is dependent on the rotational constant k. In turn, k depends on the skin's dimensions and structure, as well as its Young's modulus. Constant k varies for the three tested locations from 0.13 to 0.24.

We used a digital force gauge and DSLR camera (Mark IV, Canon) to record and later analyze the rotation angle.

6.2.5 Suction Marks

We noticed that the suction left visible marks on the skin. We investigated this undesirable effect further in Figure 6-6, by recording the marks with a camera. We believe marks were caused by fluid displacement in the tissue due to pressure from the

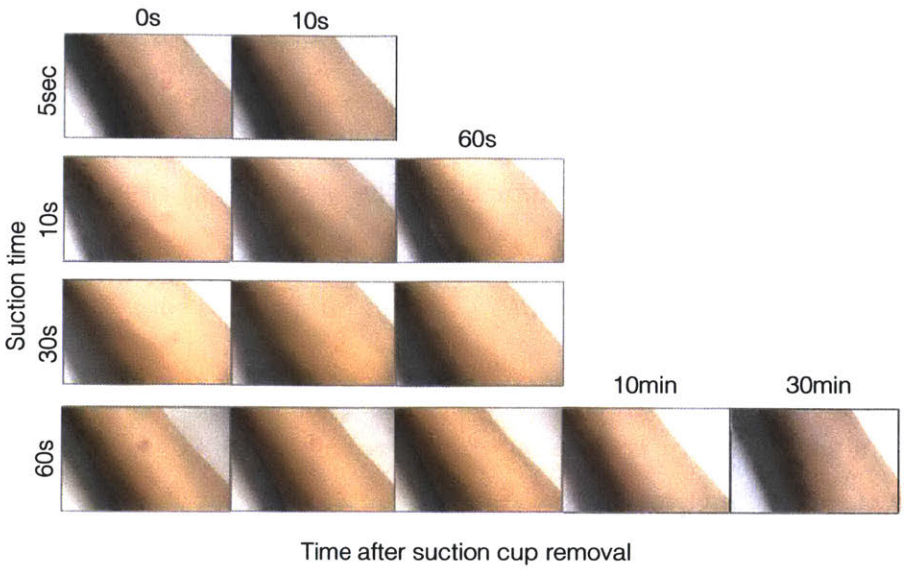

Figure 6-6: The after effect of the suction cups on the skin. The Y-axis is the duration the suction cup was applied to the skin. The snapshots are shown at different time intervals after the suction cup was removed. For example, when the suction cup was applied for 5 sec, no visible marks remained after 10 seconds.

suction cup rim [121]. The duration of time marks remained visible depended on how long suction was applied to the skin. In one participant, the marks disappeared in under 10 sec for 5 sec of suction, and under 1 minute for 10 and 30 seconds of suction. Even after 10 minutes of continuous suction, the marks disappeared in about an hour. In practice, the pumps would not operate continuously but will be duty-cycled to conserve energy.

6.3 Discussion

Irrespective of the adhesion mechanism, Epidermal Robots need to have the following: a sensor to detect adhesion state, the ability to enable and disable adhesion, and at least two degrees of freedom (preferably, three) for the end effectors. To control skin locomotion, those three features need to be combined with a digital state machine. Commonly explored robot locomotion methods, such as wheels and tracks, do not perform well on the skin. Skin locomotion is difficult but possible with the use of sensors, feedback, and digital electronics.

We determined that suction is an appropriate method for skin locomotion. Suction provides enough force to hold the robot, even with the moderate presence of hair. Highly dense hair would have to be shaved beforehand. Also, suction can be energy efficient, given that the pumps are duty cycled. Notably, for suction-based robots, the weight should not exceed 80g to minimize skin sagging. The diameter of the suction cups should be under 10mm if -10 to -30kPa vacuum pressure is used. Also, the distance between suction cups should be ideally less than 4.1mm to facilitate locomotion over most curved body surfaces. Finally, adding a thin, soft rim to the rigid suction cup will aid in adhesion to skin with hair.

6.4 Cloth climbing

This section shortly describes climbing on the clothing. Generally, the magnet mechanism in Rovables worked well, and it is miniature enough for an untethered robot. As a result, cloth climbing does not require an in-depth study.

It is crucial to quantify the force that the Rovable can pull and how it is influenced by the type of fabric. This determines how much extra weight it can carry, which enables interactions such as actuating clothing.

The force of attraction between wheels and the magnetic rod mostly depends on the thickness of clothing, as shown in Figure 6-7 (top). The measurements indicate the minimum force needed to pull wheels and magnet rod apart. Generally, thicker clothing has lower attraction forces. The maximum force is 4.2N when there is no clothing in between. Measurements were done with Series 5 force gauge (Mark-10).

The minimum force required for climbing depends both on the thickness and type of fabric, as well as the weight of the robot. The thickness is dominant, but for some materials like linen, the climbing force does not follow the trend because of the low friction coefficient. Figure 6-7 (bottom) reflects the force with the motor running at 3.7V DC on a horizontal plane. Its payload when going vertically will be the measured force minus its weight, which is 0.2N.

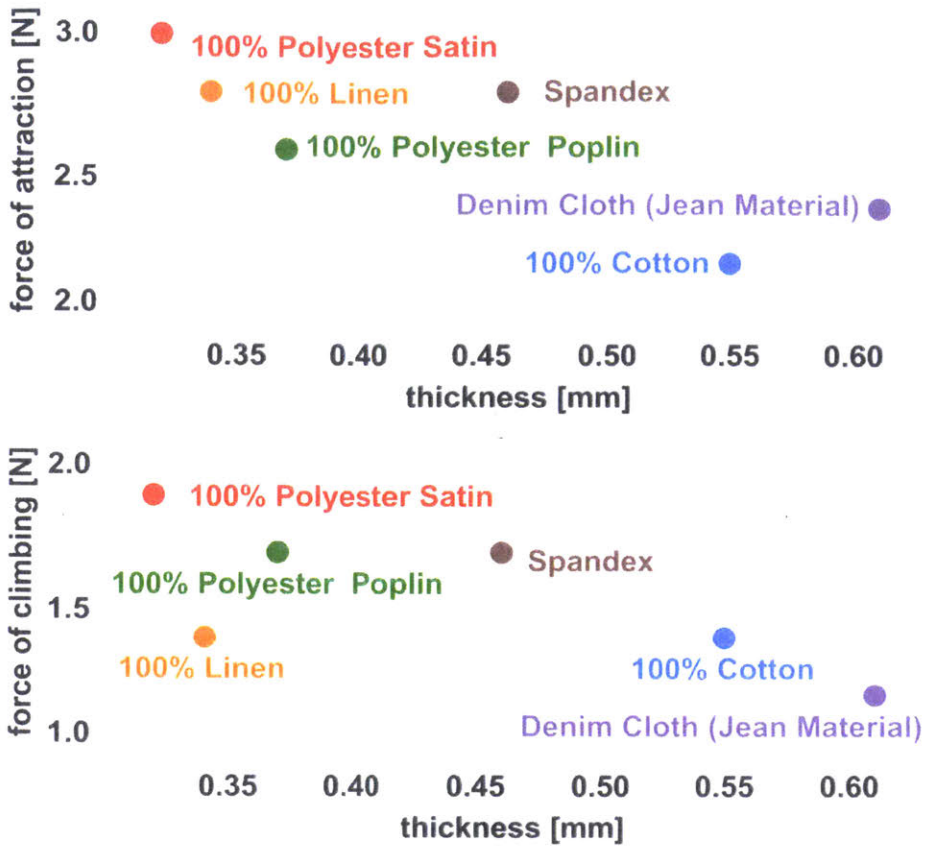

Figure 6-7: Measurement of attraction (top) and climbing forces (bottom) on different fabrics.

6.5 Chapter Summary

Climbing is one of the biggest challenges for DWT robots. In this work, we have explored in detail how to attach and climb on the skin. The exploration showed that the skin is a complex and challenging surface. Cloth climbing is simpler than skin climbing. The cloth has uniform material properties and thickness and can be held by the backside with a magnetic force.

Chapter 7

Power considerations

This chapter provides a close look at the power consumption of DWT. Robots need the ability to work for extended periods. Unfortunately, energy technology is slow to progress, with no foreseeable major improvements in the future [122]. We discuss the previous work in energy harvesting and analyze the power consumption of the robot. We also discuss the possibility of energy harvesting.

7.1 Energy harvesting technologies

A thorough review of energy harvesting in wearable devices is provided in [122, 123]. In this section, we will look at potential energy harvesting technologies and try to understand their limitations.

Electromagnetic. RF provides a useful source of wireless energy. In my master's thesis, I explored such wireless power solutions for sensors [124]. Commercial UHF (Ultra high frequency) RFID tags can provide enough energy to power a sensor and a microcontroller, as well as use backscatter for communications [125]. For example, we demonstrated that an EEG (Electroencephalogram) could be powered with UHF RFID [126]. UHF provides a relatively small amount of energy in the order of microWatts (μW), so duty cycling is usually required. Ambient RF energy from TV broadcast antennas can provide around more than 100 μW [127] in 10km proximity, but requires a large antenna.

NFC (Near-field communications) provide a much more significant amount of energy, from milliWatts to Watts. NFC is adapted for phone wireless charging and non-contact payments. We demonstrated that NFC could power small displays [128]. NFC does not use radio waves but works as an air-gap transformer between receiver and transmitter coils. As a result, NFC needs precise alignment and has a maximum range of few centimeters. The range can be increased using resonant coupling [129].

Another way to convert mechanical energy into electrical energy is by moving a magnet near a wire. Similar to electric generators, the movement generates a current inside the coil. There are commercial flashlights which create electrical energy from shaking or cranking. Significant power can be made, but this requires mechanical input.

Piezo electric. Piezoelectric materials generate electrical energy from strain on their crystalline structure. For example, a microfabricated piezoelectric material can harvest energy when placed on the surface of the heart [130]. Placed in solos of the shoes, piezoelectric materials generate electricity for every step [131]

Thermal energy. When two different metals are sandwiched together, they will produce electricity if there is a temperature gradient. Such device forms a thermo-electric generator. Such generators have been integrated into flexible fabrics [132].

Solar and optical. Solar panels can extract energy from photons proportional to their area and intensity of light. Hovewhere, solar panels provide significantly less energy indoors.

Battery technology. Most untethered robots and consumer devices are powered by lithium-polymer (LiPo) batteries. This technology provides good energy density and rechargeable chemistry. Since LiPo, there have not been major commercial breakthroughs in battery technology [133], although LiPo energy densities are steadily increasing. Batteries require many factors such as durability, energy density, charge cycles, which has not been fully satisfied with emerging technologies. LiPo battery capacities scale with volume, which does not favor small sizes, as it follows the cubic function.

Some of the recent research has focused on making solid-state batteries, which

have solid electrolyte to allow thinner and safer batteries [134]. Most LiPo batteries use gel or liquid electrolyte, which requires a thick aluminum-backed pouch for sealing and turns into gas when overheated. Another possibility is to use a lithium-oxygen chemical reaction, as oxygen is present in the air, the energy density of the battery is higher [135]

Summary. None of the energy harvesting technologies can power the robot continuously without external setups. The robot has to be powered from a battery. However, energy harvesting can provide an additional energy source for the batteries.

7.2 Power consumption of Epidermal Robots

Using a digital multimeter (U1252B, Agilent) and averaging currents over five minute periods, the mean power consumption of the robot during locomotion was found to be 1221mW. A significant part of the power is consumed by the pumps (817mW), and the rest is used by the five motors (404mW). When the robot is statically attached to the skin, the power consumption of the pumps is reduced to 30mW. This significant reduction can be achieved by monitoring the pressure sensors and only activating

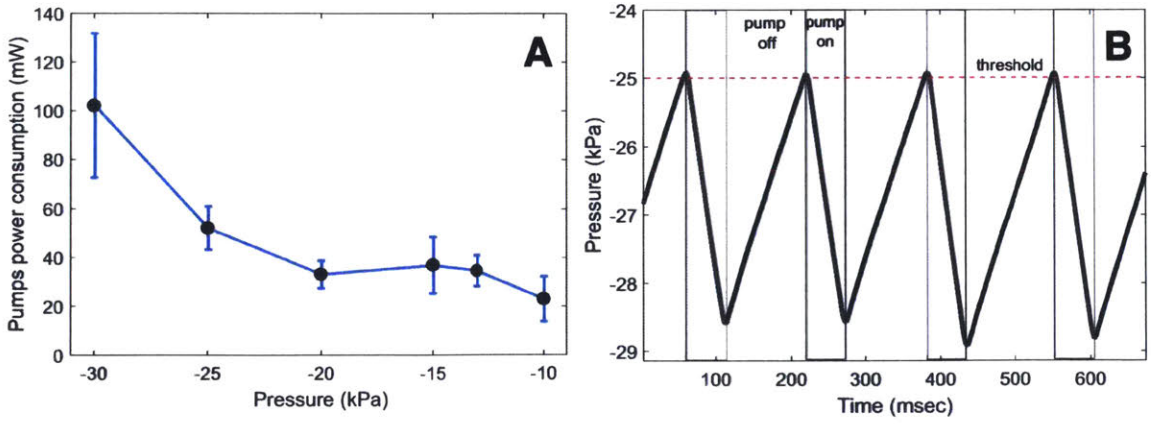

Figure 7-1: Power consumption during the adhesion experiment. A) The power consumption of the pumps required to keep the robot attached to the skin at different vacuum pressures. The pumps were duty cycled by turning on only when vacuum goes under a certain threshold. Overall, the power consumption is an order of magnitude lower than running pumps continuously at 1076mW. B) Sample pressure data showing duty cycling of the pressure to keep the pressure at the threshold of -25kPa.

the pumps when the vacuum pressure drops under -20kPa. Pumps run at a duty cycle of 2% to 5% at -20kPa pressure. Fig. 7-1 illustrates the power consumption at different pressures, and shows that -20kPa provides the most vacuum pressure while consuming the least energy. The current for each pressure threshold was measured at five different locations on the forearm.

To evaluate the feasibility of an untethered version of SkinBot, we built the prototype shown in Figure 7-2. In particular, the PCB that held the original tether was replaced by a custom PCB that contained all the electronics required for operation; 2.4 GHz radio (nRF24L01+, Nordic), an ARM-based microcontroller (ATM-SAMD21G, Atmel) and an IMU (MPU6050, Invensense). This version of the robot is powered by a 100mAh lithium polymer battery. The vacuum pumps were also added to the robot, but the torque from unbalanced weight made it unreliable for continuous vertical climbing. The electronics consumed a relatively small amount of energy (28.1mW) even with a 2-way radio transmission updating at 10Hz. Based on our measurements, the untethered robot could move continuously for around 16 minutes or remain attached to the skin for about 10 hours.

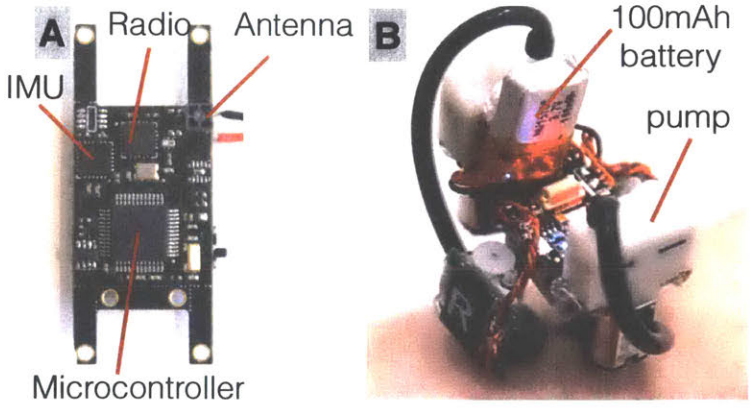

Figure 7-2: A) Circuit board and B) assembled untethered prototype of SkinBot

7.3 Power consumption of Rovables

The Rovables robot works untethered with an on-board LiPo battery. The maximum power consumption is 120.4mA (398mW), which allows for a battery life of 45 minutes

with a 100mAh battery. This is the power required with motors on and all systems active (IMU, wireless, encoders). Motors use the most energy: 91.9mA. The encoder's infrared LEDs consume 20mA. The rest of the electronics consume just under 8.5mA.

Assuming that all systems will not be active all the time, the battery life could be significantly extended. For example, optical encoders can be disabled when motors are not running. The device can wirelessly stream data for 11.8 hours if the motors and encoders are off.

7.4 Power analysis

This section looks at the power consumption of different subsystems of DWT robot. The maximum power consumption is given in most cases. It is difficult to generalize the mean power consumption, as power depends on many factors during operation, such as sleep modes and motor torque and speed. Also, during normal operation, all the subsystems are duty cycled.

To better understand the power consumption, it is best to have a realistic scenario. Let us assume that the robot moves for 5 seconds, then stops for 5 seconds to take an image. During movement, the motors, processor, IMU, and encoders are active. When stopped, the radio and camera are active for 100ms to take a picture. This time includes the time for start-up, image taking, and transfer.

Processor Modern digital electronics have low power consumption. State-of-the-art ARM-based microcontrollers consume the maximum of 8mA at 64MHz. Although, in the typical application, the average consumption is lower, as the microcontroller is often in the sleep mode, where the power consumption is in the microAmpere (μA) range. At a 50% duty cycle, assumed here, the power consumption is around 4mA.

Communications The power consumption of Bluetooth Low Energy (BLE) radio is about 5.0mA during constant transmission.

The maximum throughput of BLE is about 171kb/sec. This throughput assumes 244-byte packets are sent at transmission period of 400 ms and 2Mbit physical layer speed. The size of an uncompressed 5-megapixel image is 36Mbytes, so it is not

realistic to send raw images at such resolution over BLE. At 640x480 resolution with 10-bit per pixel, the image size is 384Kbytes. This would take 2.25 seconds to transmit At a 24% duty cycle assumed here, the power consumption is 1.2mA.

Sensors The IMU (MPU6050) maximum power consumption is 3.9mA, The gyroscope consumes the most energy (3.6mA), but it is required to track the rotation of the robot. The accelerometer is used to detect external movements. The infrared encoder consumes 10 mA, mainly used up by the infrared LED illumination. The 5-megapixel camera consumes 96 mA. Due to the complexity of integration, the camera is tethered to a Raspberry Pi. Lower power (10mA) camera, such as the OV7670 (Omnivision) can be used in the future. At a 50% duty cycle, the IMU consumes 1.8mA, and the camera runs at 1% duty cycle, hence consumes 0.96mA.

Motors The motors consume the largest amount of energy. Each DC gear motor consumes around 46mA, and the linear motor is 120mA during operation. At least two motors are required, as the robot needs at least 2 degrees of freedom. Stalling causes the motors to consume more than 200mA and can cause overheating; therefore, is avoided.

Assuming the motors are duty cycled at 50%, their power consumption is 46mA.

	Continous power	Duty cycle power	Notes
Microcontroller	8mA	4mA (50%)	nRF52832, Nordic at 64 MHz
Wireless data	5mA	1.2 mA (24%)	BLE 4.2 on nRF52832
IMU	3.9 mA	1.8mA (50%)	6-axis fusion on MPU6050
Encoders	20 mA (10mA each)	10 mA (50%)	Infrared-based
Camera	90 mA	0.96 mA (1%)	5 Megapoxel
Motor	92 mA (46mA each)	46 mA (50%)	DC gear motors
TOTAL	153mA	64 mA	
Battery life	40 minutes	1 hour and 30 minutes	Using 100mAh battery

Table 7.1: Table showing current consumption of different robot subsystems.

7.5 Chapter Summary

The motors consume more than 2/3rd of the energy and constitute an area that is difficult to optimize. Vertical climbing requires significant energy expenditure, even with the high efficiency of electrical motors. Fundamentally to move a 30-gram robot 1-meter vertically requires 0.3Joules of energy or 0.03mA. This estimate does not account for overhead such as friction and motor efficiency, which can be significant.

The camera provides an engineering challenge for integration into the robot because of the large power consumption and data rate. I believe it is possible to integrate an off-the-shelf camera. Previous research has shown that a camera can be powered with RFID [136]. Furthermore, low-resolution optical sensors with custom image processing chips (e.g., optical mouse sensor) could be used to allow better integration.

Chapter 8

Size and weight

The size and weight of the robot is one of the critical design considerations, It is essential to look at it in more details, to better understand what limits the size of the robot, and what is potentially its smallest size. Our focus is a fully functional robot that includes: microcontroller, wireless communications, actuators, and a battery.

8.1 Sizes of similar robots

To understand the size limitations of robots, its worthwhile to look at other small robots, even if they dont employ vertical climbing. In robotics literature, the definition of small has been used very loosely, as it is relative to the particular type of devices.

Mini robot. Using conventional fabrication techniques and off the shelf parts, the smallest size of an untethered robot is about 2 cm. For example, TinyTerp is 2.0 cm [137] , ALICE is also 2.0 cm and 30 grams [138], and Kilobot is 3.3 cm and 16 grams [139]. All of those robots contain microcontroller, radio and employ DC motors, to move on the flat horizontal surface. They are mostly designed for studying swarm behaviors.

Micro robot. With microfabrication techniques, the size of the robot can be further reduced. For example, recently microfabricated robots have approached 0.4cm [140], and a solar-panel powered 0.39 cm robot [141] has been developed. At sub centimeter

scales, DC motors become impractical; therefore, other actuator mechanisms such as piezoelectricity are used.

Sub-millimeter robots. Furthermore, using biological and molecular engineering, nano-sized robots were created. For example, optical tweezers use a laser to move nanoparticles [142] or a catalytic reaction can be used to move nanomotor [143]. Also, the magnetic field could be used to force magnetotactic bacteria to move objects [144].

8.2 Individual parts size

It is useful to estimate the smallest potential size of an untethered robot using off-the-shelf parts. Potentially, custon parts can be a bit smaller but would require significant development time and resources.

Electronics. Due to the constant miniaturization electronics are not the limiting size and weight part. It is possible to get a microcontroller with the size of 7x7x0.85 mm (NRF52832, Nordic), that contains a radio, as well as many peripheral interfaces. With a few passive parts and motor drives, this is enough for a self-contained robot.

Batteries. Batteries are one of the hardest components to initialize. Motors and actuators have a large instantaneous current draw, therefore require ample discharge rate. Currently, there is only one technology that can practically work in miniature robots: lithium polymer (LiPo) batteries. Such batteries have high discharge current, small size, high energy density, and can be recharged. Some of the most miniature LiPo cells have dimensions of 3x9x10 mm (GM300910H, PowerStream) and a weight of 0.33grams. The capacity of such a battery is 12mAh and maximum discharge current is 6mAh.

There are exotic smaller energy sources, such as supercapacitors. Such energy sources are ill-suited for self-powered robots, as they do not contain enough energy to power the robot continuously for a few hours. Using such energy sources would imply energy harvesting.

Actuators. Robotics require large torques; therefore, the motors need to have gearboxes (typically planetary). We successfully used 6mm geared brushed DC motors

(TGPP06-D-136, TT Motor) in the Rovables project. The smallest motor (03A, Faulhaber) that provided enough torque was 3.4mm in diameter. There are smaller motors, such as stepper motors, but such motors are not designed for high torque applications. The linear motors tend to be larger, as they require a rack-pinion mechanism or ball-screw to convert rotation into linear motion.

The skin moving robots require solenoids and pumps as well as motors. The current off-the-shelf solenoids and pumps are too large, therefore had to be placed off-the-robot. Miniaturization of such parts is possible but requires custom engineering. The smallest diaphragm pump that we found is about 8x32x18mm in size and weights 6.4 grams (SC3101PM, Skookum Electronic co.). This pump is designed for medical device applications such as a miniature arm cuff for blood pressure. Potentially, diaphragm pumps can be smaller by reducing the size of the piston. Figure 8-1 shows the dimensions of different components including piezoelectric pumps.

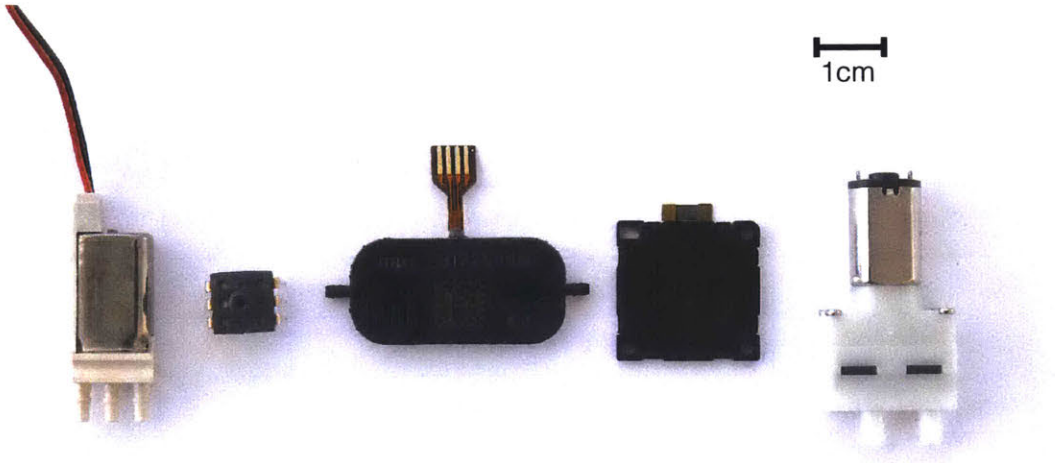

Figure 8-1: Comparison of different compoments sizes that can be used for pneumatics in epidermal robots. Left to right: solenoid, pressure sensor, piezoelectric pump, piezoelectric blower, diaphram pump with DC motor.

Mechanical. With the state-of-the-art 3D printing, the minimum resolution is about 25-100 um. With injection molding or CNC, machining resolution can be reduced to 20 um or less. Also, the materials would require about 1mm thickness to

provide enough structural rigidity. Also, the thickness of FR-4, which is used for the printed circuit boards, should be above 0.5mm to provide enough structural rigidity. The flexible electronics technology allows circuits with a thickness of 0.15mm, so it is an attractive option for miniaturization if no structural rigidity is needed.

Sensors. The robot requires sensors, which add to its size and weight. Fortunately, sensors are small in comparison to other components, as they do not need to contain moving parts. Mainly, the robot requires inertial and optical sensors. The inertial sensing can be done using a solid-state inertial measurement chip with the size of 4x4x0.9mm (MPU6050, Invensense). The optical encoders can be the size of a small surface mount LED. The camera is larger, as it requires an imaging chip, auxiliary components, and a lens. The camera that we use has die dimensions of 5x5 mm (OV6920, OmniVision). It provides 5 Megapixel resolution, which is enough for machine vision. Additional processing power and memory might be required to do real-time machine vision on-board.

	Dimensions (mm)	**Weight (grams)**
Battery	3x9x10 (GM300910H, PowerStream)	0.33
Microcontroller IC	7x7x0.85 (nRF52840, Nordic)	0.05
Mechanical PCB	0.5 x 15 x 15 (FR4)	0.35
Mechanical Structural	1.0 (SLA plastic)	1.2
Motor	12.6 x 3.4 (03A, Faulhaber)	0.43
Total Minimum	**8.75 mm (thickness)**	**2.36 grams**
Rovables	20 mm	20 grams
SkinBot	26 mm	20 grams

Table 8.1: Table showing minimum sizes and weights of different components. Size and weight of Rovables and SkinBot is shown for comparison

8.3 Chapter Summary

It appears that the minimum size and weight of a fully functional robot using off-the-shelf parts is at least 8mm thickness and 2.4 grams. This data is summarized in Figure 8.1 This number is further confirmed by looking at other miniature research robots, which achieved a size of 2 cm. State-of-the-art electronics and sensors already fit well under a centimeter. On the other hand, most batteries and actuators are well above centimeter in size. The size can be further reduced but requires novel and custom parts that are specifically designed for the application. With the current size of 2cm and weight of 20 grams, DWT robots could be further miniaturized using more specialized off-the-shelf or custom parts and extensive engineering.

Chapter 9

Applications

This chapter provides potential applications of DWT in three areas: physiological sensing, human-computer interactions, and design. The applications for Epidermal Robots were designed to highlight their access to the skin and physiological sensing. The applications of Rovables highlights human-computer interactions.

9.1 Physiological sensing

DWT robots can noninvasively sense physiological data on human skin. Some of them, such as skin mechanical properties and biopotentials, can be sensed directly by the suction cups. This is especially useful in medical sensing. Currently, most of such tests are performed manually by a doctor; therefore, they are hard to perform consistently. Furthermore, the doctor is limited by the human senses of touch, vision, and sound. The robot can test things outside of that range.

9.1.1 Skin mechanical properties

The Epidermal Robots can test the mechanical property of skin directly underneath them. This is done by applying a mechanical stimulus on the skin and measuring a response. We created two prototypes that push on the skin and pull on the skin.

Currently, such tactile sensing can be done using a robot arm with a sensor

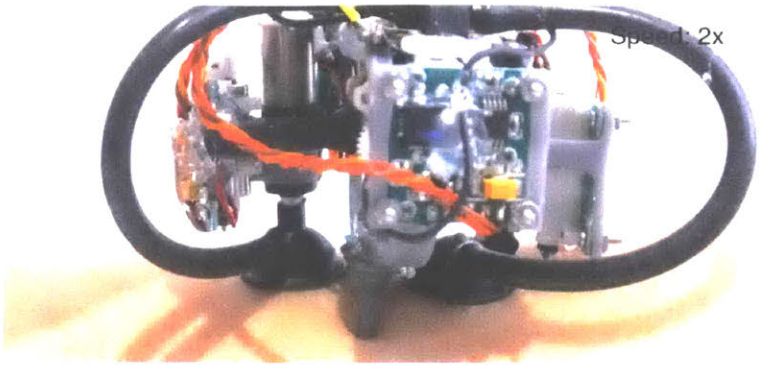

Figure 9-1: The Epidermal Eobot equiped with a plunger to test mechanical properties of the skin. In this picture, the robot is attached to forearm.

tip [145], as a hand-held [146] or stationary instrument or by hand. Providing exact measurements with those methods is challenging, as such sensing requires applying force on the skin. The body is not rigid and has many flexible joints, therefore needs to be fixed entirely. For example, if a robot arm pushes on the skin, it will create an equal reaction force. The Epidermal Robots are attached locally, so all the effects are created in a small area. The body parts do not need to be rigidly fixed.

Stiffness testing instrument design

Pushing on the skin provides information about the hardness of the skin, and can be used to derive Young's modulus[1]. This is similar to an instrument called durometer, which creates an indentation in the material to identify its hardness quickly. We equipped the robot with two vertical linear servo motor (SPMSA2005, Spektrum) and an indenter rod that pushed on the skin, as shown in Figure 9-1. The indenter had a cylindrical flat end with a diameter of 2 mm. We used two motors to increase the pushing force as well to position the rod between the two suction cups. If the rod were offset from the middle, the robot would tilt during the pushing, potentially causing detachment from the skin. The displacement of the rod was extracted by digitizing the voltage from the potentiometer of the servo, that is used for position feedback. This provided the strain measurement. The strain was unitless, as it was divided by initial strain. To measure the stress (in Newtons(N)), we added an FSR (force

[1]Stiffness defined by stress/strain ratio in the material's linear region

sensitive resistor) to the tip of the rod. An identical 0.2inch FSR sensor (FSR400, Interlink), was used in my previous work to sense gestures from wrist motions [14]. We calibrated the FSR with a digital scale (SCM2600, My Weight) to convert arbitrary voltage divider readings from the FSR into Newtons. Figure 9-2 shows the data obtained from the robot pushing on the skin. The slope of the stress vs. strain graph is defined as Young's Modulus.

The Young Modulus has large variations as reported in the literature, as it greatly depends on in-vivo or in-vitro testing, the type of testing machine, and location of the test [147] In our case we compare to Young modulus for indentation testing on the limbs and in-vivo only. Our Young modulus is slightly higher (378 kPa) than what is reported in the literature for indentation. One study reported 10.4 to 89.2 kPa [148] for lower limbs, while another study reported 21 to 195 kPa [149]. One of the potential sources of inaccuracy in our setup is the use of resistive force sensors, which has a non-linear response and is noisy. All the studies used more accurate strain-gauge based force sensor, which was too large to mount on the small robot.

The robot has to be reasonably well and stably attached to the skin, as the force exerted by the rod into the skin is transferred to the suction cups. To prevent detachment as well as influence the measurements, this force has to be less than the attachment force of the robot.

Custom wearables

Mapping the hardness of the human body has useful applications. For example, it can be used to manufacture more comfortable and efficient prosthetics using multi-material 3D printers. Ideally the prosthetic should have variable stiffness to match the elasticity of the limb, but this requires a prior map of elasticity [150, 151]. The current measurement tools require a large mechanical apparatus or multiple-camera setup. The DWT robots can be used to map the stiffness at home without the need for large machines.

Knowing the stiffness can also allow for more comfortable wearable devices. As shown in Figure 9-3, we made a concept of a 3D printed (Form 2 with durable resin,

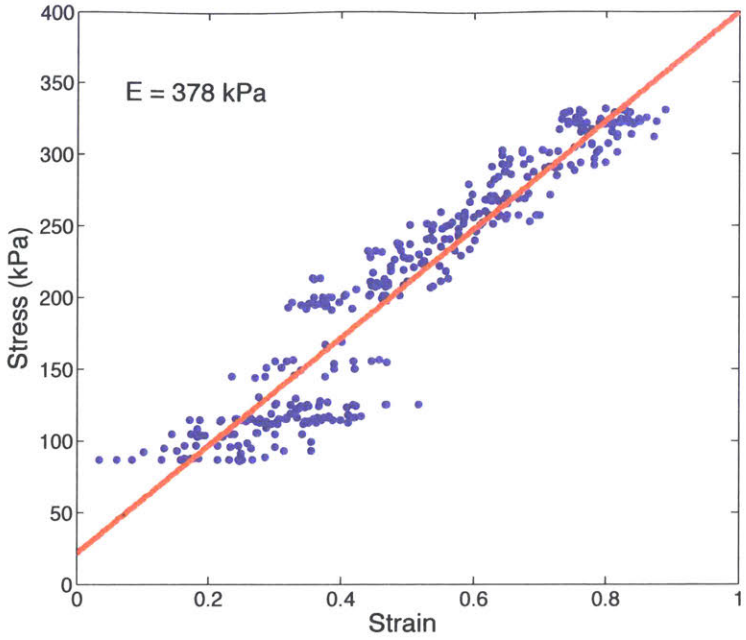

Figure 9-2: Stress vs. strain graph obtained from pushing the skin on the arm. The red line is the slope, which was used to obtain Young's modulus.

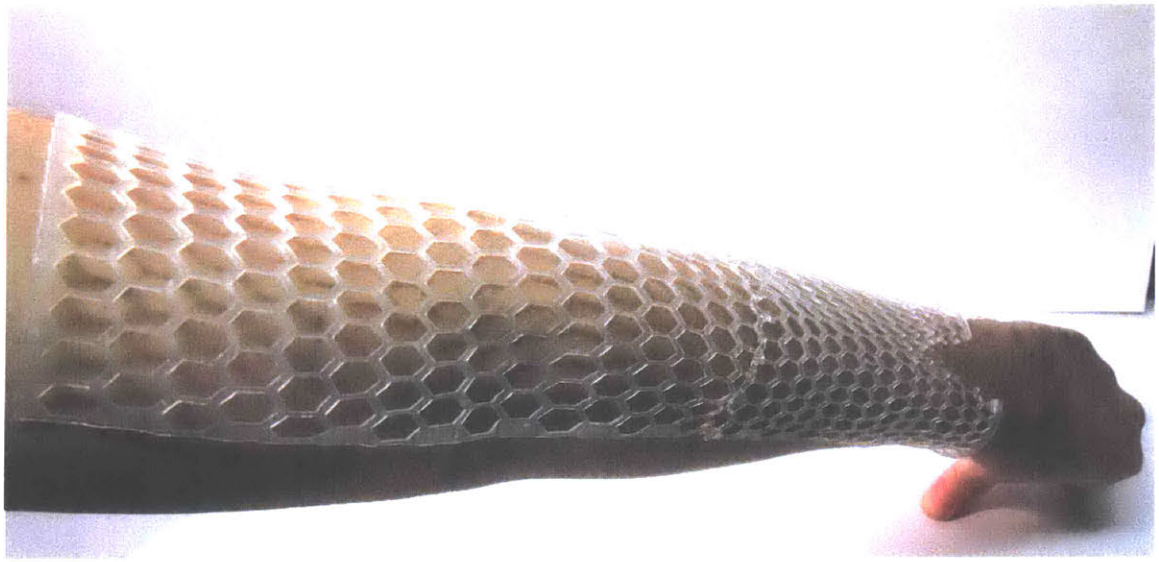

Figure 9-3: 3D printed arm brace with different stiffness segments.

Formlabs) arm brace that used 3D map and stiffness data. The stiffness was varied by changing the size of the cells in the mesh.

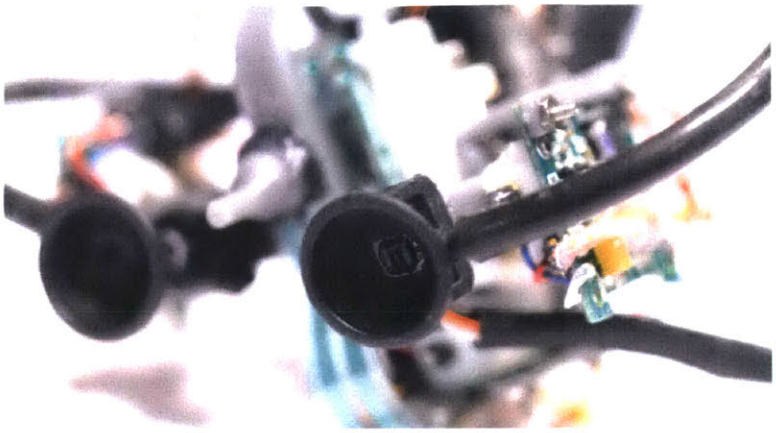

Figure 9-4: Infrared proximity sensor integrated into the suction cup of the robot.

Disease testing and prognosis.

Also, measuring and mapping relative the stiffness is useful in early disease detection. Many disorders change the mechanical properties of the skin or underlying tissues. For example, lymphoma[2] presents itself as lumps under the skin. The detection is done by the doctor by feeling the tissue with hands [152]. Such a measurement method is not systematic and largely depends on the doctor. Furthermore, research has shown that a robotic tactile sensor can be more sensitive than a human touch for skin lumps detection [153]. A tactile handheld sensor has been shown to be useful in measuring the mass size of breast lumps. [146]

Pulling on the skin also provides information about tissue's mechanical properties. This technique is often used in the cosmetics and skincare industry to understand the effect of different skin products. A tool called a Cutometer is used to pull on the skin using a vacuum and simultaneously measures how far the skin is pulled [154]. With Epidermal Robots, this technique is straightforward to implement, as the robot already uses suction for attachment. We added an infrared proximity sensor (GP2S60A, Sharp) inside the suction cup to measure the skin's bulging. Figure 9-6 shows an illustration of such a sensor. Figure 9-4 shows how such sensor is integrated inside a suction cup of the Epidermal Robot.

We developed and tested simulated lump tissue samples, as described in the lit-

[2]cancer of lymph nodes

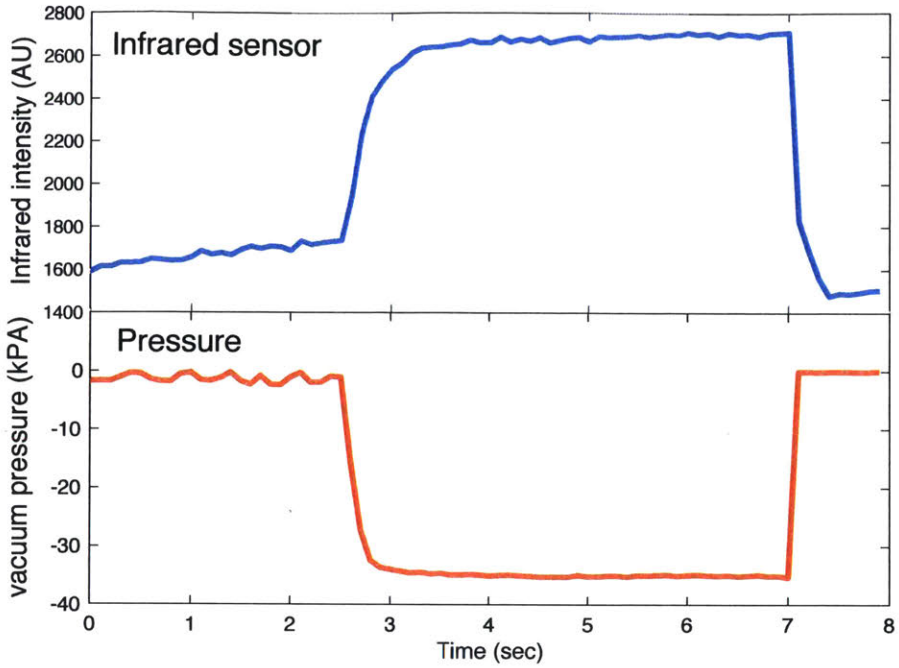

Figure 9-5: Displacement of the silicone during suction, as measured by the infrared proximity sensor inside the suction cup

erature [155]. The simulated tissues serve as ground truth. Such tissue samples are created with skin-like silicone (Ecoflex 00-30, Smooth-On) with embedded hard 3D printed plastic balls (Black resin on Form 2, Formlabs) to represent the lumps. The silicone is mixed with a pigment to be skin color. We made 21 different simulated lumps. The lumps are of various sizes (4,6,8,10 mm diameter) and are embedded at different heights (1,2,3,4,5 mm).

An example of data of skin deformation in the suction cup is shown in Figure 9-5. The data was obtained by placing the suction cup on a CNC gantry (1810-PRO, Seed Studio) and moving it in 5mm increments across the silicone sample. We used ADP5200 ($\pm$100kPa, Panasonic) pressure sensor for recording the vacuum pressure. Using a simple convolutional neural networks classifier (TensorFlow [3]) with one input and one output layer, we were able to classify the depth and the height of the sample with 66% accuracy. We also achieved 96.9% sensitivity with binary classifier (lump vs. no lump)

Multiple measurement techniques can be used simultaneously to provide better

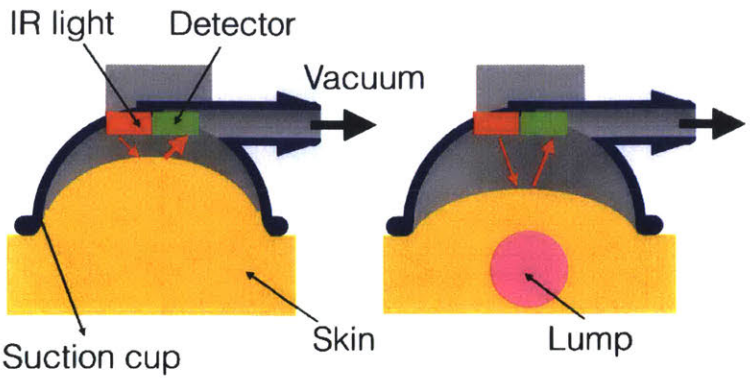

Figure 9-6: Cutometer sensor measures tissue displacement in the suction cup. The lump will change tissue properties and thus, infrared reflectance.

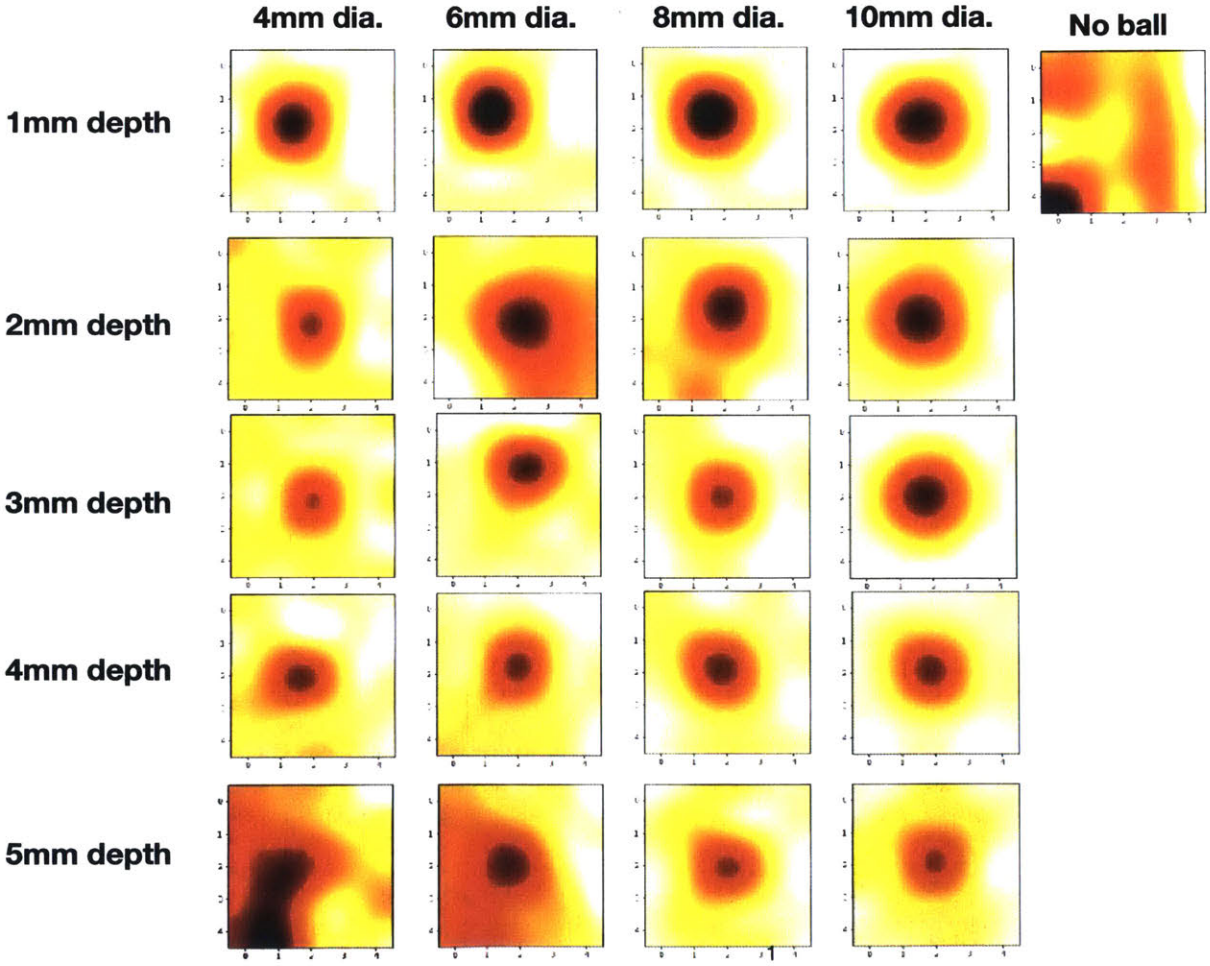

Figure 9-7: Heat map (Bessel fitting) generated by measuring displacement in a simulated tissue lump in locations 5mm apart. Grid of different lump depths and lump diameters are shown. "No ball" heat map did not contain a lump.

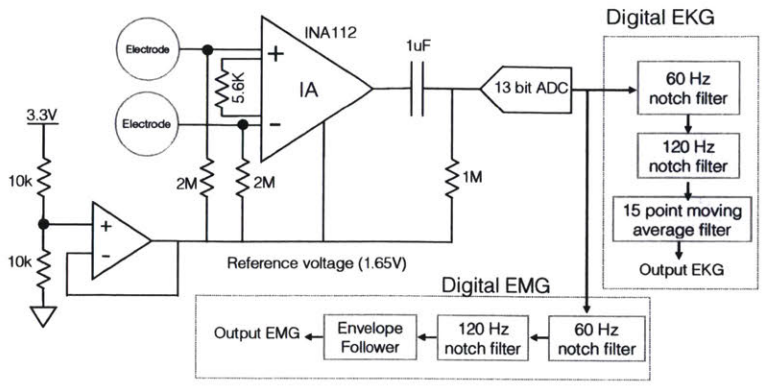

Figure 9-8: The biopotentials pickup circuit diagram. EMG and EKG had the same analog front end: instrumentation amplifier with a gain of 10. The amplifier was followed by a high pass filter of 0.16 Hz, which removed the DC baseline. To capture the complete signal shapes, the circuit was referenced to 1.65V (half of the supply).

results. The robot can combine both pushing and pulling on the skin, as well as optical imaging to collect more information.

9.1.2 Biopotentials

SkinBot contains an implementation of a circuit to monitor the electrical properties of the skin. To do so, we glued stainless steel washers (ID=9.0mm, OD=12mm, thickness=2mm) around the suction cups so they could also serve as electrodes. The electrodes can be used to capture electrocardiograms from the chest (ECG), electromyographic signals of the muscles (EMG), and electrodermal activity (EDA) from areas of the body where the density of eccrine sweat glands is high (e.g., wrists, upper arm) [156]. As the robot moved to different locations, Figure 9-9 shows EMG, ECG, and EDA traces captured from the chest, upper arm, and the interior part of the wrist, respectively. The detailed biopotential circuit diagram is shown in Fig. 9-8.

To capture biopotentials, we used an instrumentation amplifier (INA114, Analog Devices) as a front-end to reject the residual 60Hz noise. A 0.16Hz high-pass filter provided DC drift rejection, and a 30Hz low-pass filter provided a further 60 Hz noise rejection. We used quad op-amps (MCP6044, Microchip) for voltage reference and filtering. The data were digitized at 976 Hz and 13-bit resolution and further filtered with MATLAB (MathWorks). We used a digital a 60 and 120 Hz Butterworth notch

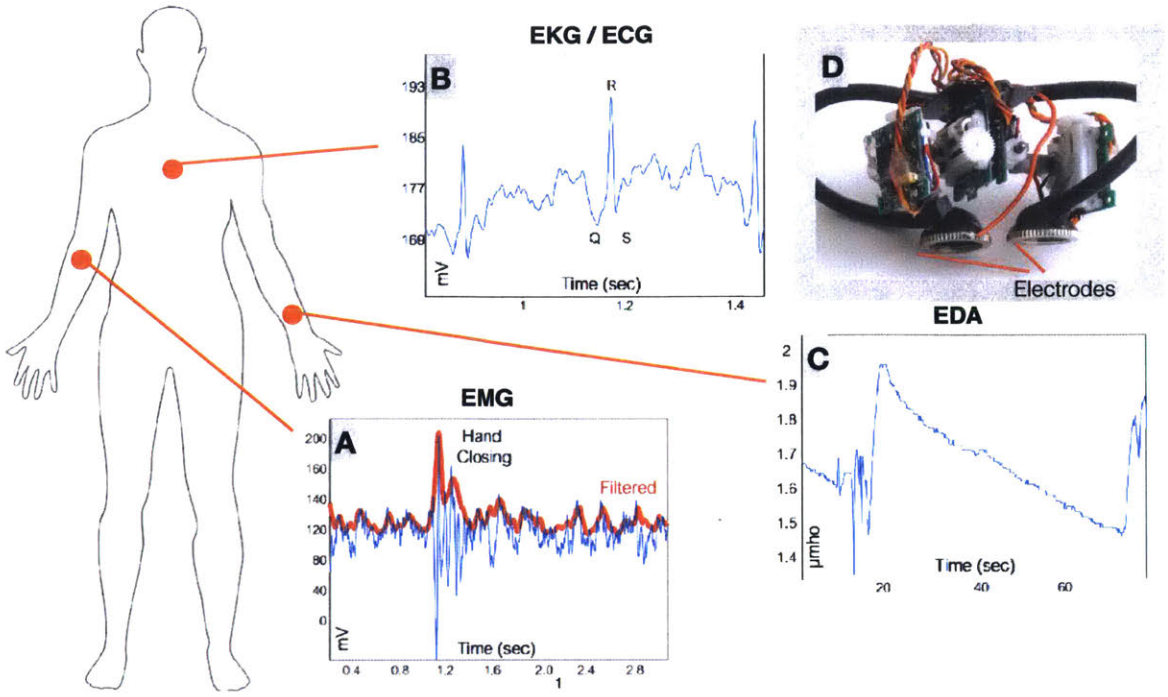

Figure 9-9: Biopotential sensing: A), Electromyographic signal measured on the upper arm when closing the hand. B), Electrocardiographic (EKG) signal measured on the chest showing the QRS complex, C), Electrodermal activity signals on the wrist in response to an auditory stimulus. D), Side view of SkinBot showing the modified suction-cups to monitor the electrical properties of the skin. Visual Imaging (middle row):

filters to remove 60Hz noise. A detailed circuit diagram is shown in Figure 9-8. The EDA was measured with a Q-sensor (Affectiva, Inc).

9.1.3 Machine Vision

The Epidermal Robot also contains a small skin-facing camera with a magnifying lens to emulate a digital dermatoscope, which is a tool that physicians use to examine the skin. The dermatoscope significantly increased the melanoma detection rate, in comparison to naked eye examination [157]. The camera module is appropriate to capture close-up snapshots of areas of interest such as birthmarks, warts, scars, irritations or scratches, and other potential anomalies. The lens provides a 10x magnification and shallow depth, so it has to be constantly refocused on the uneven

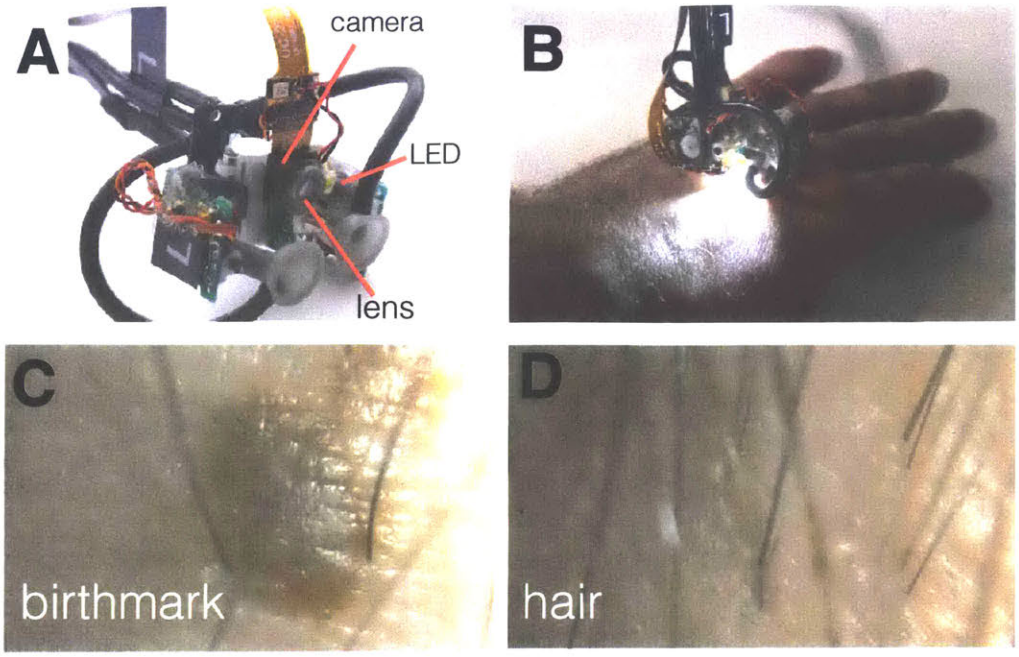

Figure 9-10: Visual imaging of the skin. a) Bottom view of the robot showing the camera sensing module. b) Epidermal robot using the camera module with a white LED for illumination. c) Camera snapshot showing a birthmark and d) Snapshot showing hair.

skin. Using the existing vertical servo motors, the robot can automatically focus by adjusting its height, or alternatively with an auto-focusing camera. Fig. 9-10 shows an example of a birthmark and dense hair captured with the camera.

The microscope was constructed using a 5-megapixel camera (OV5647, OmniVision), silicone lens (MPL15x, Cell Focus), and LED light (SM3527, Bivar) delivering 30 mW. The lens and LED were attached using hot glue. The camera was tethered to a single board computer (Raspberry Pi 3). All the video was 2592 x 1944 resolution and 30 fps.

Potentially, a nonvisible wavelength camera could be used to provide additional information.

9.1.4 Inertial Measurement Units

An inertial measurement unit (IMU) is composed of accelerometer, gyroscope, and sometimes also a magnetometer. The IMU is used for robot's navigation but can

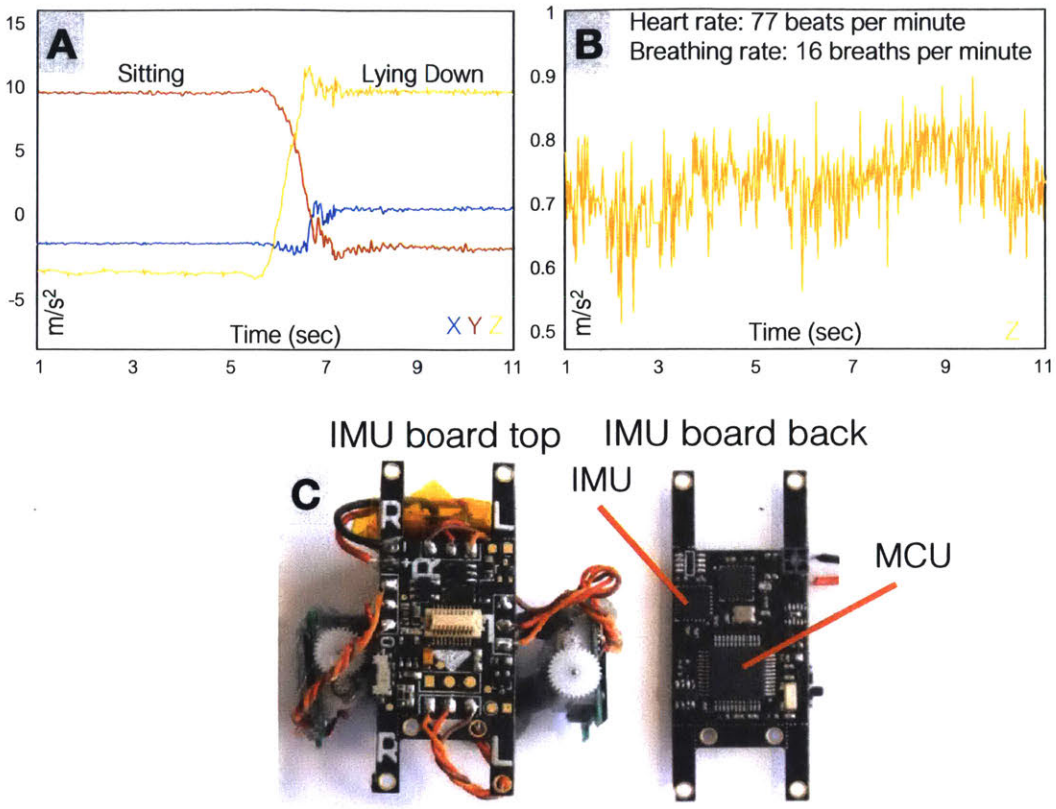

Figure 9-11: Inertial sensing with Epidermal Robot: A) changes in accelerometer data during sitting and lying down position captured on the chest, and B), cardiorespiratory motions captured on the chest. C), IMU board mounted on the robot. The backside of the IMU board contains a microcontroller (MCU) and a radio. IMU board also provides a connector to attach different modules such as an EKG module.

be used for applications such as motion capture, activity tracking, and physiological sensing. As the IMU tracks motions in relation to itself, its position on the body is very important. For Epidermal Robots and Rovables, we used a 6-axis accelerometer and gyroscope (MPU6050, Invensense), sampled at 100 Hz.

Motion capture is used to record the movement of people or objects. Motion capture has many applications, such as medicine, sports, and gaming. Depending on its body location, IMUs have been used to track different activities (e.g., typing, steps, cycling) and body posture [158]. Most of the current systems use optical tracking, which has limited use, as it requires setting up cameras around the object. Although inertial motion capture systems use on-body sensors, they need a long process of

placement and calibration of IMUs on each joint of the body (as many as 17 sensors). A shown in Figure 9-12, Rovables can become a distributed motion capture system, by using their IMUs. The process can be automated, as Rovables can travel to each joint and calibrate themselves.

We developed a kinematic chain model of the human body using the openFrameworks library [159]. The data from IMUs were fed into inverse kinematics equations to track the positions of the joints.

The motion capture can be done with Epidermal Robots and Rovables, as long as the clothing is not too loose. Attachment to the skin provides an ability to do physiological sensing of heart rate and breathing. Figure 9-11 shows accelerometer data captured while the Epidermal Robot was on the chest of a person to capture different body postures and subtle cardiorespiratory vibrations from which heart and breathing rates are extracted [160]

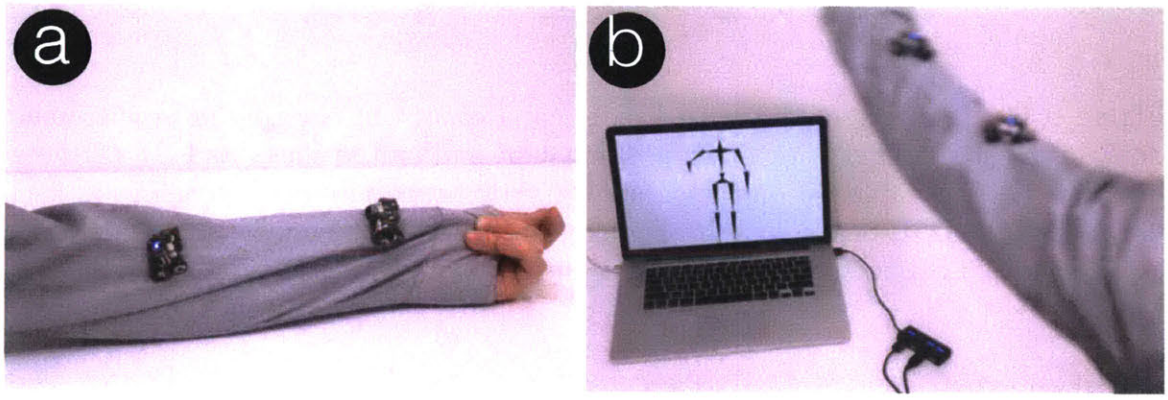

Figure 9-12: Using Rovables for motion capture. a) Rovables move to the right position on the arm. b) The kinematics of the arm is reconstructed on the screen. With more Rovables whole body skeleton can be reconstructed.

9.2 Human-computer interactions

Besides physiological sensing, wearable devices are often used for human-computer interactions, such as providing visual or tactile feedback. DWT can expand on such

applications with its locomotion abilities.

9.2.1 Wearable displays

We designed a display shield that connects to the expansion port on Rovables, as seen in Figure 9-13. The shield adds a capacitive touch display with 63 RGB LEDs (Neopixel Mini). Also, it has an ATSAMD21G (Atmel) microcontroller, which allows playing and storing animations. On each side, the shield has IR LEDs and IR proximity sensors, so it can precisely connect with another LED shield or follow an IR beacon. To make it easier to link and align with another shield, each side has two magnets. The display allows us to develop and test scenarios and algorithms where Rovables cooperate to make a larger display.

We developed a scenario where displays can become various output accessories. As an example, we developed an application scenario where one display-enabled robot is on a wrist and displays analog watch. When the user goes into a social situation, the robot moves to the chest and links up with another robot to form a name tag, as a larger display. When the user goes for a bicycle ride, the displays move to the back to form as a set of safety turn lights.

9.2.2 Tactile Feedback

Rovables can provide tactile feedback anywhere on the body. This is not possible with current wearable devices. To explore this idea, we designed a tactor that pokes the skin. The tactor is mounted on top of the Rovable, as shown in Figure 9-14. The tactor is driven by a 136:1 small gear motor. A 3D-printed rack and pinion mechanism was used to convert the motor's circular motion into linear motion.

The pushing force from the linear actuator is around 1N. But since the robot vibrates with the linear actuator, the actual force applied to the human body is less than 1N. To make a more effective tactor in the future, some stabilization mechanism for the robot will be required.

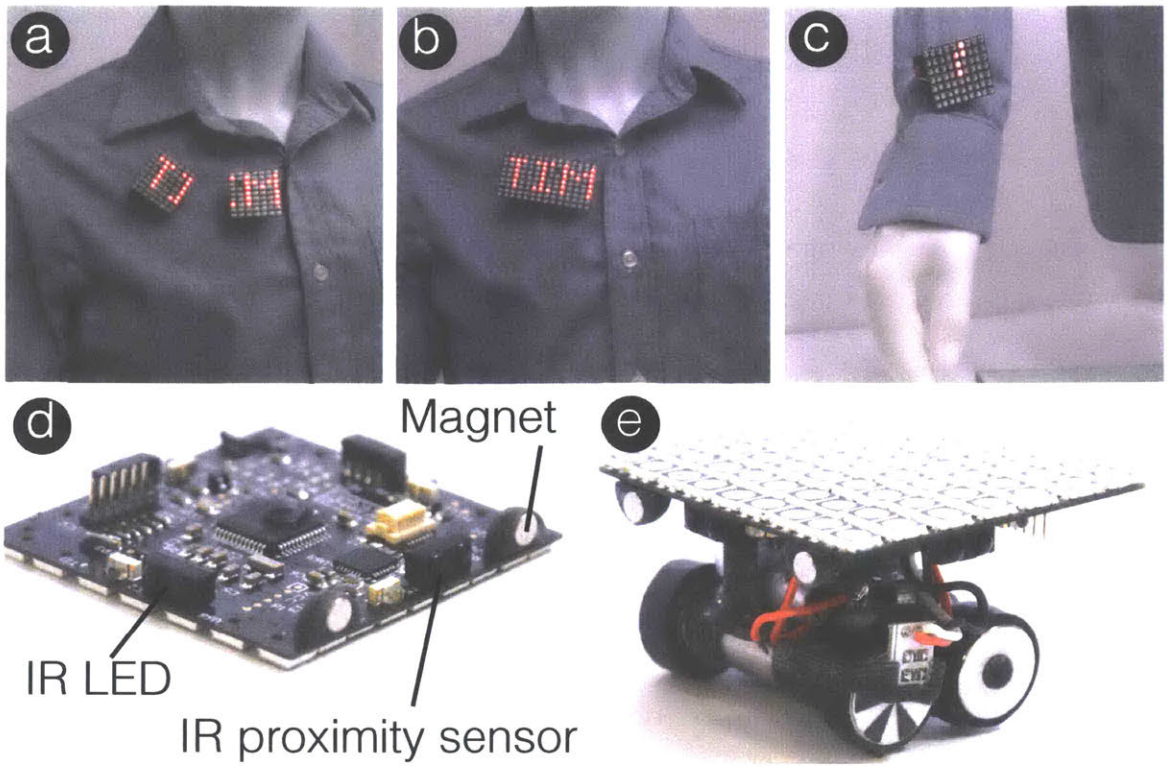

Figure 9-13: Wearable displays application. a) and b) The displays link together with magnets to form a larger name tag. c) The display can travel to the wrist to form a watch. d) The backside of the display shield exposes the IR beacon system and magnets for alignment with other displays. e) The Rovable with the attached display shield

9.3 Design and art

Because DWT is applied ultimately to the body, many design and art applications can arise.

9.3.1 Moving Fabric

By attaching the robots to clothing, they can serve beyond individual roaming elements and expand to alter the shape of the garment through movement. With the addition of a small Velcro hook on the robot casing, the robot attaches itself to the ends of a shawl which shape-changes into a scarf according to context, such as temperature change.

Figure 9-14: Tactile feedback application. We designed a linear actuator that can poke the skin. This tactor can go up and down to create tactile feedback.

Figure 9-15: Shape changing fabric. Robot self-attache to fabric shifts to become a scarf according to temperature change.

9.3.2 Interactive Moving Jewelry

Core interactions: *Hiding interfaces, timed interfaces.* With an aesthetic cover, the robot is transformed from a machine to a piece of jewelry, opening the space for decorative and functionally synthesized applications on the body. We present the example where the Rovable doubles as a brooch and microphone/speaker. It usually

serves as a decorative brooch, yet when the wearer receives a phone call, it shifts close to the neck to serve as a microphone/speaker in the case when the wearer's hands are full.

Figure 9-16: Interactive moving jewelry. Robotic brooch moves to become a shoulder microphone speaker when wearer recieves a phone call.

9.3.3 3D printing on the body

The robots could be used to 3D print on the body. This allows the clothing to be printed directly on the body. To test this concept, we created a proof of concept prototype that is based on FDM (fused deposition modeling) 3D printing. This technology deposits layers of hot thermoplastic filament. We equipped the Epidermal Robot with an extruder nozzle and a mechanism to push the filament. The extruder was taken from a 3D doodler pen. For the filament, we used a low-temperature hot melt adhesive or hot glue. We selected this material as it was safe for skin use as it melted at relatively low temperature (100°C) and was safe for skin contact.

9.4 Chapter Summary

This chapter described applications of DWT in multiple domains. We believe that meaningful applications are required for this technology to make an impact and to understand the limitations of this technology better. Rovables targeted human-computer interactions and fashion applications such as haptic feedback, displays, and mobile jewelry. Epidermal Robots mainly focused on medical applications. One of the exciting applications is mapping mechanical properties of tissues, which enables the robots to find lumps under the skin. This application allows the robots to collect data systematically, that could allow accurate machine learning.

It is conceptually challenging to create applications for DWT. The robots were not designed with one particular problem in mind, but with a vision of a new way of interaction between robots and humans. Due to technological limitations, the robots can not do anything better than other devices. It is difficult to predict future, but potentially in 5-10 years, the technology will catch on and fully enable the vision of Dynamic Wearable Technology.

Chapter 10

Challanges and Future work

The development of DWT is still in its infancy. There are many challenges and opportunities for future growth, as outlined in this chapter.

10.1 Applications

In this thesis, we demonstrated potential applications of DWT technology in medicine, human-computer interactions, and arts/fashion. However, there is still no"killer application," an application that could not be done any other way or a niche that completely justifies the robots. In its current state, the DWT can't compete with the well-developed technologies. It is not surprising, as we did not develop DWT with a single problem in mind. The main goal of DWT is to demonstrate how we can think of wearables differently, e.g., as robotic companions. Unpredictable and rapid technological development makes it hard to predict where this work will be in 5-10 years. This is especially difficult for robotics technologies. This field did not develop as we expected before: we still do not have human-like robots. This is due to both technical challenges plus the fact that robots are better able to accomplish their tasks in other forms. A future challenge for this work is to find a killer application. It is also entirely possible that there is no one killer application, and DWT provides a complimentary niche in the wearable technologies ecosystem. In any scenario, a long-term real-world deployment will be required to assess the demands of this technology thoroughly.

Many interesting sensing applications remain to be implemented. We see tremendous potential in using the robots in tomography, which is a 3D reconstruction of tissues based on spatial sensors. It is similar to what is done in MRI and CT scanners. We don't believe that our technology can see anywhere as deep as the MRI machines. The depth depends on the energy input to the transducer, and we can't input nearly as much energy into the robot as the stationary scanners. We showed, in the applications section, that we can sense about 5mm under the skin using mechanical testing. In the future, we hope to see deeper inside the body.

For examples, by equipping the robots with bright infrared LED lights and detectors, would enable Diffuse Optical Tomography (DOT) [161]. In this technique, the light is used to see inside the body, as tissues are almost transparent in near-infrared and infrared light (600-1000um wavelength). As the size and energy consumption of LEDs is not significant, it is possible to add DOT to the robots. Another possibility is to equip the robot with the ultrasound probe, which can also allow tomography [162]. The ultrasounds probe can potentially penetrate deeper than DOT but has integration challenges, such as the need for a gel for tissue impedance and high power consumption. Multiple robots could be used simultaneously as sources and receivers, or to increase the speed of the scan.

Another opportunity is using robots for intervention. The robots could be equipped with an epidermal needle to inject medicine into the tissues painlessly. Also, the robots could remove skin lesions with cryogenic spray or a micro scalpel. On the surface, the robots could be used for body care such as to remove hair, shave, or apply lotions to the skin. In the future, we hope to explore such applications.

In this thesis, we haven't explored much how the robots can cooperate with each other and work in swarms. We showed a few applications where up to three Rovables worked together to move garments. The cooperation could be used to do complex sensing tasks such as using one robot as transmitter and one as a receiver for electrical impedance tomography [163]. Also, robots working together will accomplish a job faster. Different robots could be equipped with varying instruments.

10.2 User testing

To understand the applications and the limitations of this technology, more user evaluations are required. For Rovables, limited user testing was done in a previous work [23]. The testing was mainly concerned with the robot's perception. We plan to test the robots in a normal environment while being worn for 24 hours. For the Epidermal Robots, we believe more rigorous testing is required since the robot is targeting mainly medical sensing applications. We have done testing with one participant, and only on a forearm. There is a great variation of skin mechanical properties depending on age, race, gender, and other factors. To fully understand skin locomotion, testing on different populations will be required.

For the application testing: first, the robots would be worn for a short time in defined medical applications and controlled environments. The robots could be used to measure and characterize lumps under the skin, with the ground truth obtained by a CT or MRI scanner. As technology improves, the robots could be tested in a less controlled scenario. They could be worn for 8 hours of sleep. Finally, the robots could be tested on a person going on with their every day, although the size, noise, tether, and potential discomfort associated with the robots would preclude this until more advanced versions are designed.

10.3 Adhesion and Locomotion

There is much improvement needed in adhesion and locomotion, especially for the Epidermal Robots.

Adhesion We determined that adhesion to the skin is challenging. We evaluated numerous approaches and determined that suction works the best. Even with the current approach, there is much room for improvement. Current design requires bulky pumps and solenoid valves. We plan to integrate the pump and the solenoids inside the suction cups. Previous research has demonstrated suction cups that have integrated shape memory actuated membrane instead of using an external pump [109].

Also multiple research projects have designed a suction cup that mimics octopus suckers[164, 165, 166]. Potentially, other adhesion approaches are possible such as using pinching of the skin, like a tree-climbing robot in [18].

We don't have any sensors to find the optimal spot for adhesion when the robot is taking a step. In the current approach, the robot can only detect if the vacuum seal is made. Using a camera, tactile, or distance sensor would help the robot climb faster and more reliably.

Locomotion We found locomotion using linear servo motors to be less than ideal. The current motors are fragile, and can quickly wear out, as they use a small lead-screw mechanism with plastic gears. We have not found any linear motors with similar size and torque, that can replace the current motors. Each leg of the robot has only two degrees of freedom, making it difficult to attach to curved surfaces. We believe that unconventional actuators are more appropriate and will be explored. In this thesis, we demonstrated a proof-of-concept approach to this using soft robotics.

10.4 Autonomy

We have demonstrated limited autonomous operation for the robots, and we envision that in the future such robots will roam around freely. To work in real-life applications, autonomy will have to be improved. The main challenge is to improve the accuracy of the onboard localization sensors. As we employ a dead-reckoning approach, the errors accumulate quickly. To improve the error, we need higher resolution and less noisy motor encoders. Using a high-performance IMU would also improve the error, although such a device can be bulky and draw significant power. Also, we will explore more sophisticated software algorithms, such as Kalman and particle filters.

10.5 Untethered device

The Rovables robot is untethered, but the Epidermal Robots still remain tethered. To fully realize their potential, these robots should be untethered. We found it challenging to make Epidermal Robot untethered because this would require making custom mechanical parts: motors, solenoids, and pumps. The off-the-shelf parts are too large and heavy, as the weight of the robot can't exceed 80 grams, and the center of gravity has to be designed to avoid torque on the skin.

While the analysis experiments in this thesis have been mostly performed with a tethered version of SkinBot, we believe our results are generalizable to potential untethered prototypes.

10.6 Other uses

The focus of this thesis is the human body. Potentially, the robots could be used with animals and other living creatures as well. For example, the robot could climb around an elephant to understand and map its health. If the animal is in the wild, it is hard to do any health assessment. It is not possible to bring an elephant into an MRI machine or a hospital. As DWT robots are small and light, they could be brought to the animal in the wild. Animal health is especially relevant, considering how many species are becoming endangered. As animals are prone to run and scratch off things crawling on their skin, a rugged unobtrusive robot may be critical.

Going beyond living creatures, this robot technology could be used for inspection of hard to reach places. The robot could climb different structures and detect cracks and structural problems. The Rovables could crawl on curtains and air balloons, as well as inside and outside a spaceship. Potentially, the robots could be used in disaster or conflict, and reach and measure physiological signals of a person trapped in the rubble.

Chapter 11

Conclusion

In this concluding chapter, I wanted to share ideas that could not fit anywhere else, e.g., how this work evolved over the years, and why it changed the way it did. Plus concisely summarize, what I learned by doing this research.

The main contribution of this thesis is to formulate and explore the idea of dynamic wearable technology: robots as companions living on our bodies. We demonstrated and studied this concept with two homebrew prototype robots. First, Rovables, a clothing climbing robot, that pinches fabric with magnetic rollers. Second, Epidermal robots that use suction to attach to the skin. Using the prototypes, this thesis analyzed the main design criteria of DWT; size in Chapter 4, locomotion and Adhesion in Chapter 5, Autonomy and Navigation in Chapter 8. Due to time and technological limitations, we can't fully realize the vision of autonomous skin crawling robots, but this thesis provides a path there. A big part of this thesis is to develop example applications of DWT. The applications show the importance of DWT concept and hopefully can inspire future work. The main applications area is sensing of/and around the human body. Also, we touch on applications in human-computer interactions and fashion/art.

11.0.1 Evoluation of this work

Over the years, this work has been an exciting experience of experimentation, trials, and errors. All my previous work has been on wearable electronics. It was fascinating to start blending robotics and wearables starting with a blank slate and trying every new idea. When we had the initial vision of small wearable robots, we had no idea how to implement them, as I had no robotics experience. We experimented an toyed with various mechanisms such as using wheels or grooves on the fabric. We also, purchased a lot of toys such as Hex Bugs, that move with vibrating whiskers. With Stanford collaborators, we were able to make Rovables. The magnetic wheel mechanism worked surprisingly well.

After working on the Rovables, the next logical challenge was to make skin crawling robots. The Rovables did not provide direct access to the skin, and I thought there were exciting sensing opportunities there. Climbing on the skin proved to be a challenging problem, which surprisingly has never been solved before. Initially, I tried using adhesives: wheels, tracks, and various other standard mechanisms. With trial and error, I learned that wheeled mechanisms don't work over such complex terrain. Nature confirms this, as there are no wheeled organisms. With wheels, after spinning the axis, motion and torque are created; assuming a flat ground. On the other hand, a legged robot is more challenging but provides greater control across uneven terrain. Legs are complex and delicate, and need tight control, with feedback, microcontroller, and sensors.

Once the climbing robot was operational, our next challenge was finding the right applications, and the application space is big. We entered this project motivated by a broad technical usage, as opposed to a compelling scenario. We showed that the robot could do physiological signal sensing and camera sensing, among other things. However, those applications did not drive the point as to why we need robots. Users could use their phone camera to take photos of their skin problems. An exciting area is mechanical imaging, as it can't be quickly done with existing technologies. Mechanical imaging requires contact and application of a local force with a precise

actuator. This is not possible using a phone or an electrode. Another problem with applying forces is the reaction force, which can cause unwanted deflections. As a robot already has mechanical actuators, using force is straightforward.

11.0.2 Lessons learned

There are some overall lessons that I learned in developing this work. It valuable to share those lessons:

1)Robotics are not particularly advanced at the centimeter scale. At this scale, there is not yet much market demand or many research applications. It is hard to get professional off-the-shelf parts. Centimeter scale robots are mostly concerned with hobbyists, such as remote-controlled cars, or medical applications such as insulin pumps or pressure cuffs. Most of the advances in robotics are coming from the micro-world (MEMs, microfabrication) or large platforms (e.g., drones, self-driving cars, industrial robots, and humanoid robots). Also, centimeter-sized robots are awkward for the software, as they can't run powerful operating systems or machine learning algorithms.

2) Developing a robot's autonomous operation is arduous, and I underestimated the required effort in the beginning. On the other hand, developing hardware and electronics is less daunting as they have specific functionality. By using simple physics, one can figure out the limits, such as speed and weight, and design accordingly. Working on the autonomous operation and localization does not have a precise goal, there are always improvements that can be made, and there are infinite real-world scenarios, except for very constrained environments. A designer of an autonomous system can't account for everything. Recent advances in machine learning have not been much help in this enterprise, as the size of the robot does not allow for advanced sensors and algorithms. Of course, this will develop as AI hardware progresses.

Doing a thesis on robotics invites to comment on the current state of Artificial Intelligence (AI). Hopefully, in the future, machine learning can run on small energy-constrained systems. There are indications that this will happen, as there is interest in real-time onboard image recognition, using popular neural networks (e.g., Con-

volutional Neural Nets). Intel has been a pioneer in hardware neural architectures dating back to the ETANN [167] from the 1980s, and now released much more capable digital implementation such as Neural Compute, a USB stick based neural network chip [168]. Google made hardware called Tensor Processing Unit that allows acceleration of neural network training and inference [169]. NVidia has released Jetson, a small embedded system [170] for running neural nets on robotic platforms. I believe that the most involved application of AI will be based on analyzing the data that robots are collecting using autonomous sensors. In this thesis, I demonstrated that convolutional neural networks could be used to classify the size of lumps under the skin.

3) Feedback sensors are crucial. Many hardware issues could be outsourced to sensors and computers, that compensate for bad hardware. For example, the robot can crawl on the skin using inexpensive hobby servo motors. By providing information from the vacuum pressure sensors, the servo motors can adjust themselves for correct skin attachment.

4) Frontier robotics are hard to justify. Even though our paper has won awards at technical conferences, every time, we demoed the robot projects, people asked why to do it this way over the current technologies. I found it difficult to answer that question. Almost anything a robot can currently do, a human can do better. Many people do not find the idea of DWT comfortable. It is understandable, as there are no examples of robots that live so close to our bodies. The concept of robots that live with us is of a humanoid robot or a kitchen appliance or a floor cleaner, not an insect-like crawler. In popular culture and science fiction, robots were always presented as humanoid. Even in the current world, we do not have humanoid robots, and most advanced robots are far away from us in factories. It is then a big question, as to how society will view and accept robotic companions. We will only know in 10-20 years.

Chapter 12

Appendix

The original design and software files for Rovables are in a github repository[1], and Epidermal robots are in a github repository[2]. The files provide the necessary details make the robots.

This appendix includes PCB design snopshots and schematic files for the robots.

[1]https://github.com/adementyev/Rovables-Repo
[2]https://github.com/adementyev/SkinBot

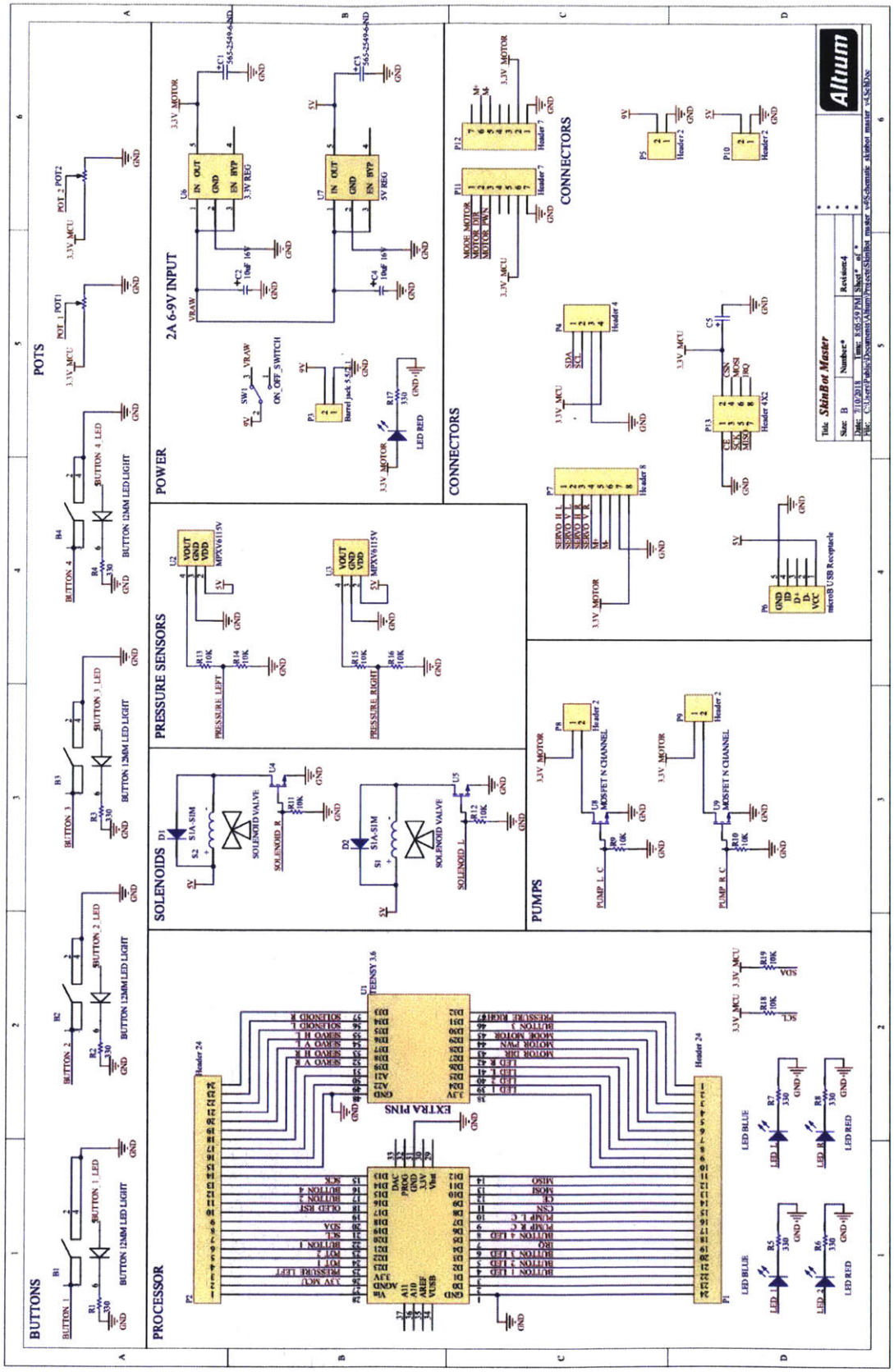

Figure 12-1: Skinbot control board

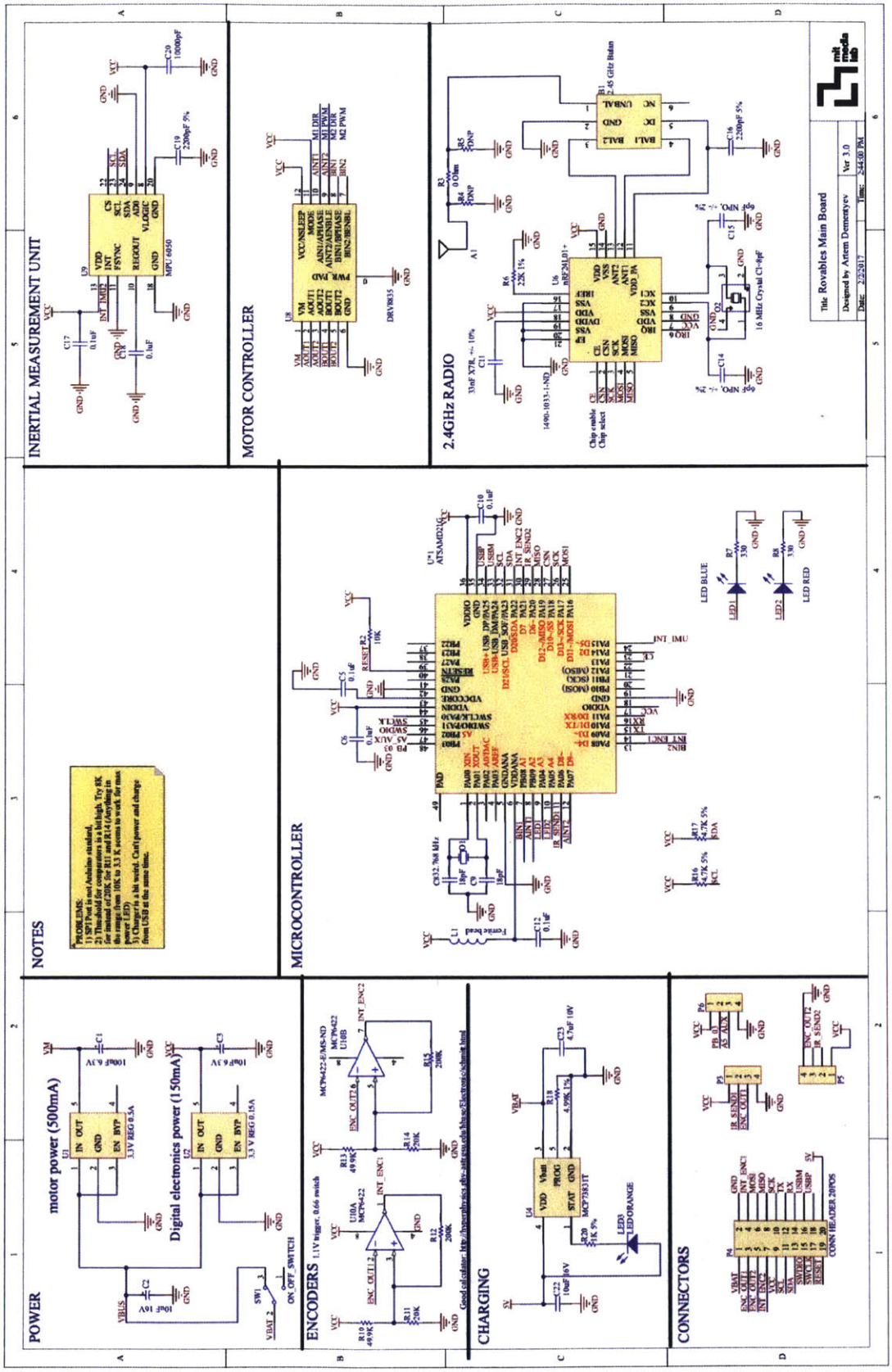

Figure 12-2: Rovables main board.

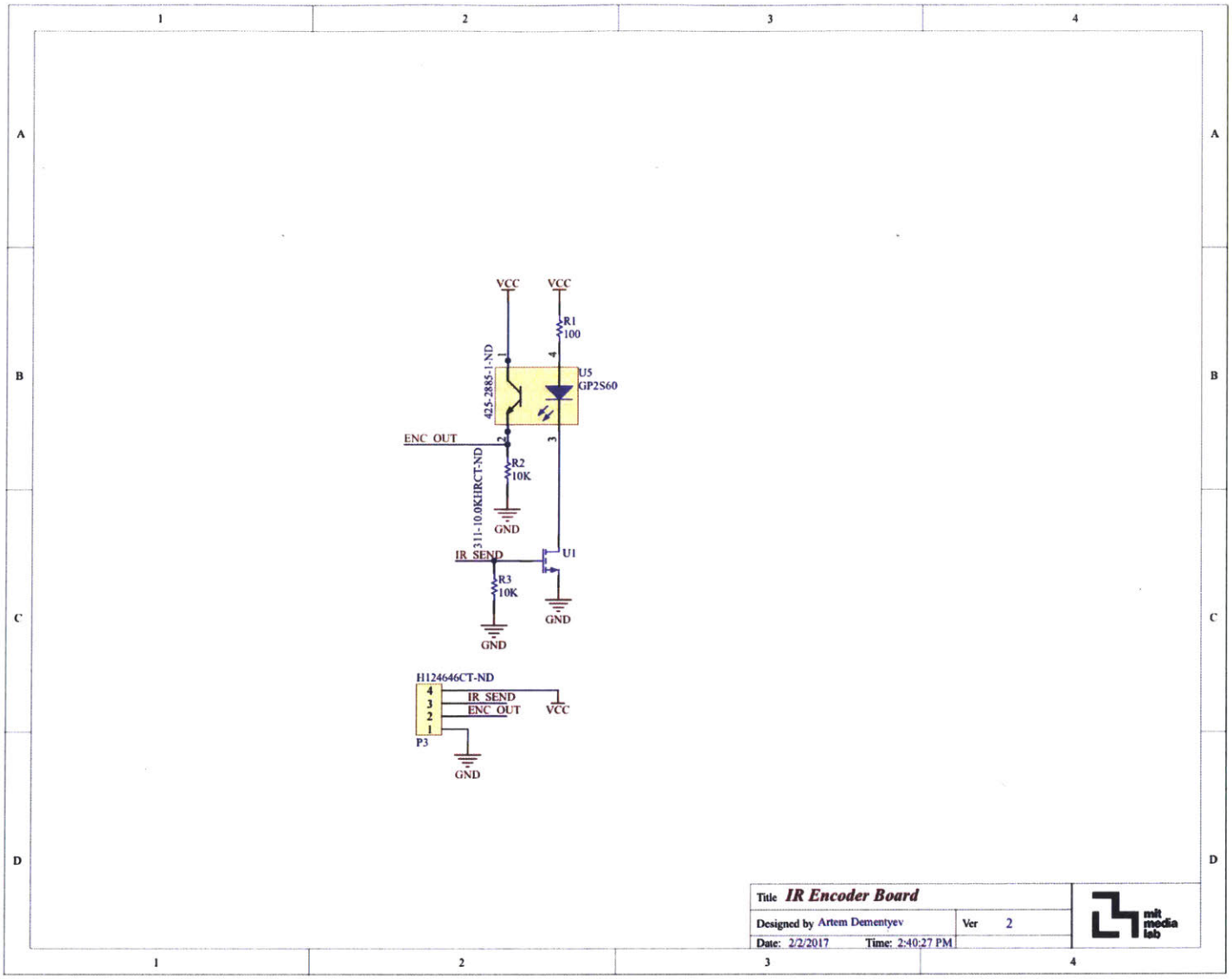

Figure 12-3: Infrared encoder board schematic for Rovables.

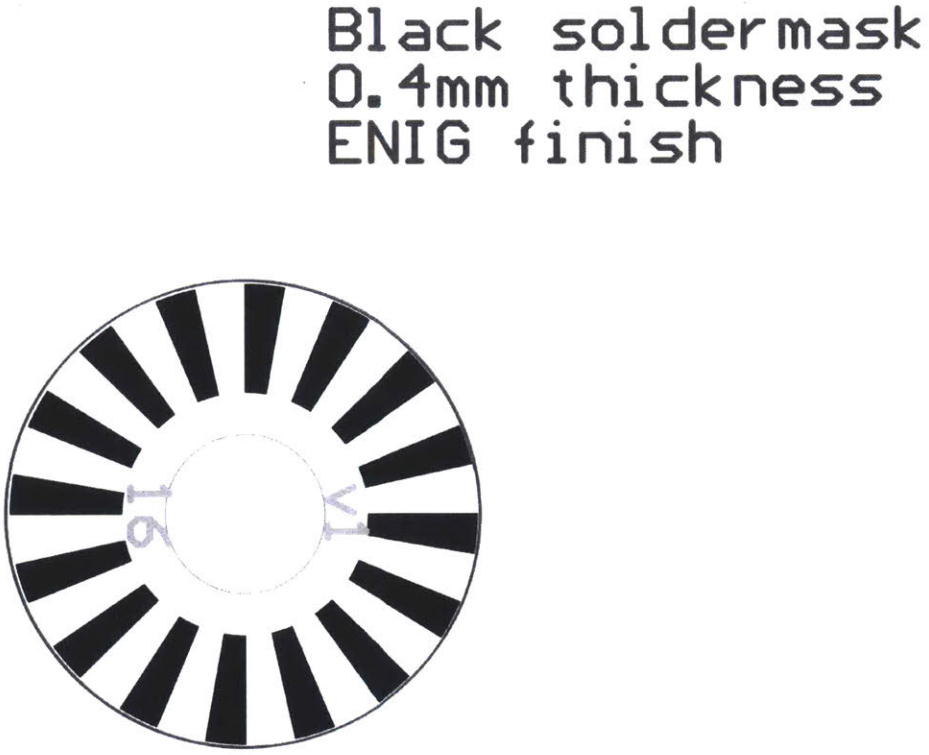

Figure 12-4: PCB Gerber of the wheel encoder pattern.

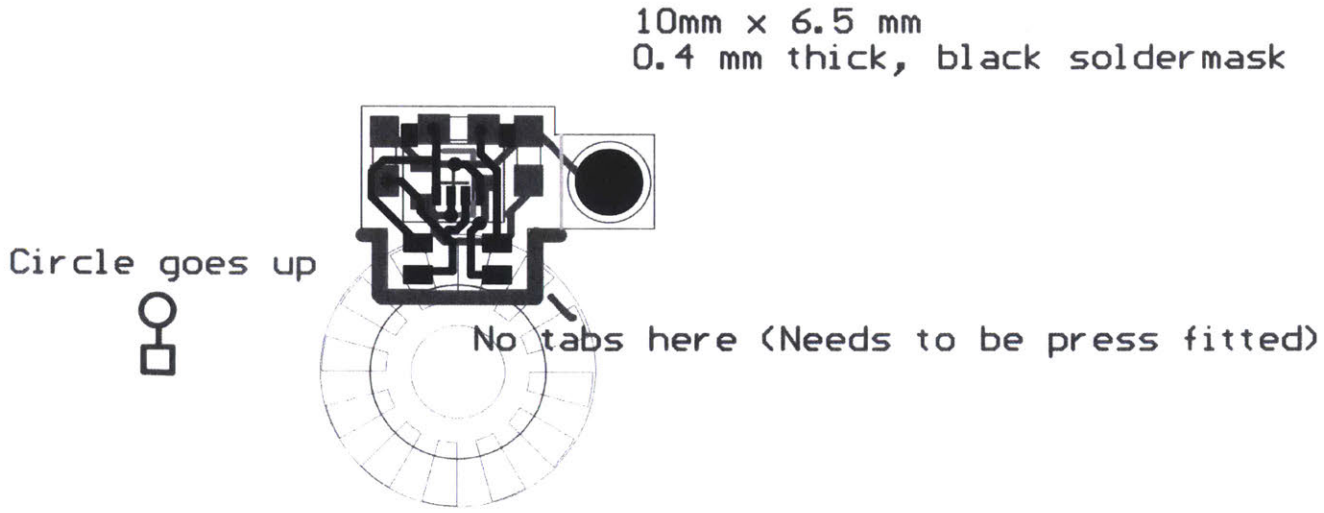

Figure 12-5: PCB Gerber of the wheel encoder board

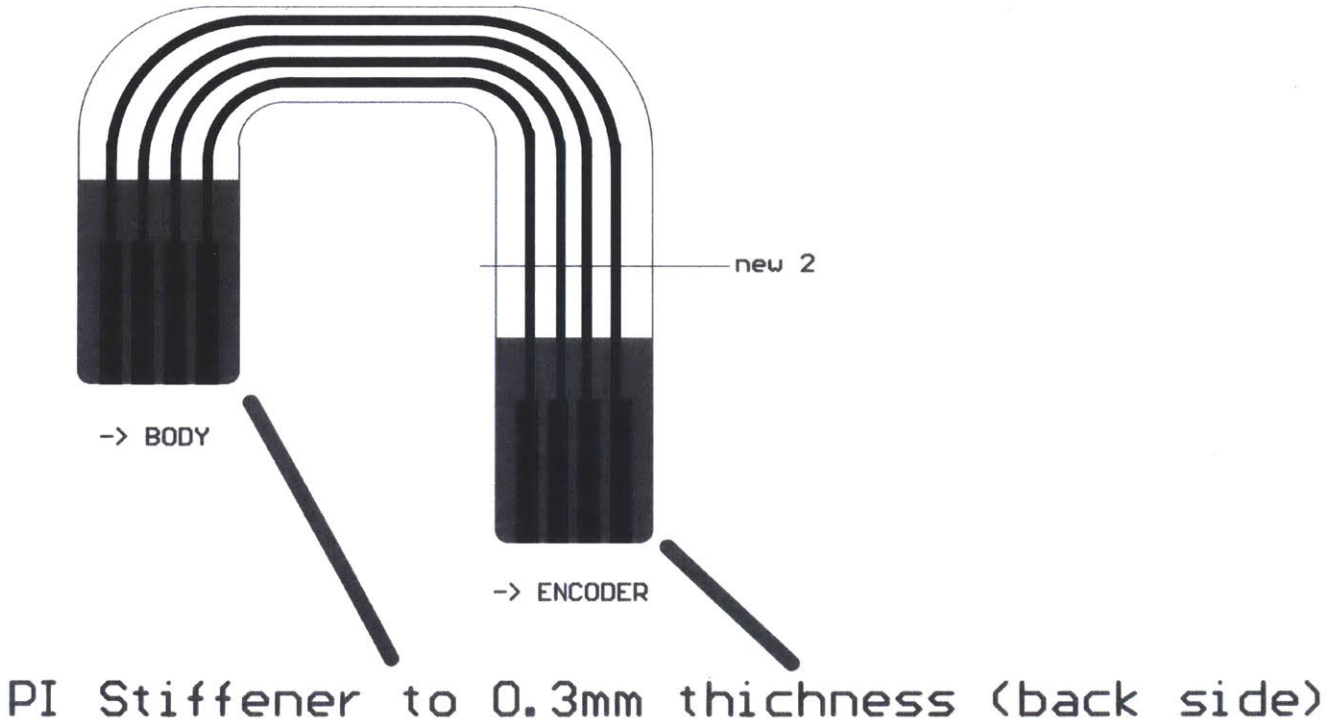

Figure 12-6: Flexible PCB of the custon cable between the encoder and the Rovables main board.

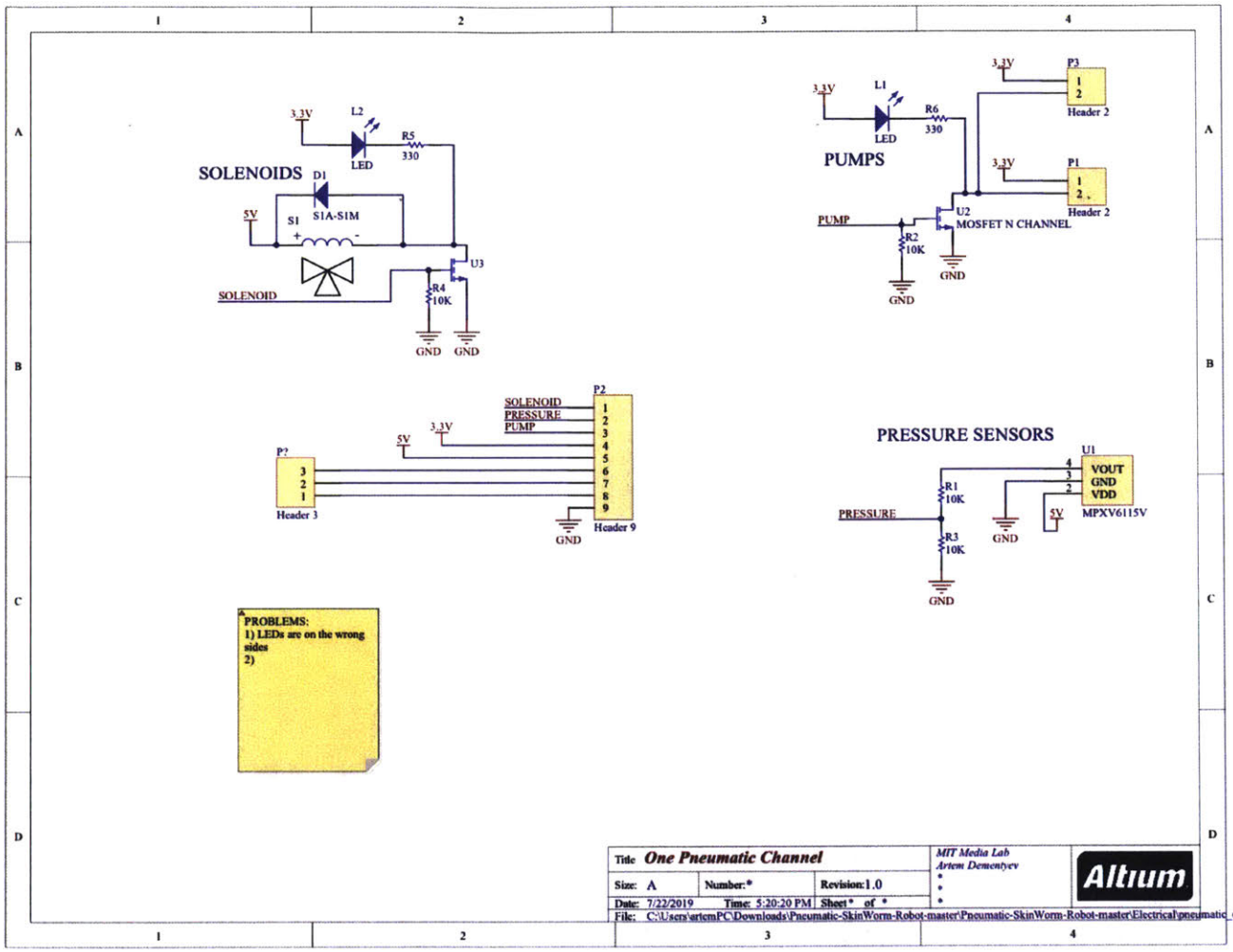

Figure 12-7: Schematic of one module for the soft robot control board

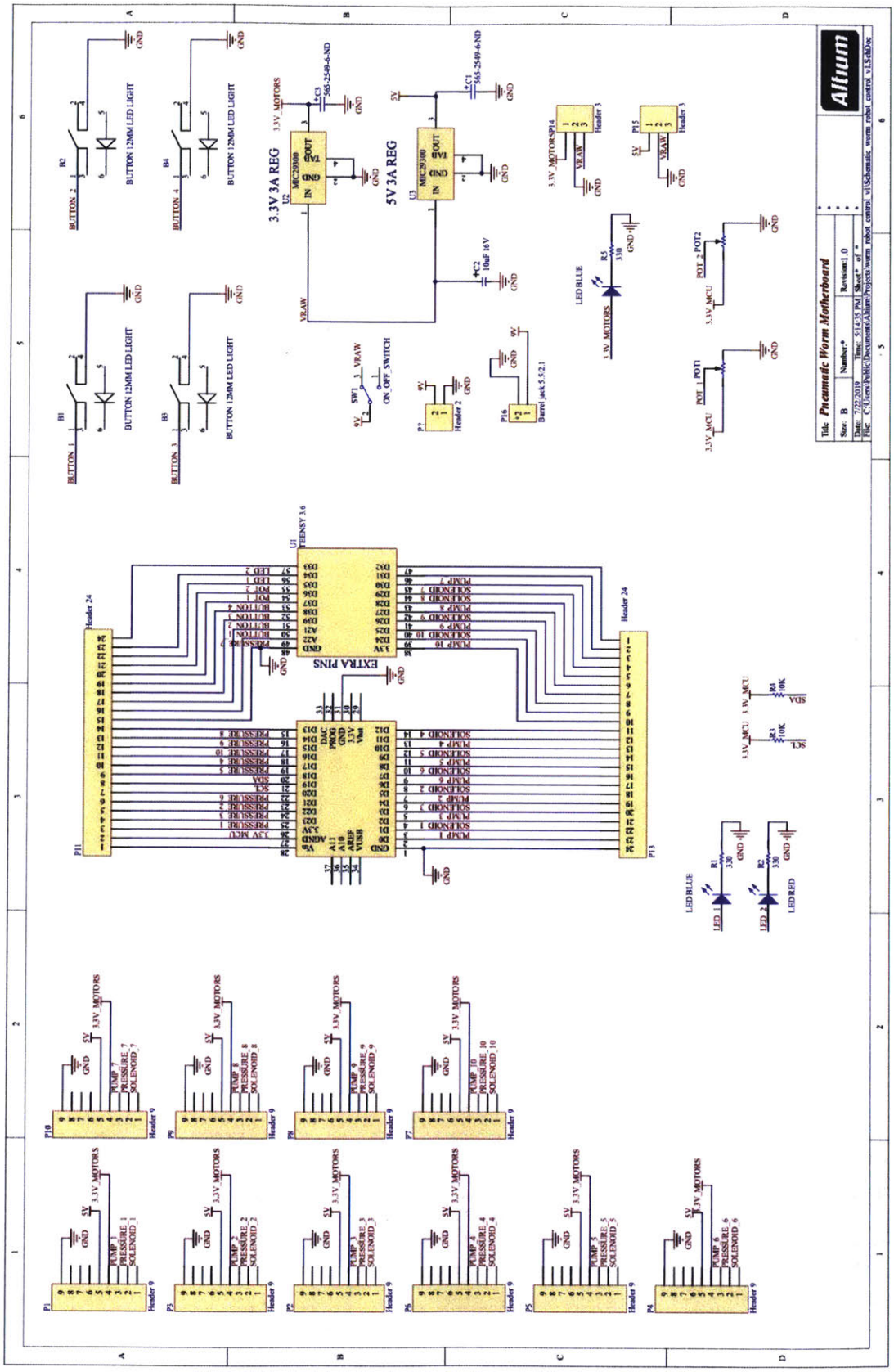

Figure 12-8: Schematic of the soft robot control board

Bibliography

[1] Artem Dementyev, Hsin-Liu Cindy Kao, Inrak Choi, Deborah Ajilo, Maggie Xu, Joseph A Paradiso, Chris Schmandt, and Sean Follmer. Rovables: Miniature on-body robots as mobile wearables. In *Proceedings of the 29th Annual Symposium on User Interface Software and Technology*, pages 111–120. ACM, 2016.

[2] Kathryn A Daltorio, Andrew D Horchler, Stanislav Gorb, Roy E Ritzmann, and Roger D Quinn. A small wall-walking robot with compliant, adhesive feet. In *Intelligent Robots and Systems, 2005.(IROS 2005). 2005 IEEE/RSJ International Conference on*, pages 3648–3653. IEEE, 2005.

[3] Martín Abadi, Paul Barham, Jianmin Chen, Zhifeng Chen, Andy Davis, Jeffrey Dean, Matthieu Devin, Sanjay Ghemawat, Geoffrey Irving, Michael Isard, et al. Tensorflow: a system for large-scale machine learning. In *OSDI*, volume 16, pages 265–283, 2016.

[4] David Silver, Aja Huang, Chris J Maddison, Arthur Guez, Laurent Sifre, George Van Den Driessche, Julian Schrittwieser, Ioannis Antonoglou, Veda Panneershelvam, Marc Lanctot, et al. Mastering the game of go with deep neural networks and tree search. *nature*, 529(7587):484, 2016.

[5] Felix Richter. The global wearables market is all about the wrist. *Statista*, 2018. `https://www.statista.com/chart/3370/wearable-device-forecast/`.

[6] Shimon Y Nof. *Handbook of industrial robotics*, volume 1. John Wiley & Sons, 1999.

[7] Kristen Warfield. People are covering live beetles in jewels to use as jewelry. *The Dodo*, 2018. `https://www.thedodo.com/in-the-wild/live-maquech-beetle-jewelry`.

[8] Ronald A Sherman. Maggot therapy for treating diabetic foot ulcers unresponsive to conventional therapy. *Diabetes care*, 26(2):446–451, 2003.

[9] Amrit Pal Singh. Medicinal leech therapy (hirudotherapy): a brief overview. *Complementary therapies in clinical practice*, 16(4):213–215, 2010.

[10] Anthony Domanico. Nixie lets you wear a selfie-taking drone on your wrist. *CNET*, 2014. `http://www.cnet.com/news/nixie-wear-a-selfie-taking-drone-on-your-wrist/`.

[11] Mathew Laibowitz and Joseph A Paradiso. Parasitic mobility for pervasive sensor networks. In *International Conference on Pervasive Computing*, pages 255–278. Springer, 2005.

[12] Artem Dementyev and Christian Holz. Dualblink: A wearable device to continuously detect, track, and actuate blinking for alleviating dry eyes and computer vision syndrome. *Proceedings of the ACM on Interactive, Mobile, Wearable and Ubiquitous Technologies*, 1(1):1, 2017.

[13] Artem Dementyev, Alexander Behnaz, and Alexander M Gorbach. 135-hour-battery-life skin temperature monitoring system using a bluetooth cellular phone. In *Biomedical Wireless Technologies, Networks, and Sensing Systems (BioWireleSS), 2013 IEEE Topical Conference on*, pages 25–27. IEEE, 2013.

[14] Artem Dementyev and Joseph A Paradiso. Wristflex: low-power gesture input with wrist-worn pressure sensors. In *Proceedings of the 27th annual ACM symposium on User interface software and technology*, pages 161–166. ACM, 2014.

[15] Hsin-Liu Cindy Kao, Artem Dementyev, Joseph A Paradiso, and Chris Schmandt. Nailo: fingernails as an input surface. In *Proceedings of the 33rd Annual ACM Conference on Human Factors in Computing Systems*, pages 3015–3018. ACM, 2015.

[16] Ken Nakagaki, Artem Dementyev, Sean Follmer, Joseph A Paradiso, and Hiroshi Ishii. Chainform: A linear integrated modular hardware system for shape changing interfaces. In *Proceedings of the 29th Annual Symposium on User Interface Software and Technology*, pages 87–96. ACM, 2016.

[17] Studio XO. Skin sucka. *Concept video*, 2013. `https://www.youtube.com/watch?v=pAE4TDMK9cY`.

[18] Tin Lun Lam and Yangsheng Xu. A flexible tree climbing robot: Treebot-design and implementation. In *Robotics and Automation (ICRA), 2011 IEEE International Conference on*, pages 5849–5854. IEEE, 2011.

[19] Markus Eich and Thomas Vögele. Design and control of a lightweight magnetic climbing robot for vessel inspection. In *Control & Automation (MED), 2011 19th Mediterranean Conference on*, pages 1200–1205. IEEE, 2011.

[20] Miroslav Dodig. Models and modelling of dynamic moments of inertia of human body. *International Journal of Sports Science*, 6(6):249–256, 2016.

[21] Lukasz Piwek, David A Ellis, Sally Andrews, and Adam Joinson. The rise of consumer health wearables: promises and barriers. *PLoS Medicine*, 13(2):e1001953, 2016.

[22] Artem Dementyev, Javier Hernandez, Inrak Choi, Sean Follmer, and Joseph Paradiso. Epidermal robots: Wearable sensors that climb on the skin. *Proceedings of the ACM on Interactive, Mobile, Wearable and Ubiquitous Technologies*, 2(3):102, 2018.

[23] Hsin-Liu Cindy Kao, Deborah Ajilo, Oksana Anilionyte, Artem Dementyev, Inrak Choi, Sean Follmer, and Chris Schmandt. Exploring interactions and perceptions of kinetic wearables. In *Proceedings of the 2017 Conference on Designing Interactive Systems*, pages 391–396. ACM, 2017.

[24] Artem Dementyev, Javier Hernandez, Sean Follmer, Inrak Choi, and Joseph Paradiso. Skinbot: A wearable skin climbing robot. In *Adjunct Publication of the 30th Annual ACM Symposium on User Interface Software and Technology*, pages 5–6. ACM, 2017.

[25] Edward O Thorp. The invention of the first wearable computer. In *Wearable Computers, 1998. Digest of Papers. Second International Symposium on*, pages 4–8. IEEE, 1998.

[26] Steve Mann. Wearable computing: A first step toward personal imaging. *Computer*, 30(2):25–32, 1997.

[27] Dung Phan, Lee Yee Siong, Pubudu N Pathirana, and Aruna Seneviratne. Smartwatch: Performance evaluation for long-term heart rate monitoring. In *Bioelectronics and Bioinformatics (ISBB), 2015 International Symposium on*, pages 144–147. IEEE, 2015.

[28] Alexandra Ion, Edward Jay Wang, and Patrick Baudisch. Skin drag displays: Dragging a physical tactor across the user's skin produces a stronger tactile stimulus than vibrotactile. In *Proceedings of the 33rd Annual ACM Conference on Human Factors in Computing Systems*, pages 2501–2504. ACM, 2015.

[29] Jun Gong, Lan Li, Daniel Vogel, and Xing-Dong Yang. Cito: An actuated smartwatch for extended interactions. In *Proceedings of the 2017 CHI Conference on Human Factors in Computing Systems*, pages 5331–5345. ACM, 2017.

[30] Junhan Zhou, Yang Zhang, Gierad Laput, and Chris Harrison. Aurasense: enabling expressive around-smartwatch interactions with electric field sensing. In *Proceedings of the 29th Annual Symposium on User Interface Software and Technology*, pages 81–86. ACM, 2016.

[31] Dae-Hyeong Kim, Nanshu Lu, Rui Ma, Yun-Soung Kim, Rak-Hwan Kim, Shuodao Wang, Jian Wu, Sang Min Won, Hu Tao, Ahmad Islam, et al. Epidermal electronics. *science*, 333(6044):838–843, 2011.

[32] Martin Weigel, Tong Lu, Gilles Bailly, Antti Oulasvirta, Carmel Majidi, and Jürgen Steimle. Iskin: flexible, stretchable and visually customizable on-body touch sensors for mobile computing. In *Proceedings of the 33rd Annual ACM*

Conference on Human Factors in Computing Systems, pages 2991–3000. ACM, 2015.

[33] Joanne Lo, Doris Jung Lin Lee, Nathan Wong, David Bui, and Eric Paulos. Skintillates: Designing and creating epidermal interactions. In *Proceedings of the 2016 ACM Conference on Designing Interactive Systems*, pages 853–864. ACM, 2016.

[34] Hsin-Liu Cindy Kao, Christian Holz, Asta Roseway, Andres Calvo, and Chris Schmandt. Duoskin: Rapidly prototyping on-skin user interfaces using skin-friendly materials. In *Proceedings of the 2016 ACM International Symposium on Wearable Computers*, pages 16–23. ACM, 2016.

[35] Adam Whiton. *Sartorial Robotics: Electronic-textiles and fiber-electronics for social soft-architecture robotics.* PhD thesis, Ph. D. Dissertation. Massachusetts Institute of Technology, Cambridge, MA, 2013.

[36] Tamami Saga, Nagisa Munekata, and Tetsuo Ono. Daily support robots that move on the body. In *Proceedings of the second international conference on Human-agent interaction*, pages 29–34. ACM, 2014.

[37] David Dobbelstein, Evgeny Stemasov, Daniel Besserer, Irina Stenske, and Enrico Rukzio. Movelet: a self-actuated movable bracelet for positional haptic feedback on the user's forearm. In *Proceedings of the 2018 ACM International Symposium on Wearable Computers*, pages 33–39. ACM, 2018.

[38] Rachel Ross. Transforming clothes. *MIT Technology Review*, 2006. `http://www.technologyreview.com/news/406705/transforming-clothes/`.

[39] Behnaz Farahi. Caress of the gaze. *Personal Website*, 2015. `http://behnazfarahi.com/caress-of-the-gaze/`.

[40] Mark Wilson. Magnetic fabric could let you change clothing instantly. *Co-Design*, 2015. `https://www.fastcodesign.com/3045349/magical-fabric-could-let-you-change-clothes-instantly`.

[41] Ernest Rehmatulla Post, Maggie Orth, Peter R Russo, and Neil Gershenfeld. E-broidery: Design and fabrication of textile-based computing. *IBM Systems journal*, 39(3.4):840–860, 2000.

[42] Yongsang Kim, Hyejung Kim, and Hoi-Jun Yoo. Electrical characterization of screen-printed circuits on the fabric. *IEEE transactions on advanced packaging*, 33(1):196–205, 2009.

[43] Liangbing Hu, Mauro Pasta, Fabio La Mantia, LiFeng Cui, Sangmoo Jeong, Heather Dawn Deshazer, Jang Wook Choi, Seung Min Han, and Yi Cui. Stretchable, porous, and conductive energy textiles. *Nano letters*, 10(2):708–714, 2010.

[44] Noémie Chocat, Guillaume Lestoquoy, Zheng Wang, Daniel M Rodgers, John D Joannopoulos, and Yoel Fink. Piezoelectric fibers for conformal acoustics. *Advanced Materials*, 24(39):5327–5332, 2012.

[45] Leah Buechley, Mike Eisenberg, Jaime Catchen, and Ali Crockett. The lilypad arduino: using computational textiles to investigate engagement, aesthetics, and diversity in computer science education. In *Proceedings of the SIGCHI conference on Human factors in computing systems*, pages 423–432. ACM, 2008.

[46] Ivan Poupyrev, Nan-Wei Gong, Shiho Fukuhara, Mustafa Emre Karagozler, Carsten Schwesig, and Karen E Robinson. Project jacquard: interactive digital textiles at scale. In *Proceedings of the 2016 CHI Conference on Human Factors in Computing Systems*, pages 4216–4227. ACM, 2016.

[47] Nicholas D Orf, Ofer Shapira, Fabien Sorin, Sylvain Dantò, Marc A Baldo, John D Joannopoulos, and Yoel Fink. Fiber draw synthesis. *Proceedings of the National Academy of Sciences*, 108(12):4743–4747, 2011.

[48] Daniel Roetenberg, Henk Luinge, and Per Slycke. Xsens mvn: full 6dof human motion tracking using miniature inertial sensors. *Xsens Motion Technologies BV, Tech. Rep*, 1, 2009.

[49] Takao Someya, Tsuyoshi Sekitani, Shingo Iba, Yusaku Kato, Hiroshi Kawaguchi, and Takayasu Sakurai. A large-area, flexible pressure sensor matrix with organic field-effect transistors for artificial skin applications. *Proceedings of the National Academy of Sciences*, 101(27):9966–9970, 2004.

[50] Artem Dementyev, Hsin-Liu Cindy Kao, and Joseph A Paradiso. Sensortape: Modular and programmable 3d-aware dense sensor network on a tape. In *Proceedings of the 28th Annual ACM Symposium on User Interface Software & Technology*, pages 649–658. ACM, 2015.

[51] Adriano Cavalcanti, Lior Rosen, Bijan Shirinzadeh, Moshe Rosenfeld, S Paulo, and T Aviv. Nanorobot for treatment of patients with artery occlusion. In *Proceedings of Virtual Concept*, 2006.

[52] Bradley J Nelson, Ioannis K Kaliakatsos, and Jake J Abbott. Microrobots for minimally invasive medicine. *Annual review of biomedical engineering*, 12:55–85, 2010.

[53] Zhiguang Wu, Jonas Troll, Hyeon-Ho Jeong, Qiang Wei, Marius Stang, Focke Ziemssen, Zegao Wang, Mingdong Dong, Sven Schnichels, Tian Qiu, et al. A swarm of slippery micropropellers penetrates the vitreous body of the eye. *Science advances*, 4(11):eaat4388, 2018.

[54] Robert J Webster, Allison M Okamura, and Nah J Cowan. Toward active cannulas: Miniature snake-like surgical robots. In *Intelligent Robots and Systems, 2006 IEEE/RSJ International Conference on*, pages 2857–2863. IEEE, 2006.

[55] DeaGyu Kim, Zhijian Hao, Jun Ueda, and Azadeh Ansari. A 5mg microbristle-bot fabricated by two-photon lithography. *Journal of Micromechanics and Microengineering*, 2019.

[56] Moshe Shoham, Michael Burman, Eli Zehavi, Leo Joskowicz, Eduard Batkilin, and Yigal Kunicher. Bone-mounted miniature robot for surgical procedures: Concept and clinical applications. *IEEE Transactions on Robotics and Automation*, 19(5):893–901, 2003.

[57] Nabil Simaan, Russell Taylor, and Paul Flint. High dexterity snake-like robotic slaves for minimally invasive telesurgery of the upper airway. In *International Conference on Medical Image Computing and Computer-Assisted Intervention*, pages 17–24. Springer, 2004.

[58] Hyun-Soo Yoon, Se Min Oh, Jin Hyeok Jeong, Seung Hwan Lee, Kyung Tae, Kyoung-Chul Koh, and Byung-Ju Yi. Active bending endoscope robot system for navigation through sinus area. In *Intelligent Robots and Systems (IROS), 2011 IEEE/RSJ International Conference on*, pages 967–972. IEEE, 2011.

[59] NA Patronik, MA Zenati, and CN Riviere. Preliminary evaluation of a mobile robotic device for navigation and intervention on the beating heart. *Computer Aided Surgery*, 10(4):225–232, 2005.

[60] Nicholas A Patronik, Marco A Zenati, and Cameron N Riviere. Crawling on the heart: a mobile robotic device for minimally invasive cardiac interventions. In *International Conference on Medical Image Computing and Computer-Assisted Intervention*, pages 9–16. Springer, 2004.

[61] Fadel Adib, Hongzi Mao, Zachary Kabelac, Dina Katabi, and Robert C Miller. Smart homes that monitor breathing and heart rate. In *Proceedings of the 33rd annual ACM conference on human factors in computing systems*, pages 837–846. ACM, 2015.

[62] Daniel McDuff, Sarah Gontarek, and Rosalind W Picard. Improvements in remote cardiopulmonary measurement using a five band digital camera. *IEEE Transactions on Biomedical Engineering*, 61(10):2593–2601, 2014.

[63] Jacob Rosen, Mitchell Lum, Mika Sinanan, and Blake Hannaford. Raven: Developing a surgical robot from a concept to a transatlantic teleoperation experiment. In *Surgical Robotics*, pages 159–197. Springer, 2011.

[64] Ashutosh Tewari, James Peabody, Richard Sarle, Guruswami Balakrishnan, Ashok Hemal, Alok Shrivastava, and Mani Menon. Technique of da vinci robot-assisted anatomic radical prostatectomy. *Urology*, 60(4):569–572, 2002.

[65] Sebastian Bitzer and Patrick Van Der Smagt. Learning emg control of a robotic hand: towards active prostheses. In *Robotics and Automation, 2006. ICRA 2006. Proceedings 2006 IEEE International Conference on*, pages 2819–2823. IEEE, 2006.

[66] Joaquin A Blaya and Hugh Herr. Adaptive control of a variable-impedance ankle-foot orthosis to assist drop-foot gait. *IEEE Transactions on neural systems and rehabilitation engineering*, 12(1):24–31, 2004.

[67] Joel C Perry, Jacob Rosen, and Stephen Burns. Upper-limb powered exoskeleton design. *IEEE/ASME transactions on mechatronics*, 12(4):408–417, 2007.

[68] Sang-won Leigh and Pattie Maes. Body integrated programmable joints interface. In *Proceedings of the 2016 CHI Conference on Human Factors in Computing Systems*, pages 6053–6057. ACM, 2016.

[69] MHD Saraiji, Tomoya Sasaki, Kai Kunze, Kouta Minamizawa, and Masahiko Inami. Metaarms: Body remapping using feet-controlled artificial arms. In *The 31st Annual ACM Symposium on User Interface Software and Technology*, pages 65–74. ACM, 2018.

[70] S Diridollou, F Patat, F Gens, L Vaillant, D Black, JM Lagarde, Y Gall, and M Berson. In vivo model of the mechanical properties of the human skin under suction. *Skin Research and technology*, 6(4):214–221, 2000.

[71] PG Agache, C Monneur, JL Leveque, and J De Rigal. Mechanical properties and young's modulus of human skin in vivo. *Archives of dermatological research*, 269(3):221–232, 1980.

[72] Artem Dementyev, Jie Qil, Jifei Ou, and Joseph Paradiso. Mass manufacturing of self-actuating robots: Integrating sensors and actuators using flexible electronics. In *2018 IEEE/RSJ International Conference on Intelligent Robots and Systems (IROS)*, pages 6099–6104. IEEE, 2018.

[73] Iris De Falco, Matteo Cianchetti, and Arianna Menciassi. A soft multi-module manipulator with variable stiffness for minimally invasive surgery. *Bioinspiration & biomimetics*, 12(5):056008, 2017.

[74] Yuanyuan Liu, Xinyu Wu, Huihuan Qian, Duan Zheng, Jianquan Sun, and Yangsheng Xu. System and design of clothbot: A robot for flexible clothes climbing. In *Robotics and Automation (ICRA), 2012 IEEE International Conference on*, pages 1200–1205. IEEE, 2012.

[75] R Nils Planken, Xavier HA Keuter, Arnold PG Hoeks, Jeroen P Kooman, Frank M van der Sande, Alfons GH Kessels, Tim Leiner, and Jan HM Tordoir. Diameter measurements of the forearm cephalic vein prior to vascular access creation in end-stage renal disease patients: graduated pressure cuff versus tourniquet vessel dilatation. *Nephrology Dialysis Transplantation*, 21(3):802–806, 2005.

[76] Dewar D Finlay, Chris D Nugent, Stefan P Nelwan, Raymond R Bond, Mark P Donnelly, and Daniel Guldenring. Effects of electrode placement errors in the easi-derived 12-lead electrocardiogram. *Journal of electrocardiology*, 43(6):606–611, 2010.

[77] Greg Welch and Eric Foxlin. Motion tracking: No silver bullet, but a respectable arsenal. *IEEE Computer graphics and Applications*, 22(6):24–38, 2002.

[78] Jeffrey Hightower and Gaetano Borriello. Location systems for ubiquitous computing. *Computer*, 34(8):57–66, 2001.

[79] Rainer Mautz and Sebastian Tilch. Survey of optical indoor positioning systems. In *Indoor Positioning and Indoor Navigation (IPIN), 2011 International Conference on*, pages 1–7. IEEE, 2011.

[80] Soo-Yong Jung, Swook Hann, and Chang-Soo Park. Tdoa-based optical wireless indoor localization using led ceiling lamps. *IEEE Transactions on Consumer Electronics*, 57(4), 2011.

[81] Roy Want, Andy Hopper, Veronica Falcao, and Jonathan Gibbons. The active badge location system. *ACM Transactions on Information Systems (TOIS)*, 10(1):91–102, 1992.

[82] Purushottam Kulkarni, Deepak Ganesan, Prashant Shenoy, and Qifeng Lu. Senseye: a multi-tier camera sensor network. In *Proceedings of the 13th annual ACM international conference on Multimedia*, pages 229–238. ACM, 2005.

[83] Frederick H Raab, Ernest B Blood, Terry O Steiner, and Herbert R Jones. Magnetic position and orientation tracking system. *IEEE Transactions on Aerospace and Electronic systems*, (5):709–718, 1979.

[84] Chao Hu, Mao Li, Shuang Song, Rui Zhang, Max Q-H Meng, et al. A cubic 3-axis magnetic sensor array for wirelessly tracking magnet position and orientation. *IEEE Sensors Journal*, 10(5):903–913, 2010.

[85] Rong-Hao Liang, Kai-Yin Cheng, Liwei Chan, Chuan-Xhyuan Peng, Mike Y Chen, Rung-Huei Liang, De-Nian Yang, and Bing-Yu Chen. Gaussbits: magnetic tangible bits for portable and occlusion-free near-surface interactions. In *Proceedings of the SIGCHI Conference on Human Factors in Computing Systems*, pages 1391–1400. ACM, 2013.

[86] Brandon Gozick, Kalyan Pathapati Subbu, Ram Dantu, and Tomyo Maeshiro. Magnetic maps for indoor navigation. *IEEE Transactions on Instrumentation and Measurement*, 60(12):3883–3891, 2011.

[87] Jeffrey Hightower, Roy Want, and Gaetano Borriello. Spoton: An indoor 3d location sensing technology based on rf signal strength. Technical report, University of Washington CSE Report# 2000-02, 2000.

[88] Fadel Adib, Zachary Kabelac, Dina Katabi, and Robert C Miller. 3d tracking via body radio reflections. In *NSDI*, volume 14, pages 317–329, 2014.

[89] Yunfei Ma, Nicholas Selby, and Fadel Adib. Minding the billions: Ultra-wideband localization for deployed rfid tags. In *Proceedings of the 23rd Annual International Conference on Mobile Computing and Networking*, pages 248–260. ACM, 2017.

[90] Nicolas Villar, Daniel Cletheroe, Greg Saul, Christian Holz, Tim Regan, Oscar Salandin, Misha Sra, Hui-Shyong Yeo Yeo, William Field, and Haiyan Zhang. Project zanzibar: A portable and flexible tangible interaction platform. In *Proceedings of the 2018 CHI Conference on Human Factors in Computing Systems*, page 515. ACM, 2018.

[91] Emidio DiGiampaolo and Francesco Martinelli. A passive uhf-rfid system for the localization of an indoor autonomous vehicle. *IEEE Transactions on Industrial Electronics*, 59(10):3961–3970, 2012.

[92] Lionel M Ni, Yunhao Liu, Yiu Cho Lau, and Abhishek P Patil. Landmarc: indoor location sensing using active rfid. In *Pervasive Computing and Communications, 2003.(PerCom 2003). Proceedings of the First IEEE International Conference on*, pages 407–415. IEEE, 2003.

[93] Andy Harter, Andy Hopper, Pete Steggles, Andy Ward, and Paul Webster. The anatomy of a context-aware application. *Wireless Networks*, 8(2/3):187–197, 2002.

[94] Nissanka B Priyantha, Anit Chakraborty, and Hari Balakrishnan. The cricket location-support system. In *Proceedings of the 6th annual international conference on Mobile computing and networking*, pages 32–43. ACM, 2000.

[95] Greg Welch, Gary Bishop, et al. An introduction to the kalman filter. 1995.

[96] Yasutaka Fuke and Eric Krotkov. Dead reckoning for a lunar rover on uneven terrain. In *Robotics and Automation, 1996. Proceedings., 1996 IEEE International Conference on*, volume 1, pages 411–416. IEEE, 1996.

[97] Johann Borenstein, HR Everett, and Liqiang Feng. *Navigating mobile robots: Systems and techniques.* AK Peters, Ltd., 1996.

[98] Richard F Lyon. The optical mouse, and an architectural methodology for smart digital sensors. In *VLSI Systems and Computations*, pages 1–19. Springer, 1981.

[99] Sooyong Lee and Jae-Bok Song. Mobile robot localization using optical flow sensors. *International Journal of Control, Automation, and Systems*, 2(4):485–493, 2004.

[100] Dominik Honegger, Lorenz Meier, Petri Tanskanen, and Marc Pollefeys. An open source and open hardware embedded metric optical flow cmos camera for indoor and outdoor applications. In *Robotics and Automation (ICRA), 2013 IEEE International Conference on*, pages 1736–1741. IEEE, 2013.

[101] Edward M Mikhail, James S Bethel, and J Chris McGlone. Introduction to modern photogrammetry. *New York*, 2001.

[102] AJ Swerdlow, J English, RM MacKie, CJ O'doherty, JA Hunter, J Clark, and DJ Hole. Benign melanocytic naevi as a risk factor for malignant melanoma. *Br Med J (Clin Res Ed)*, 292(6535):1555–1559, 1986.

[103] Yoh-suke Mukouyama, Donghun Shin, Stefan Britsch, Masahiko Taniguchi, and David J Anderson. Sensory nerves determine the pattern of arterial differentiation and blood vessel branching in the skin. *Cell*, 109(6):693–705, 2002.

[104] Alvin I Chen, Max L Balter, Timothy J Maguire, and Martin L Yarmush. 3d near infrared and ultrasound imaging of peripheral blood vessels for real-time localization and needle guidance. In *International Conference on Medical Image Computing and Computer-Assisted Intervention*, pages 388–396. Springer, 2016.

[105] Paul Birkmeyer, Andrew G Gillies, and Ronald S Fearing. Clash: Climbing vertical loose cloth. In *Intelligent Robots and Systems (IROS), 2011 IEEE/RSJ International Conference on*, pages 5087–5093. IEEE, 2011.

[106] Kellar Autumn, Metin Sitti, Yiching A Liang, Anne M Peattie, Wendy R Hansen, Simon Sponberg, Thomas W Kenny, Ronald Fearing, Jacob N Israelachvili, and Robert J Full. Evidence for van der waals adhesion in gecko setae. *Proceedings of the National Academy of Sciences*, 99(19):12252–12256, 2002.

[107] J Gray, HW Lissmann, and RJ Pumphrey. The mechanism of locomotion in the leech (hirudo medicinalis ray). *Journal of Experimental Biology*, 15(3):408–430, 1938.

[108] Cecilia Laschi, Barbara Mazzolai, V Mattoli, M Cianchetti, and P Dario. Design of a biomimetic robotic octopus arm. *Bioinspiration & biomimetics*, 4(1):015006, 2009.

[109] Hu Bing-Shan, Wang Li-Wen, Fu Zhuang, and Zhao Yan-zheng. Bio-inspired miniature suction cups actuated by shape memory alloy. *International Journal of Advanced Robotic Systems*, 6(3):29, 2009.

[110] John Charles Briggs. *Automated handling of flexible materials.* PhD thesis, Massachusetts Institute of Technology, 1988.

[111] Peng Geng, Jia Liu, Xinyu Wu, and Wei Feng. Clothbot_β: Dynamical grasping and climbing on soft cloth. In *2018 13th World Congress on Intelligent Control and Automation (WCICA)*, pages 13–20. IEEE, 2018.

[112] Guangchen Chen, Yuanyuan Liu, Ruiqing Fu, Jianwei Sun, Xinyu Wu, and Yangsheng Xu. Rubbot: Rubbing on flexible loose surfaces. In *Intelligent Robots and Systems (IROS), 2013 IEEE/RSJ International Conference on*, pages 2303–2308. IEEE, 2013.

[113] Michael P Murphy and Metin Sitti. Waalbot: An agile small-scale wall-climbing robot utilizing dry elastomer adhesives. *IEEE/ASME transactions on Mechatronics*, 12(3):330–338, 2007.

[114] Carlo Menon, Michael Murphy, and Metin Sitti. Gecko inspired surface climbing robots. In *Robotics and Biomimetics, 2004. ROBIO 2004. IEEE International Conference on*, pages 431–436. IEEE, 2004.

[115] Leoncio Briones, Paul Bustamante, and Miguel A Serna. Wall-climbing robot for inspection in nuclear power plants. In *Robotics and Automation, 1994. Proceedings., 1994 IEEE International Conference on*, pages 1409–1414. IEEE, 1994.

[116] Deepak Trivedi, Christopher D Rahn, William M Kier, and Ian D Walker. Soft robotics: Biological inspiration, state of the art, and future research. *Applied bionics and biomechanics*, 5(3):99–117, 2008.

[117] Panagiotis Polygerinos, Zheng Wang, Kevin C Galloway, Robert J Wood, and Conor J Walsh. Soft robotic glove for combined assistance and at-home rehabilitation. *Robotics and Autonomous Systems*, 73:135–143, 2015.

[118] Nikolaos G Tsagarakis and Darwin G Caldwell. Development and control of a soft-actuatedexoskeleton for use in physiotherapy and training. *Autonomous Robots*, 15(1):21–33, 2003.

[119] Nathaniel Agharese, Tyler Cloyd, Laura H Blumenschein, Michael Raitor, Elliot W Hawkes, Heather Culbertson, and Allison M Okamura. Hapwrap: Soft growing wearable haptic device. In *2018 IEEE International Conference on Robotics and Automation (ICRA)*, pages 1–5. IEEE, 2018.

[120] Charles E Clauser, John T McConville, and John W Young. Weight, volume, and center of mass of segments of the human body. Technical report, ANTIOCH COLL YELLOW SPRINGS OH, 1969.

[121] Y Lanir, S Dikstein, A Hartzshtark, and V Manny. In-vivo indentation of human skin. *Journal of biomechanical engineering*, 112(1):63–69, 1990.

[122] Joseph A Paradiso and Thad Starner. Energy scavenging for mobile and wireless electronics. *IEEE Pervasive computing*, (1):18–27, 2005.

[123] Paul D Mitcheson. Energy harvesting for human wearable and implantable biosensors. In *2010 Annual International Conference of the IEEE Engineering in Medicine and Biology*, pages 3432–3436. IEEE, 2010.

[124] Artem Dementyev. Applications of rf-powered computing systems: wearable eeg monitor and bistable display tag. Master's thesis, 2013.

[125] Alanson P Sample, Daniel J Yeager, Pauline S Powledge, Alexander V Mamishev, Joshua R Smith, et al. Design of an rfid-based battery-free programmable sensing platform. *IEEE transactions on instrumentation and measurement*, 57(11):2608, 2008.

[126] Artem Dementyev and Joshua R Smith. A wearable uhf rfid-based eeg system. In *RFID (RFID), 2013 IEEE International Conference on*, pages 1–7. IEEE, 2013.

[127] Aaron N Parks, Alanson P Sample, Yi Zhao, and Joshua R Smith. A wireless sensing platform utilizing ambient rf energy. In *Power Amplifiers for Wireless and Radio Applications (PAWR), 2013 IEEE Topical Conference on*, pages 160–162. IEEE, 2013.

[128] Artem Dementyev, Jeremy Gummeson, Derek Thrasher, Aaron Parks, Deepak Ganesan, Joshua R Smith, and Alanson P Sample. Wirelessly powered bistable display tags. In *Proceedings of the 2013 ACM international joint conference on Pervasive and ubiquitous computing*, pages 383–386. ACM, 2013.

[129] Alanson P Sample, David T Meyer, and Joshua R Smith. Analysis, experimental results, and range adaptation of magnetically coupled resonators for wireless power transfer. *IEEE Transactions on industrial electronics*, 58(2):544–554, 2011.

[130] Canan Dagdeviren, Byung Duk Yang, Yewang Su, Phat L Tran, Pauline Joe, Eric Anderson, Jing Xia, Vijay Doraiswamy, Behrooz Dehdashti, Xue Feng, et al. Conformal piezoelectric energy harvesting and storage from motions of the heart, lung, and diaphragm. *Proceedings of the National Academy of Sciences*, 111(5):1927–1932, 2014.

[131] Nathan S Shenck and Joseph A Paradiso. Energy scavenging with shoe-mounted piezoelectrics. *IEEE micro*, 21(3):30–42, 2001.

[132] Sun Jin Kim, Ju Hyung We, and Byung Jin Cho. A wearable thermoelectric generator fabricated on a glass fabric. *Energy & Environmental Science*, 7(6):1959–1965, 2014.

[133] Richard Van Noorden. The rechargeable revolution: A better battery. *Nature News*, 507(7490):26, 2014.

[134] Arumugam Manthiram, Xingwen Yu, and Shaofei Wang. Lithium battery chemistries enabled by solid-state electrolytes. *Nature Reviews Materials*, 2(4):16103, 2017.

[135] Hun-Gi Jung, Jusef Hassoun, Jin-Bum Park, Yang-Kook Sun, and Bruno Scrosati. An improved high-performance lithium–air battery. *Nature chemistry*, 4(7):579, 2012.

[136] Saman Naderiparizi, Aaron N Parks, Zerina Kapetanovic, Benjamin Ransford, and Joshua R Smith. Wispcam: A battery-free rfid camera. In *RFID (RFID), 2015 IEEE International Conference on*, pages 166–173. IEEE, 2015.

[137] Andrew P Sabelhaus, Daniel Mirsky, L Maxwell Hill, Nuno C Martins, and Sarah Bergbreiter. Tinyterp: a tiny terrestrial robotic platform with modular sensing. In *Robotics and Automation (ICRA), 2013 IEEE International Conference on*, pages 2600–2605. IEEE, 2013.

[138] Gilles Caprari, Thomas Estier, and Roland Siegwart. Fascination of down scaling-alice the sugar cube robot. *Journal of micromechatronics*, 1(3):177–189, 2001.

[139] Michael Rubenstein, Christian Ahler, and Radhika Nagpal. Kilobot: A low cost scalable robot system for collective behaviors. In *Robotics and Automation (ICRA), 2012 IEEE International Conference on*, pages 3293–3298. IEEE, 2012.

[140] Kei Iwata, Yuki Okane, Yuki Ishihara, Kazuki Sugita, Satoko Ono, Mizuki Abe, Satohiro Chiba, Minami Takato, Ken Saito, and Fumio Uchikoba. Insect-type microrobot with mounted bare chip ic of artificial neural networks. In *Micro Electro Mechanical Systems (MEMS), 2016 IEEE 29th International Conference on*, pages 1204–1207. IEEE, 2016.

[141] Erik Edqvist, Niklas Snis, Raimon Casanova Mohr, Oliver Scholz, Paolo Corradi, Jianbo Gao, Angel Diéguez, Nicolas Wyrsch, and Stefan Johansson. Evaluation of building technology for mass producible millimetre-sized robots using flexible printed circuit boards. *Journal of Micromechanics and Microengineering*, 19(7):075011, 2009.

[142] Jennifer E Curtis, Brian A Koss, and David G Grier. Dynamic holographic optical tweezers. *Optics communications*, 207(1-6):169–175, 2002.

[143] Walter F Paxton, Kevin C Kistler, Christine C Olmeda, Ayusman Sen, Sarah K St. Angelo, Yanyan Cao, Thomas E Mallouk, Paul E Lammert, and Vincent H Crespi. Catalytic nanomotors: autonomous movement of striped nanorods. *Journal of the American Chemical Society*, 126(41):13424–13431, 2004.

[144] Sylvain Martel, Charles C Tremblay, Serge Ngakeng, and Guillaume Langlois. Controlled manipulation and actuation of micro-objects with magnetotactic bacteria. *Applied Physics Letters*, 89(23):233904, 2006.

[145] Haruhisa Kawasaki, Tsuneo Komatsu, and Kazunao Uchiyama. Dexterous anthropomorphic robot hand with distributed tactile sensor: Gifu hand ii. *IEEE/ASME transactions on mechatronics*, 7(3):296–303, 2002.

[146] Parris S Wellman, Edward P Dalton, David Krag, Kenneth A Kern, and Robert D Howe. Tactile imaging of breast masses: first clinical report. *Archives of surgery*, 136(2):204–208, 2001.

[147] A Kalra, A Lowe, and AM Al-Jumaily. Mechanical behaviour of skin: a review. *J. Mater. Sci. Eng*, 5(4):1000254, 2016.

[148] Yongping Zheng and Arthur FT Mak. Effective elastic properties for lower limb soft tissues from manual indentation experiment. *IEEE Transactions on rehabilitation Engineering*, 7(3):257–267, 1999.

[149] Arthur FT Mak, George HW Liu, and SY Lee. Biomechanical assessment of below-knee residual limb tissue. *Journal of rehabilitation research and development*, 1994.

[150] Bevin Lin, Kevin M Moerman, Connor G McMahan, Kenneth A Pasch, and Hugh M Herr. Low-cost methodology for skin strain measurement of a flexed biological limb. *IEEE Transactions on Biomedical Engineering*, 64(12):2750–2759, 2017.

[151] Kevin M Moerman, Cathy A Holt, Sam L Evans, and Ciaran K Simms. Digital image correlation and finite element modelling as a method to determine mechanical properties of human soft tissue in vivo. *Journal of biomechanics*, 42(8):1150–1153, 2009.

[152] Jascha de Nooijer, Lilian Lechner, and Hein de Vries. Early detection of cancer: knowledge and behavior among dutch adults. *Cancer detection and prevention*, 26(5):362–369, 2002.

[153] James C Gwilliam, Zachary Pezzementi, Erica Jantho, Allison M Okamura, and Steven Hsiao. Human vs. robotic tactile sensing: Detecting lumps in soft tissue. In *2010 IEEE Haptics Symposium*, pages 21–28. IEEE, 2010.

[154] Hristo Dobrev. Use of cutometer to assess epidermal hydration. *Skin research and technology*, 6(4):239–244, 2000.

[155] Bin Li, Ye Shi, Adam Fontecchio, and Yon Visell. Mechanical imaging of soft tissues with a highly compliant tactile sensing array. *IEEE Transactions on Biomedical Engineering*, 65(3):687–697, 2017.

[156] W. Boucsein. *Electrodermal Activity*. The Springer series in behavioral psychophysiology and medicine. Springer US, 2012.

[157] Henrik Lorentzen, Kaare Weismann, Carsten Sand Petersen, Frederik Grønhøj Larsen, Lena Secher, and Vera Skødt. Clinical and dermatoscopic diagnosis of malignant melanoma: assessed by expert and non-expert groups. *Acta dermato-venereologica*, 79(4), 1999.

[158] Ferhat Attal, Samer Mohammed, Mariam Dedabrishvili, Faicel Chamroukhi, Latifa Oukhellou, and Yacine Amirat. Physical human activity recognition using wearable sensors. *Sensors*, 15(12):31314–31338, 2015.

[159] Tim Gfrerer. ofxskeleton. *Ponies and Light*, 2014. `http://poniesandlight.co.uk/code/ofxSkeleton/`.

[160] Javier Hernandez, Daniel J McDuff, and Rosalind W Picard. Biophone: Physiology monitoring from peripheral smartphone motions. In *Engineering in Medicine and Biology Society (EMBC), 2015 37th Annual International Conference of the IEEE*, pages 7180–7183. IEEE, 2015.

[161] David A Boas, Dana H Brooks, Eric L Miller, Charles A DiMarzio, Misha Kilmer, Richard J Gaudette, and Quan Zhang. Imaging the body with diffuse optical tomography. *IEEE signal processing magazine*, 18(6):57–75, 2001.

[162] Frank Natterer and Frank Wubbeling. A propagation-backpropagation method for ultrasound tomography. *Inverse problems*, 11(6):1225, 1995.

[163] Margaret Cheney, David Isaacson, and Jonathan C Newell. Electrical impedance tomography. *SIAM review*, 41(1):85–101, 1999.

[164] Francesca Tramacere, Lucia Beccai, Fabio Mattioli, Edoardo Sinibaldi, and Barbara Mazzolai. Artificial adhesion mechanisms inspired by octopus suckers. In *Robotics and Automation (ICRA), 2012 IEEE International Conference on*, pages 3846–3851. IEEE, 2012.

[165] FRANCESCA Tramacere, M Follador, NM Pugno, and B Mazzolai. Octopus-like suction cups: from natural to artificial solutions. *Bioinspiration & biomimetics*, 10(3):035004, 2015.

[166] Sina Sareh, Kaspar Althoefer, Min Li, Yohan Noh, Francesca Tramacere, Pooya Sareh, Barbara Mazzolai, and Mirko Kovac. Anchoring like octopus: biologically inspired soft artificial sucker. *Journal of the Royal Society Interface*, 14(135):20170395, 2017.

[167] Mark Holler, Simon Tam, Hernan Castro, and Ronald Benson. An electrically trainable artificial neural network (etann) with 10240 floating gate synapses. In *International Joint Conference on Neural Networks*, volume 2, pages 191–196, 1989.

[168] Xiaofan Xu, João Amaro, Sam Caulfield, Andrew Forembski, Gabriel Falcao, and David Moloney. Convolutional neural network on neural compute stick for voxelized point-clouds classification. In *2017 10th International Congress on Image and Signal Processing, BioMedical Engineering and Informatics (CISP-BMEI)*, pages 1–7. IEEE, 2017.

[169] Norman P Jouppi, Cliff Young, Nishant Patil, David Patterson, Gaurav Agrawal, Raminder Bajwa, Sarah Bates, Suresh Bhatia, Nan Boden, Al Borchers, et al. In-datacenter performance analysis of a tensor processing unit. In *2017 ACM/IEEE 44th Annual International Symposium on Computer Architecture (ISCA)*, pages 1–12. IEEE, 2017.

[170] Nathan Otterness, Ming Yang, Sarah Rust, Eunbyung Park, James H Anderson, F Donelson Smith, Alex Berg, and Shige Wang. An evaluation of the nvidia tx1 for supporting real-time computer-vision workloads. In *2017 IEEE Real-Time and Embedded Technology and Applications Symposium (RTAS)*, pages 353–364. IEEE, 2017.